

POLITECNICO DI MILANO



DEPARTMENT OF ENERGY

DOCTORAL PROGRAM IN ENERGY AND NUCLEAR
SCIENCE AND TECHNOLOGY

Study of innovative techniques aimed at
reducing energy consumption in domestic
refrigeration system

DOCTORAL DISSERTATION OF:
Matej Věšek

SUPERVISOR AND TUTOR:
Prof. Cesare Maria Joppolo

ASSISTANTS SUPERVISOR:
Luca Molinaroli and Andrea Olivani

THE CHAIR OF THE DOCTORAL PROGRAM:
Prof. Carlo Enrico Bottani

2013 – STEN 25th cycle

Abstract of the work

The most popular cold appliances in EU are combined two doors refrigerator-freezers. The two compartments function at very diverse air temperatures usually 4°C and -18°C. Nevertheless only the models with two compressors are currently able to evaporate refrigerant at two significantly different evaporation temperatures to match compartments air temperatures.

This PhD activity focused on the particular refrigeration circuit called sequential dual evaporator (SDE) which operates freezer (FC) and refrigerator (RC) compartments evaporators in an alternative mode with single compressor. Hence only one evaporator is cooled at the time and high evaporation temperature and COP can be achieved during RC operation. The principal problem of the SDE system is an extremely large cooling capacity delivered by volumetric compressor and low heat transfer rate at increased RC evaporation temperature.

Two innovative concepts of SDE circuit with variable speed compressor are presented in this work. The first concept employs phase change material in direct contact with visible RC evaporator to accumulate high cooling capacity. PCM then continuously absorbs heat from the RC air by natural convection at very small heat rate which has positive effect on the fresh food preservation. The RC air temperature is much more stable and resistance of the RC to grid power failure is improved.

The second concept implements supplementary loop attached to the freezer liquid line, which by passing through RC PCM can additionally subcool liquid refrigerant and shift load from the FC to RC. Theoretically shifting thermal load to RC improves overall appliance COP.

Both concepts were turned to the appliance prototypes and experimentally tested. Performance of SDE-PCM concept was compared to the performance of the baseline SDE circuit without PCM. The SDE-PCM concept showed significant improvement in the RC COP up to 29% and overall appliance COP was raised by 9%. It was also understood that refrigerant migration and design of condenser play essential role in reaching high efficiency. RC air temperature was stabilized and the RC compressor OFF period was extended from 1 hour to almost 13 hours. The concept with additional subcooling loop didn't confirm expected energy efficiency benefit and suggestions for further studies were drawn.

Wish

I hope this activity was and will be helpful in the research and development of high energy efficient refrigerator-freezer appliances with enhanced functionality and still economic in price.

By the way I can't wait the time to be able to buy one like this in the store.

Acknowledgement

On the first place I want to express my gratitude to Professor Joppolo for the possibility to pursue my studies at the Politecnico di Milano and for his calm and always positive attitude.

Whirlpool Corporation employees represented mainly by Andrea Olivani were always constructive in the discussions and open to the new ideas and I want to thank them for their support.

Advices, corrections and discussions about refrigeration topics with Luca Molinaroli from Politecnico di Milano are also greatly appreciated.

To my parents for their sincere encouragement and support without which this work would hardly became reality.

Big thank goes to my lovely wife Emilia for her continuous presence and love.

Content

Abstract of the work	i
Wish.....	ii
Acknowledgement.....	iii
Content	iv
Nomenclature	vi
1 Motivation.....	1
1.1 Refrigerants phase out in 90's	1
1.2 Two evaporation temperatures domestic refrigeration circuits	4
1.3 Energy efficiency standards for domestic refrigerators.....	10
2 Work objective identification.....	16
2.1 Object of the research	16
2.2 Problem statement	18
2.3 Objective's summary	26
2.4 Methods, tools and temporal sequence of activities	26
3 Concepts of advanced SDE refrigeration circuit	28
3.1 Heat transfer resistances of RC evaporator	28
3.2 RC evaporator with thermal accumulation	37
3.3 Compartments heat load	48
3.4 Refrigerant charge migration.....	54
3.5 Conclusions.....	55
4 Testing SDE circuit with variable speed compressor	58
4.1 Objective of the testing.....	58
4.2 Prototype instrumentation, control and acquisition	58
4.3 Test procedure	61
4.4 Experimental results	61
4.5 Thermodynamic second law analysis	72

4.6	Conclusions.....	74
5	Steady-state refrigeration circuit simulation.....	77
5.1	Model description	78
5.2	Results of the simulation	80
5.3	Second law analysis	82
5.4	Conclusions.....	85
6	Experimental testing of conceptual prototypes.....	86
6.1	Objective of the experimental testing	86
6.2	Prototype built	87
6.3	Testing equipment	90
6.4	Instrumentation	93
6.5	Experimental refrigerant pump out optimization	94
6.6	Testing procedure for energy consumption tests	100
6.7	Prototype 1 SDE-PCM experimental results	102
6.8	Heat transfer analysis.....	113
6.9	Prototype 2 (SDE-PCM-SC) experimental results	116
7	Conclusions and contribution	120
7.1	Preliminary testing.....	120
7.2	Concepts of SDE circuit with PCM.....	120
7.3	Experimental results	122
7.4	Further work	123
8	Bibliography	124
9	Appendix I.....	128
10	Appendix II	131
11	Appendix III.....	132

Nomenclature

Symbols

A	Surface area
CFC	Chlorofluorocarbon
COP	Coefficient of performance
c_p	Specific thermal capacity
DAQ	Data Acquisition
DOE	Department of energy in US
E	Emissive power, Energy
EC	European commission
EEI	Energy efficiency index
FC	Freezer compartment
FC-CV	FC suction line check valve
G	Irradiation
g	Gravitational acceleration
GWP	Global warming potential
H	Characteristic height
h	Enthalpy, convective heat transfer coefficient
HFC	Hydrofluorocarbon
J	Surface radiosity
k	Thermal conductivity
L-M	Lorenz-Meutzner cycle
N	Number of
NTC	Negative temperature coefficient
\dot{m}	Mass flow
OFF	Switched OFF
ON	Switched ON
P	Power
P/O	Refrigerant pump out phase
PCM	Phase change material
p-h	Pressure-enthalpy diagram
Q	Heat transfer rate
R	Thermal resistance

RC	Refrigerator compartment
RD	Relative difference
RPM	Crank shaft rotations per minute
SDE	Sequential dual evaporator
SEDS	Single evaporator dual source
SLHEX	Suction line heat exchanger
T	Temperature
t	Time
T-s	Temperature-entropy diagram
UA	Global heat transfer coefficient
V	Swept volume
VIP	Vacuum insulation panel
x	RC heat load ratio
pi	Pressure ratio

Greek Letters

ε	Emissivity
ρ	Density, reflectivity
β	Coefficient of thermal expansion
μ	Dynamic viscosity
ϑ	Efficiency

Subscripts/Superscripts

air	Air
amb	Ambient
aux	Auxiliary
comp	Compressor
con	Conduction
cond	Condenser, condensing
cor	Corrected
cyl	Cylinder
disch	Discharge
electric	Electric
evap	Evaporator, evaporation
ext	External
filter	Filter/dryer
int	Internal
is	Isentropic
rad	Radiation
ref	Refrigerant
removed	Removed
SC	Subcooled liquid
SH	Superheat
shell	Compressor shell
suction	Compressor suction condition
vol	Volumetric
wall	Wall

1 Motivation

Cold appliances consume approximately 15% of residential electricity consumption in EU which accounts for approximately 122 TWh/year. Refrigerators energy efficiency improved tremendously by 45% between years 1990 and 2005 and despite the population growth in EU, the absolute energy consumption of domestic cold appliances in 2007 was 15% lower than in 1990. (Bertoldi, et al., 2009) However it is still technically and economically feasible to improve energy efficiency and to save additional energy sources by developing and employing advanced technologies and strengthening energy efficiency standards in the domestic refrigeration field.

The most popular cold appliances on the EU market are the combined refrigerator-freezer appliances (2 doors appliances) which are composed of two compartments with very different temperatures; freezer compartment (FC) operating at -18°C and refrigerator compartment (RC) at 4°C . They account for more than 60% share of cold appliance sales. (Bertoldi, et al., 2009) Therefore I focused my attention on the energy improvements of combined refrigerator-freezer appliances.

Many of the marketed refrigerator-freezers employ vapor compression refrigeration circuit where both RC and FC are cooled by the same evaporation temperature. The temperature lift for cooling RC compartment is thus extremely high and causes RC operation thermodynamically inefficient which can be directly observed in the p-h diagram,

Figure 1.1.

Thus I consider circuit ability to evaporate refrigerant at two different temperatures as a basic prerequisite to make refrigerator-freezer appliance energy efficient. This condition has significantly narrowed the choice of refrigeration circuit layouts for refrigerator-freezer to be analyzed.

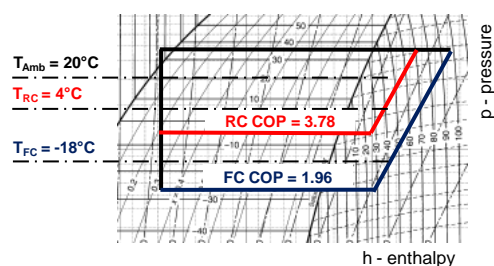


Figure 1.1 Advantage of two evaporation temperatures in refrigerator-freezer

1.1 Refrigerants phase out in 90's

Enforcing Montreal protocol in late 80's to phase out ozone layer depleting CFC refrigerants such as R12 was a starting point for searching alternative refrigerants

and in the same time also assessing new layouts of vapor compression refrigeration circuits for domestic refrigerators.

1.1.1 Alternative refrigerants

In 90's the most promising future refrigerants seemed to be zeotropic mixtures of refrigerants which exhibit temperature glide during the evaporation and condensation process. Positive impact on the thermodynamic efficiency comes from possibility to more closely match air and refrigerant phase changing temperatures. The most favorable refrigerator heat exchangers' arrangement is counter-flow. Area in the T-s (temperature – entropy) diagram between temperature curves of two heat exchanging fluids represents thermodynamic loss of the heat exchanger. Figure 1.2 shows heat exchanging process in the condenser (red lines) and in the evaporator (blue lines) with pure and mixture refrigerants with temperature glide.

It's clearly possible to see that the area representing is larger for pure refrigerants than for mixtures.

Commonly used refrigeration circuit arrangement in refrigerator-freezer before 1990 was a single evaporator circuit shown in Figure 1.3. The evaporator directly served FC and cold air was led through ducts to the RC as well. However in this solution low evaporation temperature used for cooling RC and air exchange between FC and RC have negative impact on energy efficiency and low relative humidity in the RC.

Experimental and numerical results of the tests with refrigerant mixtures in single evaporator appliances are reported in the Table 1.1. Mixtures were tested as drop-in substitutes with unchanged

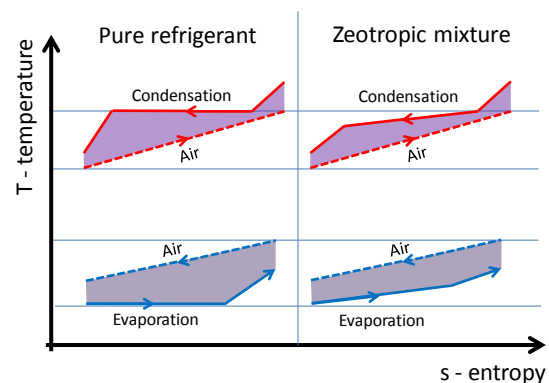


Figure 1.2 Visualization of heat exchangers thermodynamic loss for pure and zeotropic refrigerants in T-s diagram

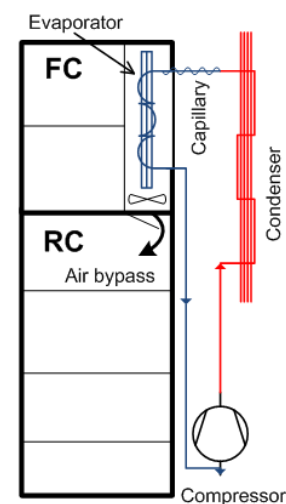


Figure 1.3 Single evaporator circuit in refrigerator-freezer

Refrigerant	Energy saving vs R12	Reference
R22/R142b	3% (simulation)	(Jung D.S., 1991)
R22(13%)/R152A	4%	(Kim K., 1993)
R290/R600	6%	(Liu, et al., 1994)
R600a	11%	(Kim, et al., 1998)

Table 1.1 Energy saving of single evaporator refrigerator with various refrigerant mixtures and pure R600s as a drop-in substitutes for R12

hardware except for the capillary tubes. Only modest up to 6% energy savings were found. Even though zeotropic mixtures are theoretically more suitable for heat exchanging processes in the domestic refrigerators their application nowadays is negligible.

On the other hand refrigeration circuit with pure isobutane R600a as a drop-in substitute for R12 systems showed even larger improvement of around 11% measured experimentally (Kim, et al., 1998). Enhancement is mainly caused by lower working pressures and lower compressor discharge temperature for R600a system. Volumetric refrigeration capacity is approximately half of that of R12. Therefore compressor volumetric flow has to be doubled to obtain same refrigeration capacity. The advantage is that in general bigger compressors are more efficient and probably 11% improvement includes this effect. R600a refrigerant charge can be reduced to approximately half versus R12 system. Isobutane is a hydrocarbon hence it's extremely flammable and only mass charges below 150g are allowed by legislation in EU.

In the currently manufactured domestic refrigerators CFC refrigerants were completely substituted predominantly by natural refrigerant isobutane, R600a in EU. In US because of strict legislation for flammable substances and also bigger appliances the most used is synthetic hydrofluorocarbons (HFC) R134a.

In the last few years policy discussions were started also about phasing out HFCs with high global warming potential (GWP). In addition new metric GWP₂₀ was proposed to evaluate GWP on the basis of 20 years instead of 100 years standard which makes the GWP difference between HFC and natural refrigerants even more noticeable. (Öko-Recherche, 2011) Policy discussions and potential new metric favor isobutane as a suitable long term future refrigerant in domestic refrigerators.

Significant energy efficiency potential, negligible environmental impact and future prospective of R600a were strong reasons to work with isobutane as a working fluid throughout my PhD work. On the other side flammability and

explosion danger and limited availability of dedicated refrigeration components approved for hydrocarbons were main practical drawbacks of R600a.

1.2 Two evaporation temperatures domestic refrigeration circuits

As a part of the effort to identify alternative refrigerants to phasing out R12 refrigerant also many innovative refrigeration circuits were introduced in 90's. I selected and further discussed only the circuits which have an ability to evaporate refrigerant at two different temperatures and were developed for combined refrigerator-freezer appliances:

- Single evaporator with sequential operation and air dampers
- Dual loop refrigeration circuit
- Two stage circuit with liquid separator
- Bypass two evaporator system
- Sequential dual evaporator circuit

1.2.1 Single evaporator with sequential operation (SEDS)

The simplest solution to allow different evaporation temperatures for RC and FC in the domestic refrigerator-freezer was presented by (Park, et al., 1998). His refrigeration circuit works only with one evaporator serving RC and FC in sequential mode, the circuit is also called single evaporator dual source refrigeration system (SEDS). Single evaporator is placed between FC and RC and air flow switching system with two dampers and two fans distributes cold air either to RC or FC, Figure 1.4. To avoid excessive air mixing between the compartments only one compartment can be cooled at a time. However certain amount of air is still exchanged between RC and FC and negatively impacts humidity level in RC. Solenoid valves after the condenser control refrigerant flow through RC or FC capillary tube and allow different evaporation temperatures for RC and FC operation.

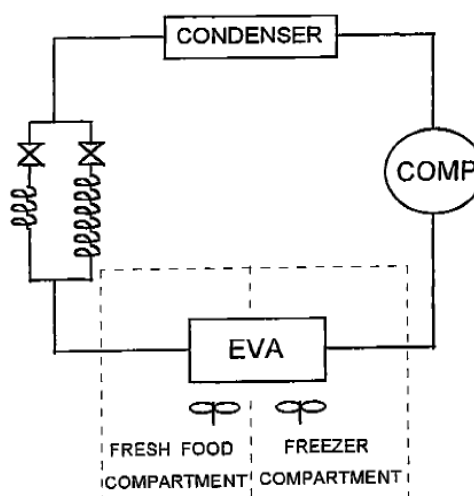


Figure 1.4 Single evaporator circuit with sequential operation in refrigerator-freezer

Experimental results of their refrigerator-freezer showed 17.3% improvement of the total energy consumed. 8.5% comes from compressor isentropic efficiency increase, 3.6% is related to shut off function of solenoid valves to prevent warm refrigerant migration to the evaporator during off periods and 5.2% is associated with more favorable operation conditions during RC cooling period.

If the bi-stable diverter valve with shut off functionality would be used instead of two solenoid valves additional 2.7% energy saving was expected. Related to shut off function preventing refrigerant migration from condenser to evaporator through capillary tubes during compressor off periods also increased requirement for starting torque of the compressor's electric motor should be discussed.

During the RC operation evaporation temperature increased by 13K, hence cooling capacity provided by compressor has increased notably. This is visible on the increased dissipation requirement on the condenser side and higher condensing temperature which decreases improvement of the RC COP, Figure 1.5. Moreover large cooling capacity shortened the RC compressor run time to only about 6% and this increased transient losses.

Numerical and experimental assessment of SEDS with two speed compressor was published by ACRC; (Kelman, et al., 1999) and (Ge, et al., 1999). The idea of two speed compressor was to decrease

cooling capacity during RC operation. The experimental results confirmed earlier simulation analyses, which predicted that achieving maximum energy savings (approx. 15%) would require a two-speed compressor having a high to low speed ratio of 5. (Ge, et al., 1999)

1.2.2 Dual loop refrigeration circuit

The domestic refrigeration system that consists of two completely separate refrigeration circuits is called dual loop system, Figure 1.6. Each circuit is controlling temperature only in one compartment. This means that each circuit can be fully optimized from refrigerant charge and from operation pressures point of view. There are no parasitical issues such as refrigerant mass charge migration or

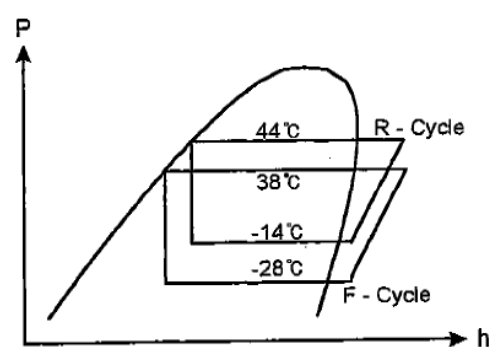


Figure 1.5 RC and FC operation conditions in the SEDS refrigeration cycle in p-h

air circulation between compartments. Dual loop set up theoretically brings considerably high energy consumption improvement.

In reality dual loop system has to use smaller compressors which are usually less efficient than the bigger ones. Moreover, there is a penalty in cost and space requirements to accommodate two separate cycles. Several experimental measurements of dual loop system were performed (Won S., 1994), (Baskin E., 1999), (Gan A., 2000).

Won reported only 4.3% energy saving versus single evaporator system using R12. Energy consumption improvement is extremely small and it is related to poor efficiency of small compressors used during testing. They estimated that small compressors with unchanged efficiency would lead to around 20% energy saving.

Baskin reported energy consumption improvement by 34.9% on the same refrigerator as was tested 10 years before him and 46-49% improvements were stated at that time. This refrigerator however apart from dual refrigeration cycle contained also other major modifications such as; thicker wall insulation, defrost heater modification, electronic temperature controller and condenser integrated in outer steel cabinet.

Gan reported up to 30% energy saving versus single evaporator system depending on the heat load ratio between freezer and food compartment. In addition he evaluated possibility to sub-cool high pressure liquid in refrigeration compartment during the FC operation. The analysis indicated however that indirect mechanical sub-cooling is not a viable alternative to decrease energy consumption.

1.2.3 Two stages circuit with liquid separator

Other system patented by (Jaster, 1990) from General Electric is using two evaporators, liquid separator, two capillary tubes and two stages compressor (or two compressors in series), Figure 1.8. The system was reported to have around 40% energy saving versus single evaporator cycle. The construction complexity

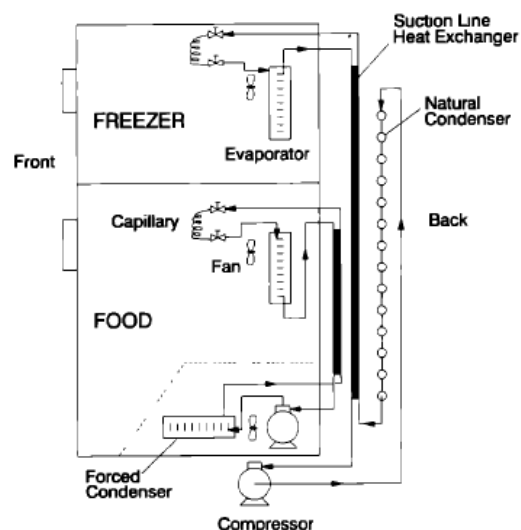


Figure 1.6 Standard dual loop refrigeration circuit in refrigerator-freezer

of the two stages system is comparable to dual loop system, but control complexity is much higher because of second stage compressor which pumps mass flows for RC and FC at once. It saves some tubing and condenser but it requires liquid separator in addition. Two stages system takes all the energy efficiency advantages of dual loop system and in addition decrease compressor work by reducing losses during compression (area A1) and expansion (A2) as it's possible to see in the T-s diagram, Figure 1.7.

There is very little information about performance of this circuit in the open source literature and it's not clear if functional prototype was ever built. The problem with efficiency of small size compressor for RC operation is avoided because second stage compressor pumps RC refrigerant mass flow together with FC mass flow. More complicate situation can occur when only one compartment needs to be cooled.

1.2.4 Bypass two evaporator system

Origin of the bypass two evaporator systems is in refrigeration circuit with separate RC and FC evaporators connected in series also called Lorenz-Meutzner (L-M) cycle. Disadvantage of simple L-M is inability to control separately the temperatures in two compartments. Therefore bypass two evaporator system was developed by adding bypass loop with dedicated second capillary tube to one of the evaporators, in order to add degree of freedom to the control system.

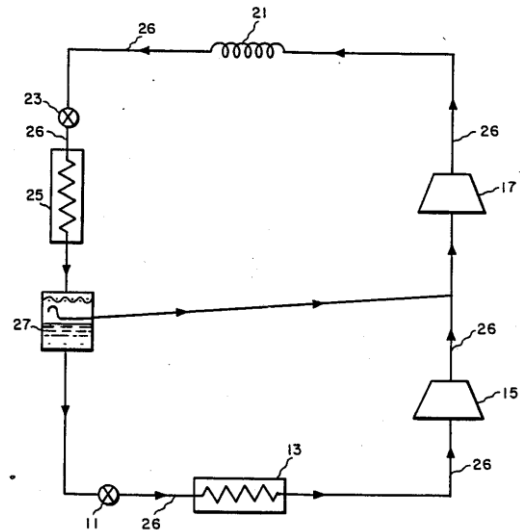


Figure 1.8 Two stages circuit with liquid separator for refrigerator-freezer

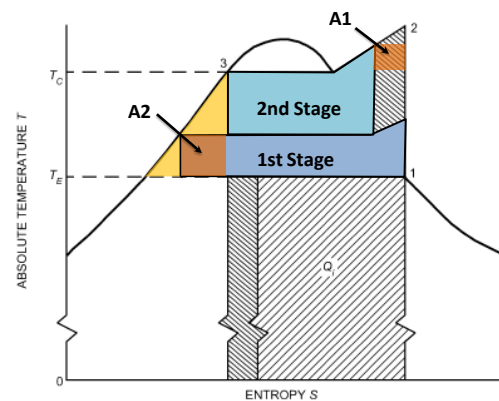


Figure 1.7 Two stage circuit in T-s diagram with indicated compression and expansion thermodynamic losses

Additional loop can pass either through FC or RC evaporator. From energy efficiency point of view optimum circuit design is Figure 1.9 (a). Where FC evaporator is first and RC evaporator is second in series loop and bypass loop passes through RC evaporator only. Thus

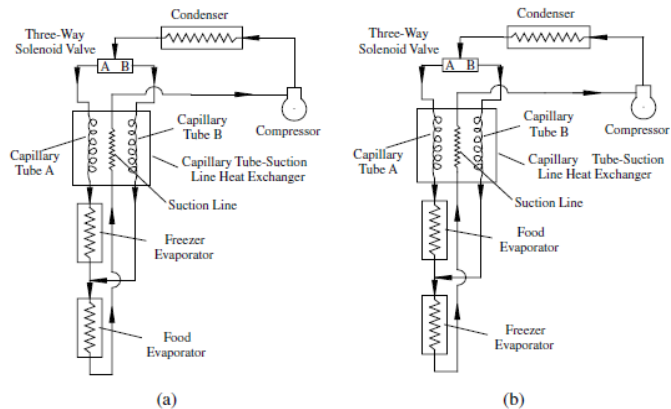


Figure 1.9 Two evaporator bypass refrigeration circuit for domestic refrigerator-freezer (Guoliang, et al., 2004)

RC evaporation temperature could be increased independently from FC operation. However in practice heat load of freezer is usually higher and it needs to be switched ON more often than RC. Hence RC evaporator is bypassed and it's placed right after the capillary tube in series loop, Figure 1.9 (b). During the operation of series loop refrigerant fluid after being partially evaporated in RC evaporator passes also through freezer evaporator and sets limit to evaporation temperature in order not to heat up FC.

Bypass circuit control technique was examined by (Simmons, et al., 1996). The result showed good independent temperature control in each compartment but it also brought a penalty of around 10% in energy consumption versus L-M cycle. Also more complex modified Lorenz-Meutzner (ML-M) cycle with bypass loop was tested by (Simmons, et al., 1996). Bypass circuit had an intercooler between high pressure and low pressure refrigerant to recover unused heat. This set up again showed very good temperature control in compartments and brought smaller penalty to energy saving. If this penalty is subtracted from the net cycle improvement of 12.1% versus single evaporator system than the ML-M cycle with bypass has still a net improvement of 6.5%.

1.2.5 Sequential dual evaporator circuit

Appliance equipped with sequential dual evaporator (SDE) refrigeration circuit contains one compressor and condenser followed by refrigerant flow diverting electro-valve and two evaporators connected in parallel and placed in corresponding compartments, Figure 1.10. The circuit extracts heat from FC and RC in alternating mode, in other words only one evaporator works at the time.

Therefore during RC operation it allows higher evaporation temperature and higher compressor COP. There is no air exchange between two compartments and as the system requires only one compressor it has a considerable cost advantage versus dual loop appliances.

SDE circuit was first time introduced in open literature in 1992 and experimentally tested with R12 and R152a resulting in 2.3% and 6%

energy saving over single evaporator system charged with R12. It was predicted that the circuit would not be willingly accepted by refrigerator manufacturers because of small experimental energy saving, increased system complexity and reduced reliability (Sand, et al., 1992). Opposite became truth when one year later Whirlpool Corporation submitted a patent with several modifications to the SDE circuit (Cur, et al., 1995). Later on experimental tests performed on the prototype with new RC evaporator increased evaporation temperature by 10K and brought improvements in energy consumption of 8.5% in SDE refrigerator charged with isobutane (R600a) versus system with two evaporators in series (Lavanis, et al., 1998). Issues with improper refrigerant charge of the loops and charge migration during ON and OFF cycle were reported.

SDE circuit applied to side-by-side domestic refrigerator appliance gained an energy improvement of 7.8% over the system with evaporators in series. Moreover it was stated that by implementing refrigerant recovery sequence (R/S) between FC and RC operation additional energy saving of 1.8% was achievable (Won Jae, et al., 2011). In this study inverter equipped compressor was utilized and was set to run at 52% cooling capacity during RC operation. More details about impact of compressor speed on RC evaporation temperature were not available.

Another study published by General Electric described experimental results on SDE circuit with PCM placed in three locations FC, RC and also used for sub-cooling during FC operation. They claimed good energy saving potential for RC as its COP was high but overall energy benefit was not visible (Tulapurkar, et al.,

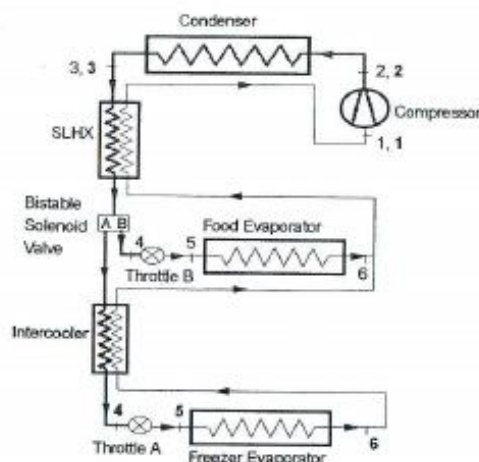


Figure 1.10 Sequential dual evaporator (SDE) circuit for refrigerator-freezer appliance

2010). Very little information was provided about experimental prototype and about compartments operation control strategy.

In all the studies of SDE circuits evaporation temperature during RC operation was reaching values around -20°C if measured by pressure transducer and around -16°C when measured with surface thermocouple at the RC evaporator inlet, which could at the end easily correspond to -20°C real evaporation temperature. Therefore there is still a large potential to increase RC evaporation temperature to values much closer to RC air temperature.

1.2.6 Conclusions

Based on this literature survey, SDE circuit is the strongest candidate to be successfully applied to refrigerator-freezer appliance from energy efficiency potential, food preservation, economic and reliability points of view. Major difficulty of SDE circuit is to address excessive cooling capacity at high RC evaporation temperature. High cooling capacity and small heat transfer to the air was the limiting factor in previous studies.

1.3 Energy efficiency standards for domestic refrigerators

Starting from 70's cold appliance energy efficiency standards and various labeling schemes are in force in majority of industrialized countries and are being implemented also to industrializing economies worldwide, Figure 1.11. Number



Figure 1.11 International use of policy measures in 2006 (Presutto, 2008)

Standard	EU 96	EU 10	EU 12	EU 14	US 01	US 14
Worst energy class (Figure 1.13)	C	A	A+	A+	B	A
Max Energy Standard kWh/year	595	412	329	315	510	408
vs EU 96	0%	-31%	-45%	-47%	-14%	-31%
Energy efficiency index (EEI)	79	55	44	42	68	55

Table 1.2 Comparison of EU and US energy standards for refrigerator-freezer with 72L freezer, 199L refrigerator, energy class A++, stated energy consumption 230 kWh/year

of nations implementing energy efficiency requirements is growing rapidly. The most common policies and measures for cold appliances are labeling and efficiency requirements. Even non-EU European countries are interested in implementation of EU regulations for refrigerators and freezers.

To see performance differences comparison of the different efficiency requirements for cold appliances around the world would be very interesting. However often the standards used to measure the energy consumption and the other parameters are based on different measurements methods which makes comparisons difficult.

I compared at least efficiency standards in EU and US. Legislation in both economies has been updated several times in the past 20 years. The Table 1.2 summarizes the evolution of energy efficiency standards and shows the number difference between EU and US limits. Calculation was done for one selected refrigerator-freezer appliance with internal net storage volumes 72L and 199L of freezer and refrigerator respectively and it is based on the European commission directive and (DOE, 2009) (DOE, 2005) (European Commission, 2010). The appliance is available on the EU market, rated in A++ energy class and consumes 230kWh/year. From the comparison it's possible to see that EU legislation is little bit more demanding than in US. For example: from the year 2014 new appliances will have to have energy efficiency index (EEI) lower than 42 in EU and in US it can be still as high as 55 EEI. Between 1996 and 2014 domestic refrigerator-freezers had to improve their energy efficiency by almost 50% in order to be accepted on the EU market.

1.3.1 Technical studies for European Commission and DOE

To support such a strengthening of the energy efficiency standards for domestic cold appliances, European Commission (EC) and US Department of energy

(DOE) had worked extensively on the assessment of energy efficient technologies applied to domestic refrigerators.

In 2007 EC carried out a preparatory study to analyze the technical, environmental and economic aspects of refrigerating appliances typically used in household in order to correctly propose future energy consumption standards. In the technical part several technologies were analyzed and their impact on the overall energy consumption was estimated. The technologies were divided into two main categories; available and not yet available. List of the most significant technologies is presented in the Table 1.3. Promising technologies with largest energy efficiency improvements are; vacuum insulation panels (VIP) and variable speed high efficient compressors with efficiency enhancements close to 15%.

However, European committee of domestic equipment manufacturers stated that in EU study not enough attention was given to the calculation of cross-technology effects between the three fundamental technology options (insulation increase, compressor efficiency and heat exchanger improvements). By other words refrigerator cabinet with increased insulation requires less cooling capacity and smaller compressors, but these smaller compressors are generally less efficient.

EU study mentioned also sequential dual evaporator system and cited work of Radermacher's team and 8.5% energy efficiency improvement (Lavanis, et al., 1998). But the results of experiments performed

Technologies in 2005-2009
Gas-filled panels
Vacuum insulated panels
Insulation foam thickness increase
Variable anti-sweat heating
Adaptive defrost systems
HEX size increase
Phase change material usage
Cycles with bistable solenoid valve
Non-azeotropic refrigerant mixtures (Lorentz-Meutzner cycle)
Two compressors systems
High efficiency reciprocating compressor
Two speed compressor
Variable speed compressor
- reciprocating
- rotary
- linear
Fully vacuum insulated compartment
CO2 compressor
Oil free compressor
More isothermal compressors
Aerogels as insulating materials
Integration of alternative cooling technologies TE sub-cooling

Table 1.3 Technologies considered for improving domestic refrigerator efficiency of EC and DOE studies (in red are not yet available technologies)

during COLD-II study showed limited potential of this circuit for overall energy saving and thus it was not considered further in the study.

In 2009 also Department of Energy in US carried out similar study with the same objective. To assess potential energy saving of different technology options they used computer simulation program ERA which was developed based on the experimental results.

Regarding SDE refrigeration circuit DOE is also skeptic about the application in the future because of extensive patent literature discussing dual-evaporator systems and its modifications which limits further spreading of the technology. Moreover DOE was not aware of any commercialized refrigerators using SDE approach at the time of the study. Therefore this technology was screened out from the assessment.

From EC and DOE studies it's evident that SDE technology is not mature enough to be implemented in refrigerator-freezer in the short term. Further applied research and development is required to bring this technology to the acceptable level.

1.3.2 EU labeling scheme – past and future

According to European Commission directive from January 1994 on all domestic refrigerator appliances on sale have to present “energy label” showed in the Figure 1.12. It's a label which informs customer about energy efficiency of the product he is interested in. Products are divided into categories marked by letters from G till A where A is the most efficient. During the years appliances were getting rapidly more efficient and most of the products occupied the highest class A. Thus further differentiation of A class was essential and was done by adding +. Currently the most efficient appliances hold the label with A+++.

Besides letter marking also numerical index assessing energy efficiency was developed and it's called energy efficiency index (EEI). Calculation of this index is in detail described in the European directive 2010/30/EU, (European Commission, 2010). It takes into consideration several aspects



Figure 1.12 Energy label

such as storage volume, standard temperature of the compartments, appliance climatic class, built-in or self standing and many other parameters. Correspondence of EEI and letter classes is shown in Figure 1.13. On the secondary y-axis is reported also yearly energy consumption

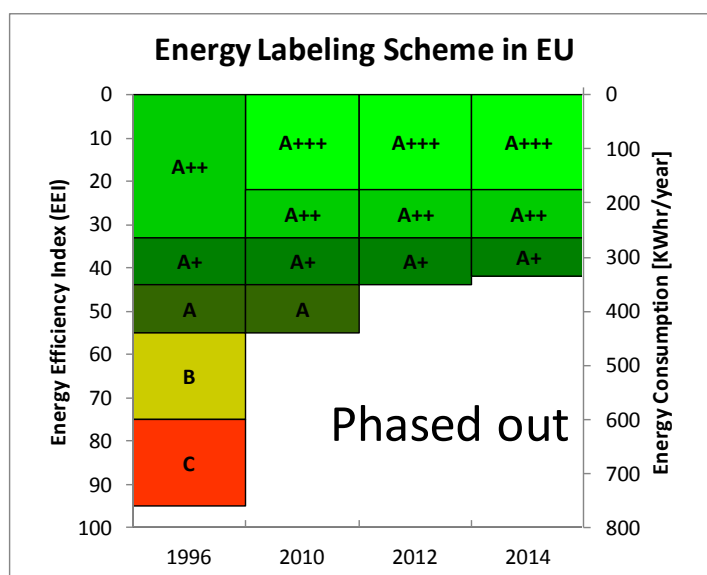


Figure 1.13 Correspondence of energy efficiency index, letter classes in different years and yearly energy consumption for standard size European refrigerator-freezer

of typical European bottom-mount refrigerator-freezer appliance.

For vapor compression type cold appliances (representing today 95% of the market), minimum energy requirements are showed in Figure 1.13. Following energy efficiency requirement roadmap was published in (Bertoldi, et al., 2009):

- From July 2010: The current Class A becomes the new minimum energy performance requirement (EEI<55).
- From July 2012: The current Class A+ becomes the new minimum energy performance requirement (EEI<44).
- From July 2014: Stronger requirements than the current Class A+ becomes the new minimum energy performance requirement (EEI<42).

The best appliances today reach EEI bellow 22 and are in the class A+++. The good question would be how much more the energy efficiency can be improved and for what cost? And how much benefit would it bring to the end user?

Standard size appliance with EEI 22 consumes yearly around 170kWh. If the price is considered to be 0.22 EUR/kWh (approximately Italian residential electricity price) the yearly electricity bill for refrigerator-freezer would be less than 40 EUR showed in Figure 1.14. Compared to A class appliance of the same size we could save up to 60 EUR per year on the electricity bill. If we consider 10 years refrigerator life it's easy to calculate justifiable price difference between A and A+++ class appliances for the end user. But because of already very small

energy consumption the available space for customer EUR saving is shrinking, unless the electricity cost will increase significantly in the future.

Potential for further energy saving based on the current measures is rapidly decreasing.

The energy consumption mentioned on the energy labels refers to laboratory conditions which are usually being very far from real end user conditions.

Real consumption of the refrigerator might be very

different depending mainly on the position of the appliance, frequency of door opening amount of food stored in the refrigerator, room temperature and other aspects of the usage. Therefore in the future while developing new standards it might be more important to focus the attention to real end user energy consumption.

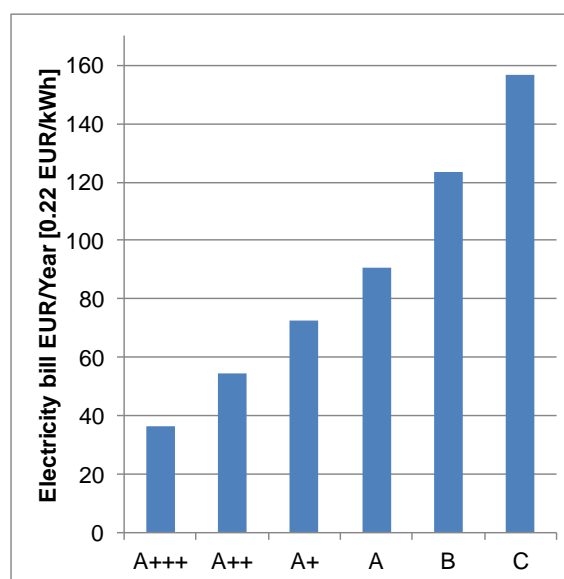


Figure 1.14 Yearly electricity bill for standard size European refrigerator-freezer in various energy classes, electricity price 0.22EUR/kWh

2 Work objective identification

Area of domestic refrigeration is very competitive and innovative field. Most of the manufacturers try to protect their technology knowhow by national and international patents and share minimum possible information with the competition. However academic research activities are frequently supported by domestic refrigerator manufacturers, same as my PhD work. This work was performed in the cooperation with advanced development center of Whirlpool Corporation in Cassinetta di Biandronno in Italy. Therefore also the objective of the PhD thesis was defined in the way to offer space for academic research and in the same time to be useful for further activities of the company.

Despite the fact that Whirlpool Corporation owns a comprehensive intellectual property portfolio and knowledge around sequential dual evaporator circuit (SDE) and vacuum insulation panels (VIP) technologies when I was starting my PhD work in 2010, there was no domestic refrigerator-freezer appliance on the market which would be implementing SDE technology. Open source literature survey performed in the previous chapter 1.2 confirmed real potential for improvements in refrigerator-freezer appliance energy efficiency by employing SDE circuit, but also revealed challenges related to management of large cooling capacity provided by compressor at increased evaporation temperature. Therefore application of SDE circuit to European bottom-mount refrigerator-freezer became the keystone for developing my research.

2.1 Object of the research

The PhD study focuses on the improvements of bottom-mount built in domestic refrigerator-freezer with SDE refrigeration circuit, developed to the prototype stage by Whirlpool Corporation in its previous projects. Appliance has two compartments; on the bottom is located freezer compartment operating at temperature bellow -18°C and on the top refrigeration compartment to preserve fresh food at non freezing temperatures around 5°C . Freezer is used for freezing fresh food and prolonged storage of frozen food. Compartments are insulated from ambient environment by thick layer of polyurethane foam blown by cyclopentane including vacuum insulation panels (VIP) in somewhat unknown positions. The circuit is charged with environmentally friendly but extremely flammable refrigerant, isobutane R600a.

Bottom-mount appliance equipped with sequential dual evaporator refrigeration circuit contains two evaporator loops (refrigeration compartment RC – green and freezer compartment FC – blue) connected in parallel, bi-stable diverting electro-valve, shared condenser and compressor, Figure 2.1. The circuit extracts heat from FC and RC in alternating mode, in other words only one evaporator works at a time. Heat transfer mode for FC evaporator is forced convection and in RC it is natural convection. Natural convection is preferred mode of heat transfer in refrigeration compartment because it prevents fresh food from intense dehumidification.

Whirlpool's previous experimental research on SDE circuit led to the creation of this prototype showed in Figure 2.2 which was the starting point of my research activity. This prototype has shown minimal or no performance improvements versus comparable two evaporators bypass circuit refrigerator-freezer.

SDE circuit refrigerator-freezer prototype was built based on the standard built-in, bottom-mount appliance. Basic external dimensions of the refrigerator-freezer were 1735x540x514mm, height x width x depth. Storage volumes are 209 and 83L for refrigerator and freezer compartments respectively. Low thermal conduction vacuum insulation panels (VIPs) were used in the FC door and sides to decrease FC heat

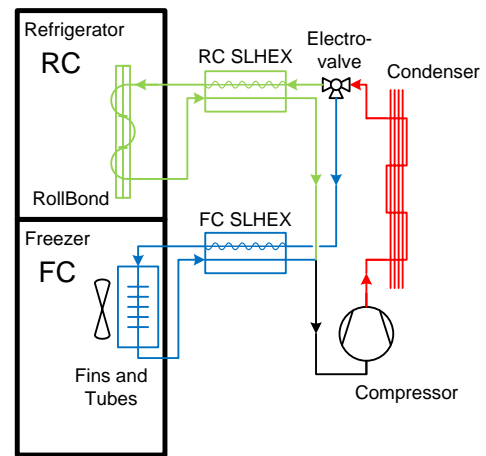


Figure 2.1 SDE circuit in bottom-mount refrigerator-freezer with visible roll-bond evaporator in RC



Figure 2.2 Whirlpool's existing SDE cycle refrigerator-freezer prototype

loads. Visible roll-bond evaporator was clamped to the inner side of cabinet's back wall in the way that both evaporator sides are used for heat transfer, see Figure 2.3. RC contained also a slow running fan which actually didn't have any effect on the heat transfer coefficient during cooling period. Roll-bond evaporator was connected to the compressor through counter flow capillary tube in suction tube heat exchange with the entire length approximately 1.4m completely foamed in to the cabinet's back wall. RC capillary tube was designed to allow 8L/min volume flow of the N₂.

FC evaporator was a fins and tubes type with 50 Al fins and roughly 5.5m length of Al tube arranged in 2 rows with 9 tubes per row. FC Evaporator was "no frost" with forced convection, placed on the back wall of FC and was not modified versus serial production appliance. System was charged by 32g of R600a.

Compressor was Embraco VEMZ9C variable speed type. Speed was adjustable by external frequency modulator in the range from 1600RPM to 4500RPM recommended by manufacturer. The high to low speed ratio was almost 3. Condenser was natural draft with steel tube covered by steel plate with fins cut and bended. The bi-stable electro-valve was placed on the liquid line after the filter/drier. The appliance control board did not exist.



Figure 2.3 Visible roll-bond evaporator in SDE circuit prototype refrigerator-freezer

2.2 Problem statement

The energy efficiency advantage of SDE circuit comes from its ability to evaporate refrigerant at high temperature during RC operation. Operating compressor at high evaporation temperature increases its COP which is visible from the Figure 2.4. Compressor's COP is a ratio of cooling capacity to power consumption of the compressor.

$$COP = \frac{Q_{evap}}{P} \tag{eq 1}$$

The main question is how to increase the evaporation temperature during RC operation? And why other studies didn't succeed to reach evaporation temperatures higher than approximately -20°C? We should analyze what happens at elevated evaporation temperature with power and cooling capacity and why COP is increased.

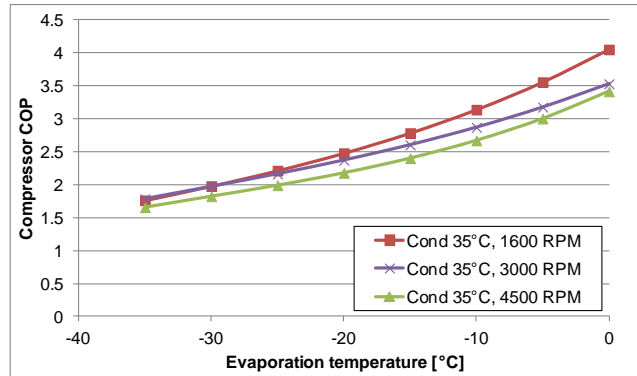


Figure 2.4 Compressor’s COP as function of evaporation temperature at various speeds for compressor VEMZ9C

2.2.1 Cooling capacity

Cooling capacity can be written as refrigerant mass flow (\dot{m}) multiplied by enthalpy difference of exiting ($h_{suction}$) and entering (h_{sc}) refrigerant flow to the evaporator.

$$Q_{evap} = \dot{m}(h_{suction} - h_{sc}) \tag{eq 2}$$

Compressors used in the domestic refrigerators are usually volumetric reciprocating 2 pistons compressors. In the volumetric compressors pumped refrigerant mass flow is calculated according to the following equation:

$$\dot{m} = \rho_{suction} \vartheta_{vol} V_{cyl} N_{cyl} RPM / 60 \tag{eq 3}$$

$\rho_{suction}$ is suction density of the refrigerant at the inlet to the compressor. It is a thermo physical property of refrigerant fluid. For R600a it has a strong sensitivity to suction pressure (evaporation temperature) and weak dependence on suction temperature as can be observed in the Figure 2.5. The density rises in

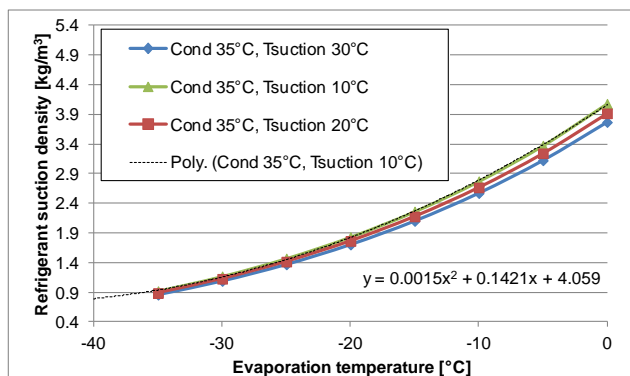


Figure 2.5 R600a refrigerant suction gas density as a function of evaporation and suction temperatures

quadratic manner with evaporation temperature and extremely increases refrigerant mass flow. ϑ_{vol} is compressor's volumetric efficiency and it is usually defined by compressor manufacturer, or can be deduced from compressor data sheet. It depends on the evaporation temperature but the dependence is much weaker than for the suction density which is visible in Figure 2.6.

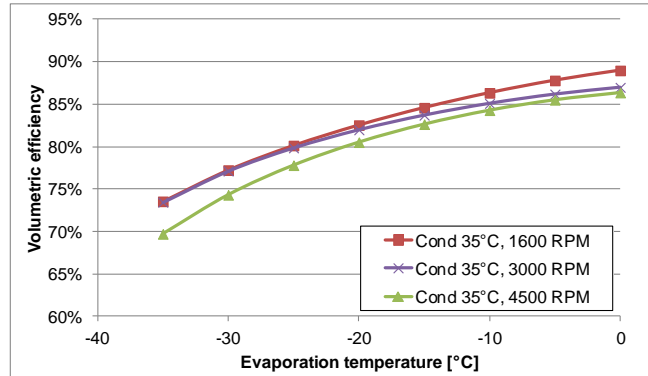


Figure 2.6 Compressors volumetric efficiency as a function of evaporation temperature

Moreover from the eq 3 it is visible that the compressor's crankshaft RPM can linearly modulate refrigerant mass flow.

Based on this analysis refrigerant mass flow is much higher at elevated evaporation temperature which is caused in the first place by higher refrigerant suction density and in the second place by volumetric efficiency. Mass flow can be reduced by smaller swept volume less number of cylinders and lower crankshaft RPM.

Looking to the p-h diagram of R600a Figure 2.7 and keeping sub-cooling degree and superheating temperature constant we can directly assume that enthalpy difference across the evaporator will change only marginally and

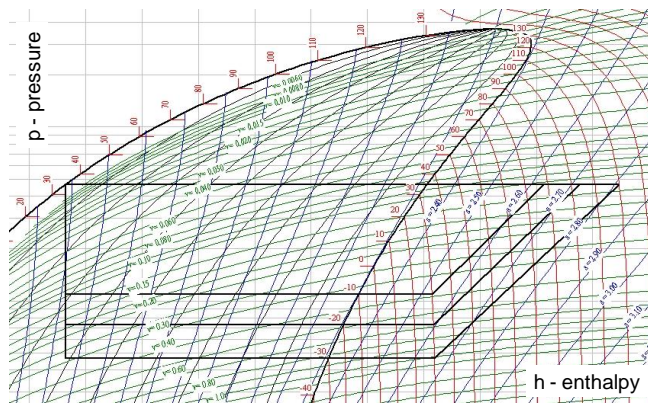


Figure 2.7 p-h diagram of R600a with refrigeration cycles with 3 different evaporation temperatures

therefore can be considered constant. *Understanding this assumption we get to the conclusion that cooling capacity rises with almost the same intensity as suction gas density. This could mislead us also to the conclusion that COP improvement is related to higher cooling capacity which is incorrect hypothesis. In the next I will show why it is wrong by analyzing compressor power impact on the COP.*

2.2.2 Impact of compressor and operating condition on the COP

Performing similar analysis of the compressor power we can write the power in the following form:

$$P = \frac{\dot{m}(h_{is} - h_{suction})}{\vartheta_{is}} \quad \text{eq 4}$$

ϑ_{is} is compressor's isentropic efficiency and it's usually defined by the manufacturer. h_{is} is enthalpy at compressor discharge pressure, defined by isentropic compression of the refrigerant fluid. The numerator of eq 4 is by other words isentropic compression work. It's a minimum work required to compress real gas from suction pressure to discharge pressure. If we substitute eq 2 and eq 4 to eq 1 and eliminate \dot{m} we obtain COP as a function of compressor isentropic efficiency and cycle enthalpies.

$$COP = \vartheta_{is} \frac{(h_{suction} - h_{sub})}{(h_{is} - h_{suction})} \quad \text{eq 5}$$

Interesting is that COP is not dependent on refrigerant mass flow in this theoretical analysis. COP is a function of type of refrigerant, compressor isentropic efficiency and operating condition. Refrigerant was selected to be R600a isobutane.

Isentropic efficiency represents impact of compressor choice on the COP. It is an overall efficiency of the compressor and in reciprocating piston compressors it is mainly defined by losses arising from friction, refrigerant flow, valving system, heat dissipation and in hermetic compressors also electrical motor losses. Selection of correct size of the electric motor is crucial to reach high efficiency of the compressor. Figure 2.9 shows compressor isentropic efficiency as a function of operating condition or in other words operating pressure ratio which also represents load to electric motor. It's possible to see that the compressor VEMZ9C from Embraco was designed to run at pressure ratio of around 10 corresponding to low evaporation temperatures.

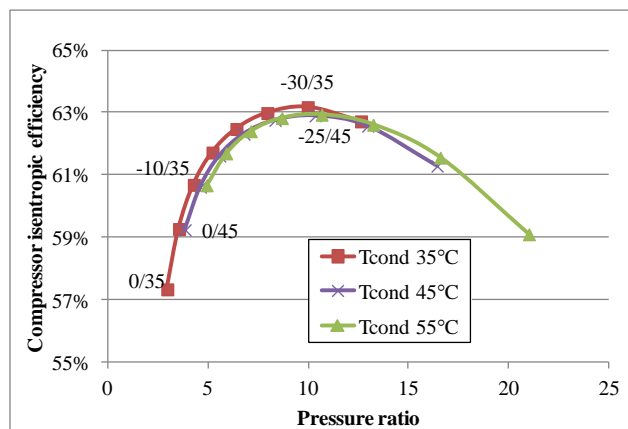


Figure 2.8 Isentropic efficiency as a function of pressure ratio (load) for variable speed compressor VEMZ9C

Operating condition		Isentropic efficiency		Thermodynamic COP		COP
Cond [°C]	Evap [°C]	Value	Change	Value	Change	
35	-30	63.2%	0%	3.05	0%	1.93
	-10	60.7%	-3.9%	5.04	65.3%	3.06
	0	57.3%	-9.2%	6.91	126.6%	3.96

Table 2.1 Impact of compressor's isentropic efficiency and refrigerant fraction on the COP at elevated evaporation temperatures keeping condensing temperature constant

Standard operating condition of the freezer compartment is approximately -30°C to -25°C evaporation and 35°C to 45°C condensing temperatures which is exactly area of maximum isentropic efficiency.

If we want to run the refrigerator compartment at elevated evaporation temperatures between -10°C and 0°C and keep the condensing temperature unchanged our isentropic efficiency can drop to 61% or even 57% from 63%. Only 2.5% decrease in isentropic efficiency is already equal to approximately 4% decrease in COP. All the values are summarized in the Table 2.1.

In sequential dual evaporator system only one compressor is used for operation of both FC and RC. Optimum would be if both compartments could be operated as close as possible to the peak of isentropic efficiency. Of course pressure ratios are different for FC and RC operation and thus compromise in the selection of compressor is required.

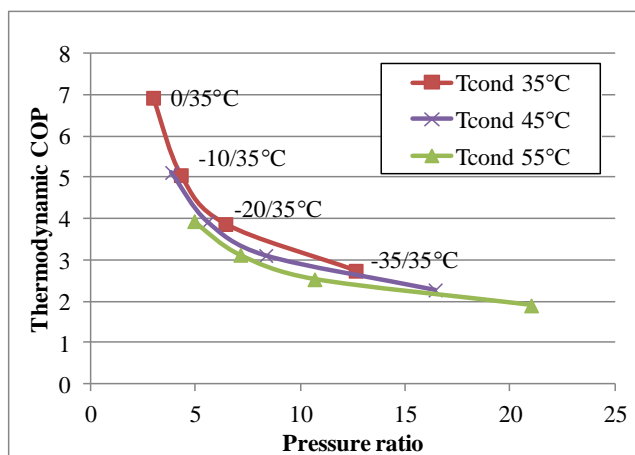


Figure 2.9 Impact of pressure ratio on the refrigerant fraction of the COP for isobutane

The fraction part of the eq 5 characterizes impact of refrigerant fluid on the COP at the selected condition and it's called thermodynamic COP. In the Figure 2.9 we can see how the thermodynamic COP changes with pressure ratio for isobutane. At lower pressure ratios the fraction increases almost exponentially. Comparing increase of the thermodynamic COP for conditions $-30/35$ and $-10/35$ we observe the growth of more than 65%, which is showed also in the Table 2.1.

Thus we can conclude that lower pressure ratio has a strong positive effect on the COP which is significantly higher than the penalty caused by isentropic efficiency at low pressure ratio. If possible it's wise to select compressor in the way that high isentropic efficiency is available at both FC and RC operating conditions.

2.2.3 Evaporation temperature manipulation

In the previous chapter I showed that elevated evaporation temperature is a basic requirement to reach high COP. Also I demonstrated that cooling capacity provided by the compressor is strongly dependent on the evaporation temperature and it increases in quadratic manner with increasing evaporation temperature.

In the following I illustrate that evaporation temperature is dependent on the balance between cooling capacity provided by the compressor and heat transfer rate to the evaporating liquid refrigerant in the evaporator. I focus my attention only to the RC evaporator and write steady-state energy balance:

$$Q_{evap}(T_{evap}, \vartheta_{vol} V_{cyl} N_{cyl}, RPM) = UA_{RC\ evap}(T_{RC} - T_{evap}) \quad \text{eq 6}$$

Where:

- T_{evap} is evaporation temperature
- T_{RC} is temperature in RC compartment
- $UA_{RC\ evap}$ is RC evaporator global heat transfer coefficient between evaporating liquid and RC air temperature

We can solve the equation by graphical method. I plotted in the graph separately left and right side of the equation as a function of evaporation temperature. Intersections of the curves determine the resulting evaporation temperature.

As discussed above the cooling capacity can be nicely modulated by size of the compressor or RPM of the crankshaft. Compressor VEMZ9C is a variable speed type with modulation range from 1600RPM till 4500RPM. In the Figure 2.10 I have displayed two cooling capacity curves corresponding to 3000RPM and 1600RPM and 35°C condensing temperature.

Other two curves are representing heat transfer rate of the evaporator at two different $UA_{RC\ evap}$ coefficients. The UA value is assumed to be constant over the range of evaporation temperatures for each curve (red $UA = 3.8WK^{-1}$ and purple $UA = 8WK^{-1}$). In reality UA value is not constant, it can be subdivided into area of heat exchange A and overall heat transfer coefficient U, where U is dependent on parameters such as refrigerant mass flow, shape of the evaporator and tubes, material of evaporator, evaporation temperature and other.

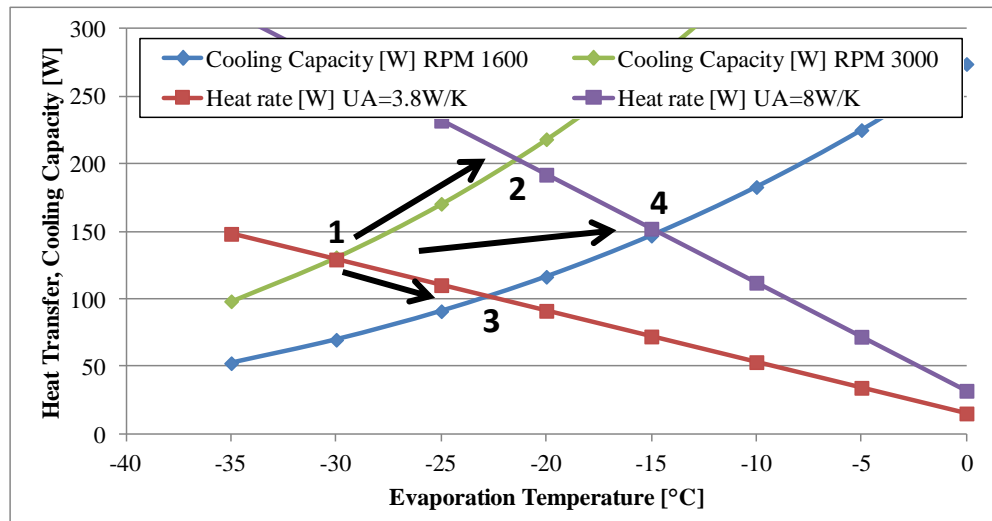


Figure 2.10 Solution of evaporator's steady-state energy balance by plotting compressor cooling capacity and evaporator heat transfer rate as a function of T_{evap} (red line $UA = 3.8\text{W/K}$ and purple line $UA = 8\text{W/K}$)

Based on the results in Figure 2.10 there are three main approaches to increase evaporation temperature in the refrigeration cycle:

- Increase the heat transfer rate to the evaporating fluid
- Decrease cooling capacity provided by compressor
- Combination of the two approaches mentioned higher

The intersection points of the curves are marked with numbers from one to four. Point 1 is a starting point when compressor is running at nominal speed 3000RPM and heat transfer to the evaporator is governed by natural convection with UA value around 3.8W/K . The RC evaporation temperature is equal to approximately -30°C which is very low and close to the evaporation temperature during FC operation. Heat absorbed by refrigerant from RC is equal to 125W .

2.2.3.1 $UA_{RC\text{ evap}}$ increase

If we pass from natural convection to forced convection as it was used in (Won Jae, et al., 2011) our heat transfer coefficient can double or even triple. Coming back to Figure 2.10, with more than double UA value (purple line) we move on the green line to the new intersection point number 2 with purple curve. Evaporation temperature grows by 8K to the new value of 22°C . Potentially the COP can rise from 2 to 2.4 (+20%) according to the Figure 2.4 if we keep constant condensing temperature. The rate of heat removal from the RC increases to 200W . This is a huge growth of cooling capacity by approximately 60% and the heat absorbed by refrigerant in RC needs to be also dissipated on the

condenser side which can have an impact on the increasing condensing temperature. Larger heat removal from RC decreases the compressor run time and in the same time it also raises compressor ON/OFF cycling frequency and thus increases transient losses. Both increased condensing temperature and transient losses place penalty on the potential COP growth. In addition capillary tube has to be modified in order to accommodate higher refrigerant mass flow rate.

2.2.3.2 Compressor RPM decrease

On the other side if we decide to decrease compressor RPM to minimum 1600 instead of increasing UA value we move from point 1 to point 3 on the red line. The evaporation temperature theoretically grows to -23°C by 7K and the heat removal rate decreases to approximately 100W. In theory the COP could raise from 2 to almost 2.4 same as in the previous case. In addition decreased heat dissipation requirements on the condenser side can lower the condensing temperature and hence further improve COP. Small cooling capacity also means that compressor run time increases and ON/OFF cycle period length extends and has a positive impact on the transient losses.

Reducing compressor RPM is a better choice versus modifications on the heat transfer side, because of no penalty from higher condensing temperature and transient losses. Disadvantage of this approach is limited minimum RPM of the compressor defined by manufacturer. Choosing a smaller compressor could lead to further enhancement of the evaporation temperature with risk of smaller compressor's isentropic efficiency. New generation of linear piston domestic refrigeration compressors with modulation capabilities almost from 0% to 100% is entering the market but the technology is not yet widely available.

2.2.3.3 Combination of both

Obviously the combination of low compressor RPM and high evaporator UA brings the highest potential for improving COP and overall refrigerator efficiency. It means to move in the Figure 2.10 from point 1 to point 4 and increase evaporation temperature by 15K to -15°C and COP from 2 to 2.8 (+40%). The heat removed from RC is only slightly higher than in the point 1, thus only minor changes are expected to the ON/OFF cycle period length and condensing temperature.

2.3 Objective's summary

I have a sequential dual evaporator cycle in the refrigerator-freezer domestic appliance and I want to increase RC evaporation temperature as high as possible to improve RC compressor COP and thus also overall appliance energy consumption.

I showed that evaporation temperature can be raised by decreasing compressor's cooling capacity and/or increasing heat transfer rate to the RC evaporator. Combination of both approaches is required to bring significant (+40%) improvement to RC COP. In addition I want to keep natural convection as a preferred heat transfer mode in the RC. Thus the main question is:

- ***How do I increase in a clever way heat transfer rate to the evaporating refrigerant liquid and still keep natural convection heat transfer mode to RC air?***

There is also the second question which appears after RC evaporation temperature is increased. It is related to the impact on the overall appliance energy efficiency:

- ***How RC evaporation temperature impacts overall refrigerator-freezer appliance COP?***

The PhD activity offered answers to these principal questions and it formed many other questions which should be answered in the future studies.

2.4 Methods, tools and temporal sequence of activities

In order to provide scientific answers to the objective questions I performed theoretical analysis of the problem and proposed conceptual solutions to the problems. During this analysis I developed and used simple numerical models for refrigeration circuit components and system. I already showed part of the analysis which led me to the problem definition. In the next chapter I demonstrate conceptual solutions to the problem.

Afterward I carried out experimental campaign on the existing Whirlpool's SDE refrigerator-freezer appliance prototype to get a feeling about testing domestic refrigerators and to understand experimentally impact of compressor speed on the evaporation temperature. Later on I used preliminary experimental results to develop steady-state refrigeration circuit model to closer predict energy efficiency improvements of the proposed concepts.

In the following step together with Whirlpool model shop I built two refrigerator-freezer prototypes implementing conceptual solutions. I instrumented the prototypes with thermocouples and pressure transducers and made modifications to the control and acquisition hardware to be able to operate the prototypes. I run simplified energy consumption tests in the environmental chambers to verify concepts functionality and energy saving potential. In the last step I performed analysis of measured data and I drew the conclusions and suggestions for further development of the concepts.

3 Concepts of advanced SDE refrigeration circuit

In this chapter I present conceptual solutions how to increase COP of refrigerator-freezer appliance with SDE circuit without passing to forced convection heat transfer in the refrigeration compartment. I show how the application of phase change material in contact with evaporator can increase RC evaporation temperature and RC COP.

I also analyzed the impact of RC COP on the overall appliance COP and energy consumption. Based on the COPs of each SDE circuit loop and the RC heat load ratio I evaluated the dependence of overall appliance COP. I proposed concept to shift load from FC to RC by mechanical sub-cooling using PCM in the RC to improve overall appliance COP.

In the first part of the chapter I performed basic heat transfer resistance analysis of RC roll-bond evaporator and identified the bottom neck of the evaporator heat transfer.

3.1 Heat transfer resistances of RC evaporator

RC evaporator is a visible roll-bond evaporator. Roll-bond evaporator is made of two aluminum plates which are bonded at large part of their surface. Not bonded surface area creates channels which are inflated by high pressure gas during production process. One side of evaporator thus includes puffed up channels and is not completely flat. Even if the sides of roll-bond evaporator are not the same I assume the area to be equal for simplification of the calculations. Visible evaporator means that the evaporator plate is placed directly inside the RC cavity in parallel with back wall inner liner preserving roughly 2 cm

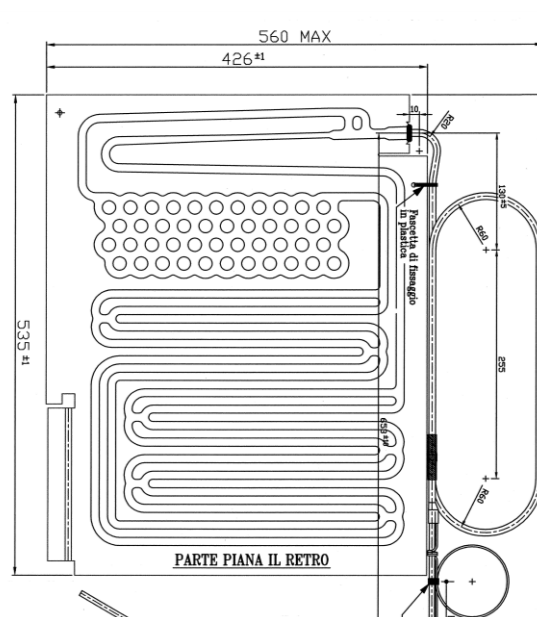


Figure 3.1 Basic sketch of visible roll-bond evaporator for refrigeration compartment

		(Hermes, et al., 2008)	Whirlpool's prototype	Unit
Area external	A_{ext}	0.288	0.456	m ²
Area internal	A_{int}	0.180	0.211	m ²
Evaporator height	H	0.481	0.535	m
Channel internal diameter	d_1	0.013	0.0055 ²	m
Channel external diameter	d_2	0.016 ¹	0.0085	m
Channel length	L	4.4	2x6.12	m
Distance from the wall	S	0.020 ¹	0.020	m
Air channel ratio	S/H	0.042	0.037	-
Refrigerant		R134a	Isobutane	-

Table 3.1 Basic dimensions of the roll-bond evaporators used in the study of Hermes (Hermes, et al., 2008) and in Whirlpool's prototype; ¹ estimated – value not mentioned in the text; ² hydraulic diameter

gap between the wall and the evaporator. In Figure 3.1 is presented sketch of the roll-bond evaporator used in Whirlpool's prototype. Basic dimensions are 42.6x53.5cm (one side area approx. 0.23m²) and further dimensions are reported in the Table 3.1.

As the RC evaporator is visible it decreases refrigerator internal volume by around 6L and thus also indirectly the European energy efficiency index (EEI) which is based on the net storage volume. The appliance with 72L freezer and 199L refrigerator storage volume and consuming 230kWh/year falls into the energy class A++ with EEI 30.7, the 6L lower RC volume increases marginally EEI to 31 and still preserves the energy class of the appliance.

On the other hand both sides (front and back) of the evaporator are functional surfaces for heat transfer to the RC air and also there is no additional thermal resistance of inner liner conduction as it's in the case of foamed in evaporator. Thus the global heat transfer coefficient of the evaporator is improved. Moving the evaporator out of the foam has also a positive impact on the increased thermal resistance of the refrigerator back wall. Theoretically visible evaporator is more efficient solution than foamed in evaporator. This was the reason why Whirlpool implemented it to the prototype.

I used analogy with electric circuit to model heat transfer process in the RC evaporator. As both walls of the evaporator are functional the heat transfer circuit has two parallel branches, Figure 3.2 Heat transfer circuit between evaporating refrigerant and RC air. I split overall evaporator heat transfer resistance into two main elements, air and evaporator structure resistance. The reason for this division

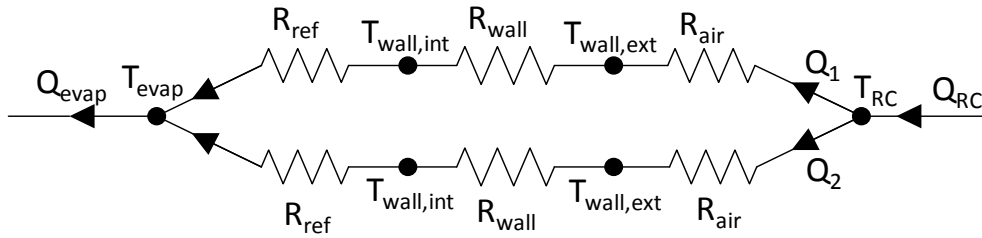


Figure 3.2 Heat transfer circuit between evaporating refrigerant and RC air

is ability to measure evaporator surface temperature and evaluate the two resistances in the future experiments with relatively simple thermocouple equipment.

3.1.1 Analysis of similar roll-bond experimentation

Similar visible roll-bond evaporator was analyzed numerically and experimentally by group of Hermes (Hermes, et al., 2008), Figure 3.3. Described numerical simulation is problematic to be reproduced because it's a computationally heavy first principle distributed mathematical model which included refrigerant flow model, 2D heat diffusion model in the evaporator plate and heat transfer to the refrigeration cabinet. However the interesting part of the paper are the experimental results because there are available all the necessary data to calculate principle heat transfer resistances of the evaporator as described in Figure 3.2. Basic dimensions of the evaporator are reported in the Table 3.1 and experimental data with calculated thermal resistances are reported in

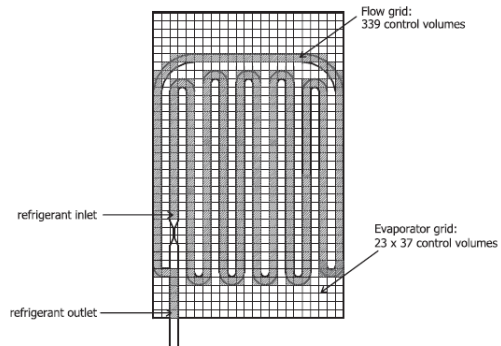


Figure 3.3 Roll-bond evaporator in the study of Hermes (Hermes, et al., 2008) with mesh

Table 3.2. Refrigerant R134a was used in experimental testing of Hermes.

Based on the experimentally measured temperatures and heat transfer rates results I have calculated heat transfer thermal resistances, by using following equations:

$$Q_1 = Q_2 \quad \text{eq 7}$$

$$Q_{evap} = Q_1 + Q_2 = Q_{RC} \quad \text{eq 8}$$

$$R_{air} = \frac{(T_{RC} - T_{wall,ext})}{Q_1} \quad \text{eq 9}$$

$$R_{wall} + R_{ref} = \frac{(T_{wall,ext} - T_{ref})}{Q_1} \quad \text{eq 10}$$

$$R_{wall} = \frac{\ln\left(\frac{d_2}{d_1}\right)}{\pi L k_{Al}} \quad \text{eq 11}$$

I assumed that heat transfer rates in both branches are equal to each other, eq 7 and eq 8 therefore also all the thermal resistances are mirrored. In reality mainly the air heat transfer resistance R_{air} might be different for each branch because of protruded channels on one side of the evaporator plate which could cause turbulent behavior of the boundary layer. The presence of 2 cm air channel between evaporator and back wall of the refrigerator was assumed and has also an impact on the air thermal resistance.

Evaporator to air thermal resistance was calculated by eq 9. The thermal

Test	Experimentally measured					Calculated			
	p_{evap}	T_{evap}	$T_{wall,ext}$	T_{RC}	Q_{evap}	R_{air}	$R_{ref}+R_{wall}$	R_{wall}	$(R_{ref}+R_{wall})/R_{air}$
	Mpa	°C	°C	°C	W	KW ⁻¹	KW ⁻¹	KW ⁻¹	ratio
#1	0.121	-22.1	-20.5	-3.2	43.7	0.792	0.074	7e-5	9%
#2	0.123	-21.7	-20.2	-4.7	37.6	0.824	0.082	7e-5	10%
#3	0.124	-21.5	-19.9	-3.9	39.8	0.804	0.084	7e-5	10%

Table 3.2 Measured experimental results from (Hermes, et al., 2008) for roll-bond evaporator and calculated heat transfer resistances

resistance of evaporator wall and flow boiling heat transfer resistance were calculated together by equation eq 10, because internal evaporator wall temperature was not measured. Anyhow I have determined the conduction thermal resistance of the evaporator wall based on Fourier's law eq 11, assuming aluminum tube with inner, outer diameter and length (d_1 , d_2 and L respectively) and aluminum thermal conductivity $205 \text{ Wm}^{-1}\text{K}^{-1}$, (Engineeringtoolbox, 2013). Resistance of the aluminum wall is three orders of magnitude smaller than the resistance between evaporating liquid and internal wall and thus could be neglected in the further calculations.

Looking at the calculated resistances R_{air} and R_{ref} I could conclude that R_{air} is approximately ten times higher than R_{ref} . Conduction thermal resistance in the evaporator wall can be neglected. It makes sense to focus on the air side heat transfer to decrease overall evaporator resistance.

3.1.2 Evaporator's air thermal resistance

It's necessary to underline that evaporator to air thermal resistance in this case includes natural convection and the radiation heat transfer to the evaporator surface. I have used solution to the governing equations of laminar boundary layer and three more empirical correlations to estimate natural convection heat transfer coefficient for the Hermes and Whirlpool evaporators. Very much simplified radiation heat transfer was predicted by radiosity method. The results of calculated thermal resistances were compared to the ones determined experimentally in chapter 3.1.1 and the closest matching correlation was selected for further use. To evaluate properties of fluids at different conditions I have implemented well know electronic library of thermodynamic and transport properties of fluids Refprop Version 8 developed by NIST. The library was connected with excel by add-in for convenience to perform calculations.

3.1.2.1 Natural convection

The natural convection heat transfer coefficient correlations can be divided into two main groups; derived from boundary layer governing equations and empirical correlations. Correlations are based on the dimensionless numbers such as Grashof (Gr), Prandtl (Pr), Rayleigh (Ra) and Nusselt (Nu). The numbers have to be evaluated for each determination of the heat transfer coefficient. In the next I made a quick description of the main dimensionless numbers and reported equation to calculate it. Numbers calculated for 3 test conditions of Hermes roll-bond evaporator are reported in the Table 3.3.

Grashof number (Gr) describes ratio between buoyancy and viscous forces acting on the fluid in the presence of thermal gradient. Its value can be used to determine whether boundary layer flow is turbulent or laminar same as Ra. In very viscous fluids the fluid movement is more restricted and natural convection is usually laminar. Grashof number is calculated according to the following equation:

Test	eq 12	eq 12	eq 13	eq 14	eq 19	eq 16	eq 17	eq 18
	Gr_s	Gr_H	Pr	Ra	Nu_s	Nu_1	Nu_2	Nu_3
#1	3.5e+4	4.9e+8	0.73	3.6e+8	3.4	71.1	71.6	89.9
#2	3.2e+4	4.5e+8	0.73	3.2e+8	3.3	69.3	69.9	87.0
#3	3.3e+4	4.6e+8	0.73	3.3e+8	3.3	69.7	70.2	87.6

Table 3.3 Dimensionless numbers for estimating natural heat transfer coefficient for 3 tests performed on the roll-bond evaporator used in the study of Hermes (Hermes, et al., 2008)

$$Gr = \frac{H^3 \rho_{fluid}^2 g \beta (T_{wall} - T_{RC})}{\mu_{fluid}^2} \quad \text{eq 12}$$

Where, H is a characteristic dimension, for evaporator it's the height of the wall in the direction of the natural convection flow. β is coefficient of thermal expansion of the fluid. It's derived from density change of the fluid with temperature at the constant pressure $\beta = -\frac{1}{\rho} \left(\frac{\partial \rho}{\partial T} \right)_p$

Prandtl number (Pr) describes ratio between momentum diffusivity and thermal diffusivity in the working fluid and it's dependent only on the properties and state of the fluid. In the heat transfer problems Prandtl number strongly influence relative growth of the velocity and thermal boundary layer. By other words if $Pr \gg 1$ (such as oils) the momentum boundary layer will be much thicker than the thermal boundary layer. Prandtl number is calculated by following equation:

$$Pr = \frac{c_p \mu}{k} \quad \text{eq 13}$$

Rayleigh number (Ra) is a simple multiplication of Pr and Gr number. It's used to define transition in the natural convection boundary layer from laminar to turbulent flow. Transition to the turbulence flow has a strong effect on the heat transfer and is estimated to happen for $Ra > 10^9$.

$$Ra = PrGr \quad \text{eq 14}$$

Nusselt number (Nu) defines convection to pure conduction heat transfer ratio. Large Nu number means large convection heat transfer coefficient.

$$Nu = \frac{hH}{k} \quad \text{eq 15}$$

Many of the natural heat transfer correlations are based on the Nu. For a given geometry the Nu is a function of position variable and dimensionless numbers Grashof and Prandtl and it defines local heat transfer coefficient. Moreover the average convective heat transfer coefficient can be obtained by integration over the heat transfer surface and getting rid of dependence on the position variable. In the next I introduce four correlations from the literature to calculate average natural convection heat transfer coefficient between evaporator surface and surrounding air. In all the calculations the roll-bond evaporator surface temperature was assumed to be uniform. Properties of air were evaluated at average temperature between evaporator surface and undisturbed air temperatures. All the resulted heat transfer coefficients are reported in the Table 3.4 together with corresponding thermal resistances.

For the vertical surfaces with assumption of laminar flow ($Ra > 10^9$) similarity solution to the governing equations of the boundary layer can be resolved (Incropera, et al., 2007). The resulting average Nusselt number is following and average convection heat transfer coefficient can be derived from the formula:

$$\overline{Nu}_H = \frac{4}{3} \left(\frac{Gr_H}{4} \right)^{1/4} g(Pr) = \frac{\bar{h}H}{k} \quad \text{eq 16}$$

Where $g(Pr)$ is an interpolation formula of the dimension less temperature gradient. Two more empirical correlations were used to determine the same heat transfer coefficient for vertical cold plates (eq 17 from (Incropera, et al., 2007) and eq 18 from (Janssen, et al., 1991). The resulting coefficients are presented in the Table 3.4.

$$\overline{Nu}_H = 0.68 + \frac{0.67 Ra_H^{1/4}}{\left[1 + \left(\frac{0.492}{Pr} \right)^{9/16} \right]^{4/9}} \quad \text{eq 17}$$

$$\overline{Nu}_H = 0.85 Ra_H^{\frac{12 + \log(Ra)}{90}} \quad \text{eq 18}$$

In addition to the described correlations I examined also empirical correlation for natural heat transfer coefficient in the parallel plate channels. If the air channel dimensions (S – plates distance and H – channel height) are selected properly the natural convection is enhanced versus stand alone vertical plate. In our case one plate is considered to be isothermal and the other adiabatic with H/S ratio equal to 24. The equation was taken from (Incropera, et al., 2007).

$$\overline{Nu}_S = \left(\frac{144}{\left(Ra_S \frac{S}{H} \right)^2} + \frac{2.87}{\left(Ra_S \frac{S}{H} \right)^{1/2}} \right)^{-1/2} \quad \text{eq 19}$$

3.1.2.2 Radiation heat transfer

Thermal radiation heat transfer in contrast to convection and conduction doesn't require heat transfer matter because it's transmitted by electromagnetic waves. Radiation heat transfer rate Q_{rad} is represented by radiative interactions occurring at the surface A . It's equal to the difference between the surface radiosity J and irradiation G , Figure 3.4.

$$Q_{rad} = A(J - G) \quad \text{eq 20}$$

Radiosity is defined as a sum of emissive power and reflected irradiance and can be written as:

$$J = E + \rho G \quad \text{eq 21}$$

Where, ρ is reflectivity. Emissive power E can be expressed as a black body emissivity E_b defined by Stefan-Boltzmann law multiplied by surface emissivity ε . In addition reflectivity can be expressed in terms of emissivity $(1-\varepsilon)$ as well. Resulting radiosity expression is

$$J = \varepsilon E_b + (1 - \varepsilon)G \quad \text{eq 22}$$

The only unknown in the eq 22 is the irradiance G which is actually equal to the radiosity of surrounding surfaces multiplied by the view factor. Making an assumption that only two surfaces exchange heat by radiation and both of them are straight equal size surfaces we can consider the view factor to be equal to 1. After these assumptions the problem of radiation heat transfer can be written in the system of two algebraic equations with two unknowns J_1 and J_2 radiosities for each surface. Solving the system and substituting J_1 and J_2 to the eq 20 I obtained radiative heat transfer rate and I could determine radiative heat transfer coefficient h_r . The first surface was considered to be painted aluminum plate with emissivity equal to 0.9

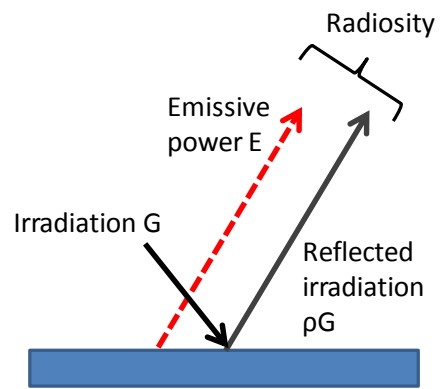


Figure 3.4 Radiosity and irradiation

(Engineeringtoolbox, 2013) and uniform temperature $T_{\text{wall,ext}}$. The second surface imitated inner compartment wall from plastic with emissivity 0.91 (Engineeringtoolbox, 2013) and uniform temperature assumed to be equal to T_{RC} . In reality temperature of internal compartment walls is higher than T_{RC} but this difference was neglected. The resulting radiation heat transfer coefficient is reported in Table 3.4.

From the results in Table 3.4 it's possible to see that all the convection correlations predict heat transfer coefficient in the same range. Correlation based on the air channel eq 19 gives the highest heat transfer coefficient, thus the air channel enhances the heat exchange. For further analysis I have selected the correlation eq 18 because it estimates the highest convective heat transfer from standard correlations. Convective heat transfer is responsible for approximately

Heat transfer coefficients [$\text{Wm}^{-2}\text{K}^{-1}$]						
	Convective				Radiative	
Test	h_s eq 19	h_1 eq 16	h_2 eq 17	h_3 eq 18	h_r	$h_3/(h_r+h_3)$
#1	3.90	3.41	3.44	3.67	3.35	52%
#2	3.79	3.32	3.35	3.55	3.32	52%
#3	3.82	3.35	3.37	3.58	3.35	52%

Thermal resistances [KW^{-1}]						
	Calculated				Measured	
Test	R_{airS}	R_{air1}	R_{air2}	R_{air3}	R_{air}	$R_{\text{air3}}/R_{\text{air}}$
#1	0.96	1.03	1.02	0.99	0.79	125%
#2	0.98	1.04	1.04	1.01	0.82	123%
#3	0.97	1.04	1.03	1.00	0.80	125%

Table 3.4 Evaporator surface heat transfer convective and radiative coefficients and thermal resistances calculated by utilization of natural convection correlations and radiosity method at three test conditions taken from the study of Hermes (Hermes, et al., 2008) and compared to air thermal resistance determined experimentally

52% of overall heat transfer to the evaporator. The remaining 48% of heat rate is caused by radiative heat transfer. This is closely corresponding with predictions of (Hermes, et al., 2008). Comparison of calculated and measured thermal resistances shows that empirical correlations overestimate the measured thermal resistance by approximately 25%. The mismatch can be explained by the accepted assumptions that evaporator surface is completely flat and temperature of the compartment walls equals to air temperature.

3.1.3 Evaporator's wall thermal resistance

As it was already suggested in chapter 3.1.1 the evaporator wall thermal resistance can be estimated by eq 11. It's very difficult to measure directly internal wall temperature during operating the circuit. Therefore the theoretical estimation remained the only option to be utilized in this study.

To calculate roll-bond evaporator wall thermal conduction heat transfer resistance I assumed its geometry to be a simple aluminum tube. This is a very drastic simplification but the resulting resistance is 4 orders of magnitude smaller than air convection resistance Table 3.2. Even though in reality wall conduction resistance is expected to be higher it should not play the major role in the heat transfer to the evaporating liquid.

3.1.4 Flow boiling heat transfer

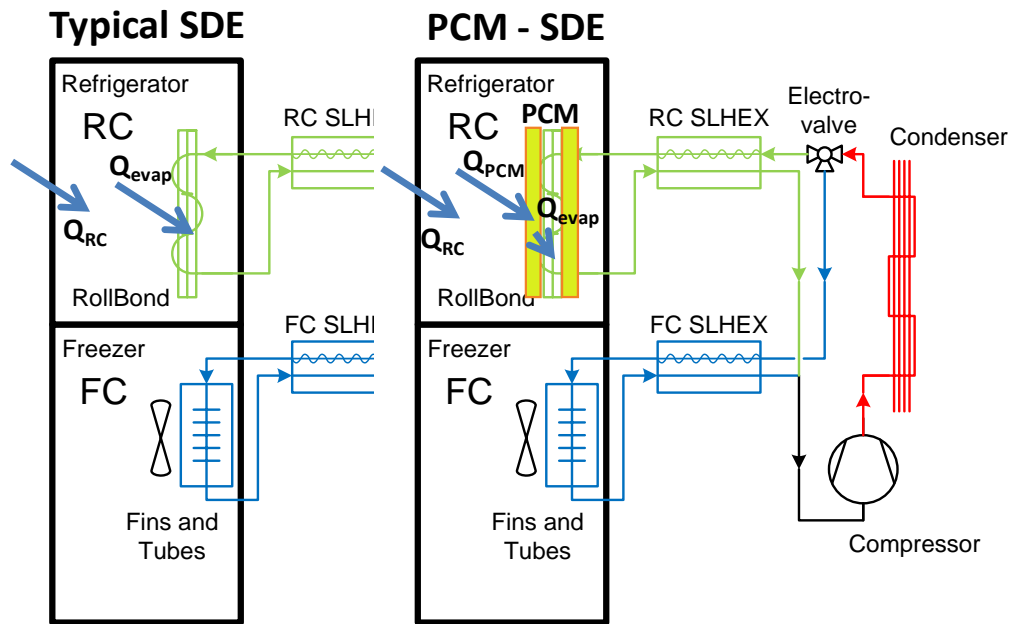
Evaporating flow heat transfer is a complex phenomenon, dependent on many aspects such as flow velocity, vapor quality, flow regime, refrigerant, shape and orientation of the channel and many others. Usually empirical correlations utilizing dimensionless numbers are employed but the differences in results of these correlations can be in some orders of magnitude. Therefore I used resistance determined experimentally in Table 3.2 in my further calculations.

3.2 RC evaporator with thermal accumulation

As I showed in the previous chapter the thermal resistance on the air side causes the highest restriction to the heat transfer rate to the evaporating fluid. In order to allow operation of the RC at the higher evaporation temperature the heat rate to the fluid has to be increased. The idea of my PhD thesis is to use thermal cold storage based on phase change material which is in direct contact with the wall of the roll bond RC evaporator. By this solution the mode of heat transfer on the external surface of the evaporator is changed from air natural convection heat transfer to conduction heat transfer in the phase changing material. Conduction heat transfer coefficient in PCM depends on the material itself and the state of the material. The thermal resistance of PCM can be much lower than for natural convection.

The latent heat thermal capacity of the PCM storage is utilized to provide sufficient heat rate to the evaporating fluid during the PCM charging process (RC evaporator in operation) and thus increases evaporation temperature. Another advantage of the cold thermal accumulator is that it absorbs heat from the refrigeration compartment continuously even when the compressor is OFF eq 24. This allows that the same amount of thermal energy is removed from RC by much lower heat transfer rate, thus natural convection can be preserved as preferred heat transfer mode in the RC. In addition continuous removal of the heat by PCM from RC stabilizes RC temperature. Comparison of heat transfer processes occurring in the typical and PCM SDE refrigerator-freezer are compared in the Figure 3.5.

Cooling capacity of typical domestic refrigerator compressor is always much larger than heat load of the compartment thus surplus energy provided by the compressor during ON period has to be stored. In case of the standard design SDE refrigerator-freezer the surplus thermal energy is accumulated in a sensible heat of the compartment air, shelves and evaporator eq 26. This has a direct effect on the



		Typical SDE		PCM - SDE	
Energy balance		$Q_{RC}t = Q_{evap}t_{ON}$	eq 23	$Q_{RC}t = Q_{PCM}t$	eq 24
				$Q_{PCM}t = Q_{evap}t_{ON}$	eq 25
Energy storage		$E_S = MC_p\Delta T_{RC}$	eq 26	$E_S = ML$	eq 27
Time ON cycle		$t_{ON} = \frac{E_S}{Q_{evap} - Q_{RC}}$			eq 28
Time OFF cycle		$t_{OFF} = \frac{E_S}{Q_{RC}}$			eq 29
Cycling frequency		$f_{RC} = \frac{Q_{RC}(Q_{evap} - Q_{RC})}{Q_{evap}E_S} = \frac{1}{t} = \frac{1}{t_{ON} + t_{OFF}}$			eq 30
Cooling capacity	$Q_{evap} = UA_{evapRC}(\bar{T}_{RC} - T_{evap})$	eq 31	$Q_{evap} = UA_{evapPCM}(T_{PCM} - T_{evap})$	eq 32	
Air - PCM heat rate	$Q_{PCM} = UA_{PCM-RC}(T_{RC} - T_{PCM})$			eq 33	

Figure 3.5 Comparison of energy balances in typical SDE and PCM - SDE refrigerator

RC air temperature cycling. On the contrary in PCM - SDE refrigerator the surplus energy during the operation of RC evaporator is stored in the latent heat of PCM and there is no effect on the air temperature of RC eq 27. In the PCM - SDE refrigerator RC temperature to a certain sense is decoupled from the compressor operation.

Interesting is that compressor run fraction t_{ON}/t depends for both refrigerators only on the compartment heat load Q_{RC} and cooling capacity of the compressor Q_{evap} and it's not dependent on the thermal storage capacity. However the compressor

cycling frequency is strongly influenced by thermal capacity. The larger the capacity of the thermal storage the fewer cycles of the compressor are required. Thus another advantage of PCM – SDE refrigerator-freezer is less transient operation time and less transient losses because of lower compressor cycling frequency.

In the eq 24 I made an assumption that heat load of the RC Q_{RC} is equal to heat transfer rate to the PCM Q_{PCM} . In real operation conditions of the refrigerator the heat load of RC is varying with many aspects such as ambient temperature, external ventilation and the consumer habits. Hence also Q_{PCM} should vary according to the heat load of the RC. The energy balance between Q_{RC} and Q_{PCM} can be also written in the following form:

$$UA_{PCM-RC}(T_{RC} - T_{PCM}) = UA_{RC}(T_{AMB} - T_{RC}) + Q_{aux} \quad \text{eq 34}$$

If we want to keep the temperatures T_{RC} and T_{PCM} constant we have to consider variable UA_{PCM-RC} to match variable heat load to the compartment. Therefore variable speed RC fan is an obligatory component in the final production design of the refrigerator-freezer. However if we consider laboratory conditions without any auxiliary heat loads Q_{aux} to the RC and constant ambient temperature T_{AMB} we appreciate the importance of suitable design of UA_{PCM-RC} and UA_{RC} .

3.2.1 Thermal accumulation with PCM

The basic question is which material to choose for the PCM storage accumulation in contact with RC evaporator for the best performance of the system. Fundamental classification of substances used for thermal energy storage purposes is shown in Figure 3.6. Two main groups utilized are solid-liquid and gas-liquid PCMs.

The easier to implement are obviously solid-liquid phase change materials and are also the most used in the research. The real application of PCM materials to marketed cold appliances does almost not exist yet or it's very limited. On the other hand there are several research papers in the literature

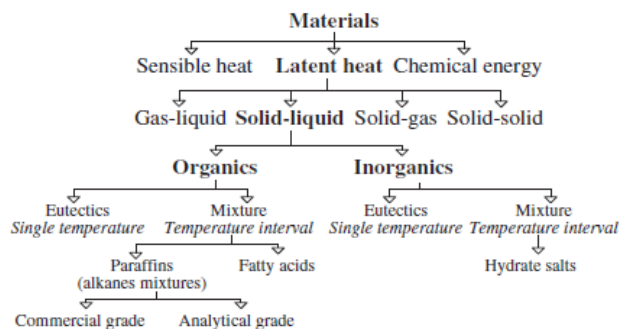


Figure 3.6 Classification of substances used for thermal accumulation (Abhat, 1983)

dealing with solid-liquid PCMs applied into the freezer compartment (Gin, et al., 2010), (Oro, et al., 2012), (Tulapurkar, et al., 2010) and into the refrigeration compartment (Azzouz, et al., 2009) (Tulapurkar, et al., 2010). Obviously the difference between the RC and FC PCMs is in the phase changing temperatures. Gas-liquid phase changing materials are utilized widely as a main working fluid in the vapor compression cycles almost in every domestic refrigerator. However stationary application of gas-liquid PCMs for thermal accumulation was not exploited yet. ☺ This is mainly because of extremely large volume change between gas and liquid and problems with its compensation. The volume change occurs also in the solid-liquid PCMs and it is important to consider it during design phase of the PCM container, in order to avoid fatigue failures during the operation.

3.2.1.1 Literature survey PCMs in refrigeration compartment

Application of PCM into refrigeration compartment is more interesting for my research activity so I discuss two available papers in more details. The work of (Azzouz, et al., 2009) was performed on the single cavity domestic refrigeration appliance where PCM pocket was attached from the back side of the evaporator and foamed into the cabined wall Figure 3.7. PCM used was eutectic mixture of water and salt. By changing the salt concentration in the water he could obtain phase changing temperature between 0°C and -9°C. In experimental study he used water and eutectic mixture at -3°C. In his experimental study he managed to increase evaporation temperature by almost 4K with water and 3K with eutectic mixture. He concluded 10% to 30% increase in COP depending on the thermal load and 5 to 9 hours cycle period of the refrigerator.

Work of (Tulapurkar, et al., 2010) done for General Electric is even

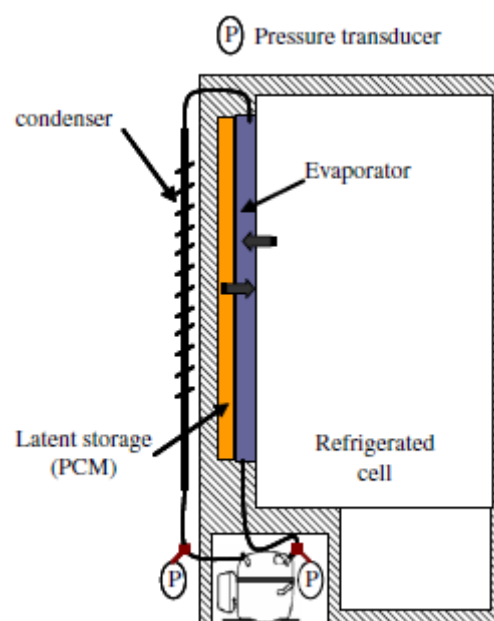


Figure 3.7 PCM in contact with evaporator in a single cavity refrigerator (Azzouz, et al., 2009)

more interesting because they applied PCM to the side by side refrigerator-freezer appliance with SDE circuit. But there are not many details about prototype design explained in the paper. However from the Figure 3.8 it seems that RC PCM heat exchanger was placed on the suction tube exiting from the RC evaporator. This assumption confirms also

relatively high RC evaporation temperature

around -20°C . He concluded potential of the setup to increase energy efficiency by 8% though the experiments didn't confirm it. It's not clear what type substance was used as PCM but it was changing phase at -2°C , so probably it was some water mixture.

3.2.2 Selection of PCM

There are several important criteria to consider during selection of phase change material for domestic refrigerator:

1. Phase changing temperature
2. High thermal conductivity (both solid and liquid) and low supercooling
3. Latent heat of storage
4. Compatibility with food environment and evaporator material
5. Thermal volumetric expansion
6. Cycling stability (components separation)
7. Availability and cost

Refrigeration compartment operates at air temperatures around 4° to 5°C . The first criterion thus limits the PCM choice possibilities to materials with PC temperature close to zero or below. In my study I have considered three substances; pure

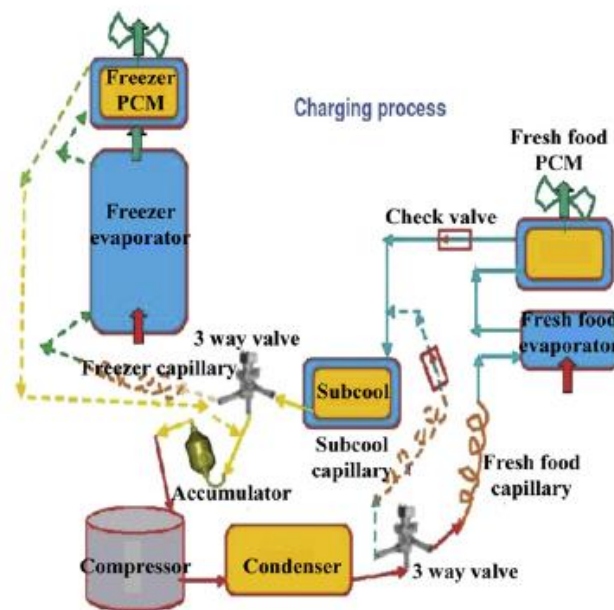


Figure 3.8 Sequential dual evaporator circuit with PCM applied to both refrigeration and freezer compartments and used also for subcooling (Tulapurkar, et al., 2010)

Water			
Mass concentration	Latent heat	Phase change temperature	Thermal conductivity liquid
kgkg ⁻¹	kJkg ⁻¹	[°C]	Wm ⁻¹ K ⁻¹
0.0%	334	0	0.560
Water + Ethylene glycol			
8.4%	321	-2	0.535
14.0%	313	-4	0.517
18.4%	306	-6	0.503
22.3%	300	-8	0.491
25.7%	295	-10	0.481
Water + NaCl			
6.3%		-4	0.55
12.6%		-8	0.52

Table 3.5 Properties of pure water and two mixtures of water with ethylene glycol and salt NaCl (MEglobal, 2008) (Martinez, 2011)

water, and two mixtures glycol-water and salt-water. Basic properties such as phase change temperature, latent heat and thermal conductivity for different mass concentration are presented in the Table 3.5. The water is the best candidate for the PCM material. It has highest thermal conduction coefficient and largest latent heat from the evaluated materials. It's not a mixture hence there is no problem with cycling stability. It's widely available and compatible with food. There is a volume change between water and ice of approximately 9% which has to be considered in the design phase of the PCM pocket. The only problem might be insufficient temperature lift between ice and RC air temperature causing very small heat transfer rate.

3.2.3 PCM freezing-melting test

I performed very simple test of freezing and melting PCMs in the bottles equipped with T type thermocouple placed directly in the PCM on the centerline of the bottle. The thermocouple reading was recorded by acquisition system. The test was performed with water, 10%, 20% and 30% volume concentrations of ethylene glycol with water and 6.3% and 12.6% weight concentration of NaCl with water.

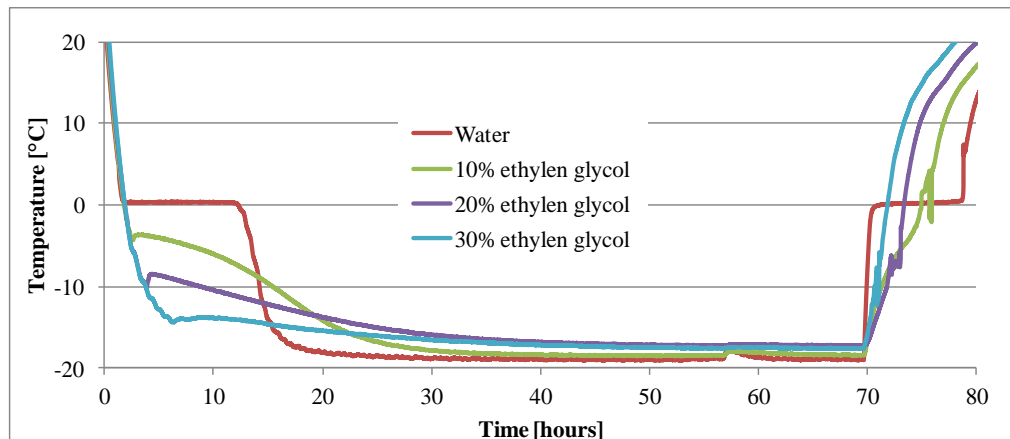


Figure 3.9 Freezing and melting experiment with water and ethylene glycol solutions

Recorded temperature profiles for ethylene glycol mixtures are reported in Figure 3.9 and salt solution temperatures are in Figure 3.10.

The results for water corresponded exactly with the theory and water ice mixture was for a very long time at temperature 0°C during freezing and also during melting. From the measured results small supercooling is visible during the start of the freezing phase for all mixtures except 6.3% salt concentration. The results for mixtures showed nicely observable freezing phase at temperatures below zero °C. The temperature is not constant during the freezing phase as it's for water but it's slightly decreasing. The passage from two phase mixture to completely frozen PCM is not visible. Somewhat surprising observation was made during the heating up period. The temperatures of melting mixtures (except 6.3% NaCl concentration) were rising almost like during sensible heating up. Only a small "temperature distortion" happened at temperature close to assumed melting point. After zooming closer the heating section of ethylene glycol mixtures in Figure 3.11 the previously identified temperature "distortion" is actually a constant

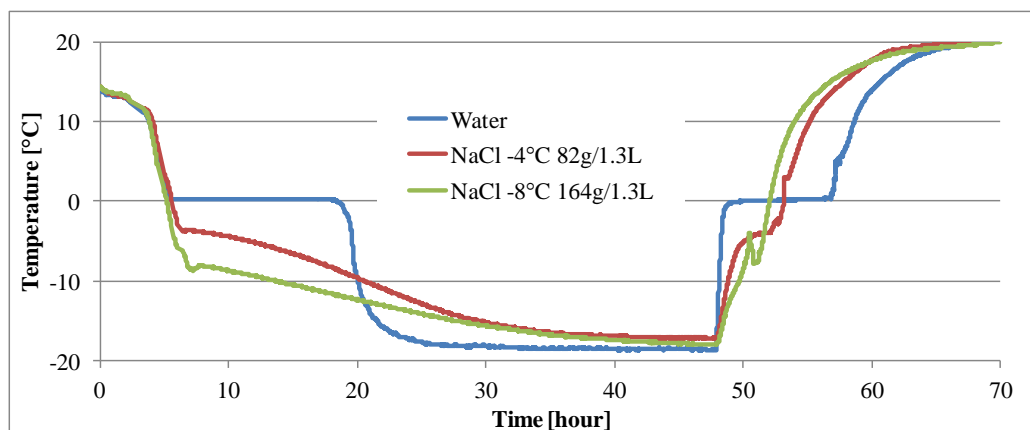


Figure 3.10 Freezing and melting experiment with water and NaCl solutions

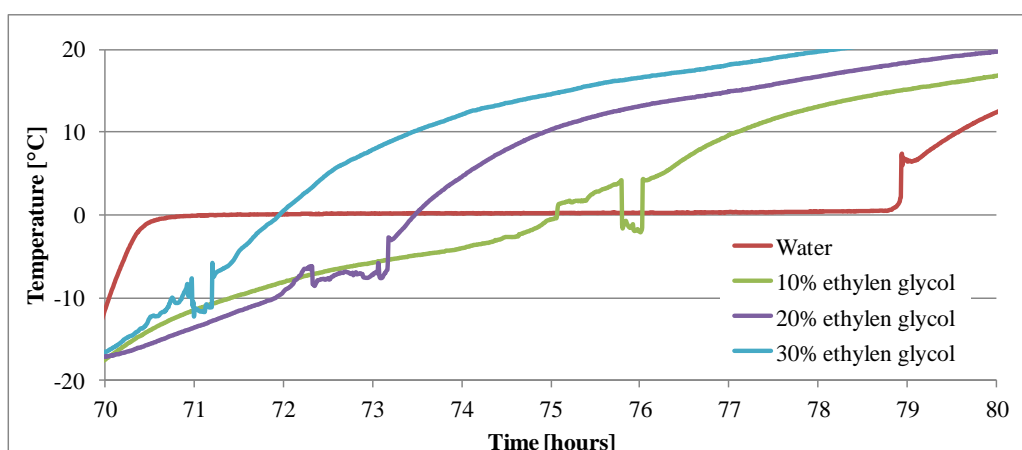


Figure 3.11 Melting phase of water ethylene glycol solutions with superheating phenomena

temperature phase changing with large superheating necessary to initiate the melting process. Such a large superheating might cause problems in cooling of the RC. For example mixture of 10% ethylene glycol should melt at the temperature close to -3°C . However the melting of the PCM is initiated only after the PCM temperature raises to more than 4°C . Actually this could mean that PCM made of 10% ethylene glycol and water would never melt as the temperature in RC is approximately 4°C to 5°C .

These findings lead me to the conclusions that water is the best PCM for utilization in the RC. PCM pocket and refrigeration cabinet design should be adjusted to the small temperature lift between melting water and RC air temperature. Solution of water and NaCl with freezing temperatures higher than -4°C could be utilized as well.

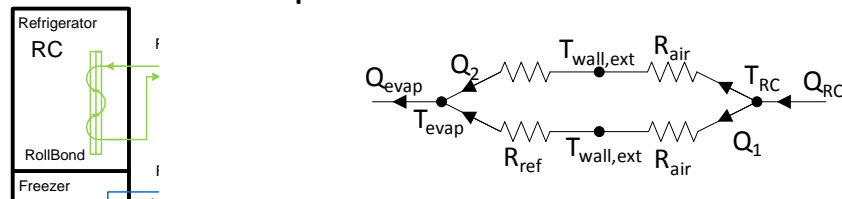
3.2.4 Thermal resistance of RC evaporator with PCM accumulator

The PCM pocket can be in contact with both sides of the roll-bond evaporator or it can be attached to only one and second side can directly cool the compartment air. Both cases are analyzed by heat transfer modeling and compared to RC roll-bond evaporator without PCM. The dimensions of the evaporator were taken from Table 3.1 for Whirlpool roll-bond. Analogy with electric circuit was again used to sketch thermal resistances, capacity, temperatures and heat rates Figure 3.12.

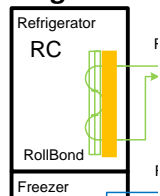
In the model of the evaporator several important assumptions were made:

- Thermal resistances of PCM were calculated from thermal conductivity coefficients of water ($k_{\text{ice}}=2.18\text{Wm}^{-1}\text{K}^{-1}$, $k_{\text{water}}=0.58\text{Wm}^{-1}\text{K}^{-1}$)
- The thickness of ice and water was assumed to be constant 5mm

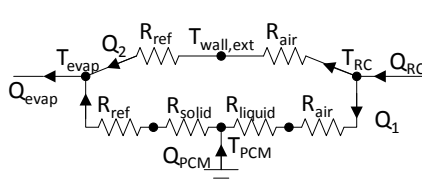
No PCM roll-bond evaporator



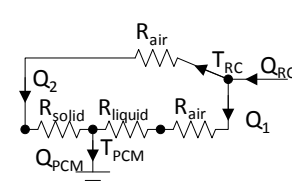
Single side PCM



PCM charging



PCM discharging process



Double side PCM

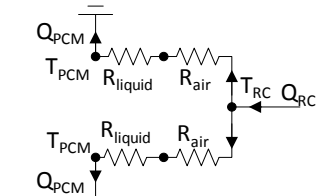
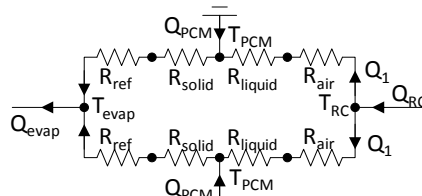
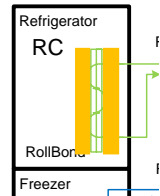


Figure 3.12 Heat transfer processes modeled by thermal resistances in visible roll-bond evaporator and roll-bond with PCM pocket on one side and on both sides

- Thermal resistance R_{ref} was kept constant $0.08KW^{-1}$ as it was determined in the Table 3.2
- Correlation eq 18 chapter 3.1.2.1 was used to evaluate air convection heat transfer coefficient
- Radiation heat transfer coefficient was determined according to the chapter 3.1.2.2
- Evaporation temperature was calculated from compressor data sheet at compressor speed 1600RPM with assumption of constant condensing temperature $35^{\circ}C$
- COP was evaluated based on compressor data sheet
- Compartment temperature was assumed to be constant $4^{\circ}C$

The simulation was performed first on the roll-bond evaporator without PCM and

Whirlpool's roll-bond evaporator No PCM								
T_{cond}	T_{evap}	$T_{wall,ext}$	T_{RC}	R_{ref}	R_{air}	Q_{evap}	Power	COP
$^{\circ}C$	$^{\circ}C$	$^{\circ}C$	$^{\circ}C$	KW^{-1}	KW^{-1}	W	W	
35	-25.34	-21.76	4	0.08	0.58	89.3	40.7	2.20

Table 3.6 Results of heat transfer simulation for simple roll-bond evaporator without PCM and at 1600 RPM

results are summarized in the Table 3.6.

In the following simulations PCM temperature was varied from 0°C till -8°C and impact on the evaporation temperature, heat removal rate from the RC, thermal resistance on the air side and compressor COP were observed in both cases single side PCM and double side PCM. Evaporation temperatures for single side PCM are generally approximately 3K lower than for double side PCM Figure 3.13. With decreasing phase changing temperature also refrigerant evaporation temperature is decreasing.

Behavior of COP is copying that of evaporation temperature which can be observed in the Figure 3.14. Compressor COP of single side PCM evaporator is roughly 7% to 10% worse than double side PCM evaporator. When water is used as a PCM the COP increase versus evaporator without PCM is maximal and reaches roughly +35% and +45% for single and double PCM respectively.

In the Figure 3.15 are plotted results for heat transfer resistance on the air side between PCM and RC air temperature. It's possible to see that with smaller temperature lift the resistance is growing rapidly. The cause is decreasing convective heat

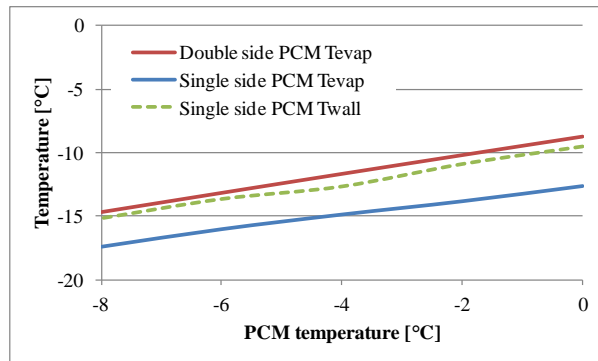


Figure 3.13 Evaporation and evaporator wall temperatures at various fusion temperatures of PCM

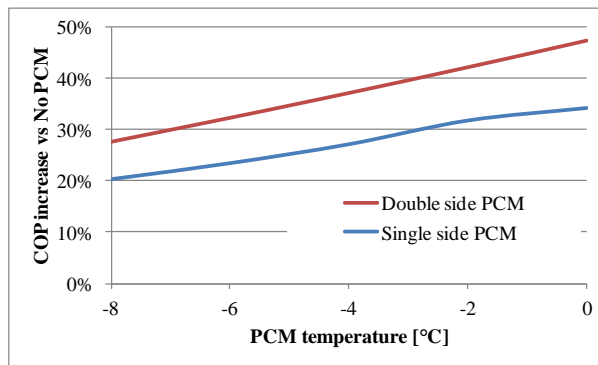


Figure 3.14 Compressor COP at various fusion temperatures of PCM

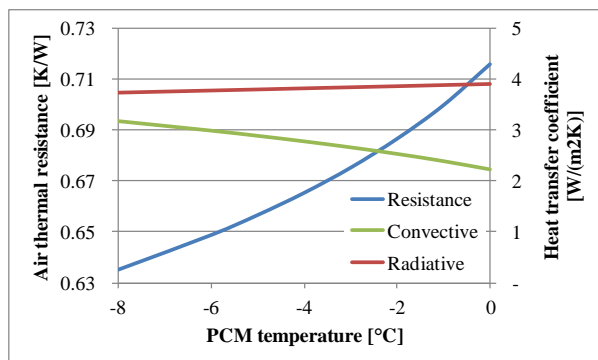


Figure 3.15 Thermal resistance of air to PCM and convective and radiative heat transfer coefficients at

transfer coefficient which is dependent on the temperature lift between T_{RC} and T_{PCM} . Radiative heat transfer coefficient is not changing almost at all.

Maybe the most important topic in this heat transfer exercise was to evaluate amount of heat being

absorbed from RC by PCM during charging and discharging process Figure 3.16. For the double side PCM evaporator only one value exists as the heat transfer rate between PCM and RC is not dependent on the evaporator operation. The heat transfer rate is very small only approximately 11W when water is used as PCM and the heat removal is increasing with decreasing phase changing temperature. For single side PCM roll-bond the heat removal rate is different for charging and discharging process. During the discharging process it is almost the same as for double side PCM evaporator. But during the charging process the evaporator surface temperature is much lower than PCM temperature and thus results in the higher heat rate. We should consider that correlation which was used for the estimation of convective heat transfer coefficient is underestimating the real coefficient by approximately 25%, therefore the real heat removal rate might be higher.

Depending on the ambient temperature and insulation of the refrigeration compartment the calculated heat removal rate can be sufficient even with water as a PCM during the steady-state operation. But the design of double side PCM evaporator has no chance to pull down the temperature in RC during the start up of the appliance in reasonable time, unless RC fan is employed to increase convective heat transfer rate. I mentioned already before that the RC fan is basically a must for the production design appliance even if it brings extra heat to the RC and consumes additional electric power. However in my testing prototype I decided not to implement RC fan mainly because it requires a complex changes to the currently used fans ducts and control strategy. To allow temperature pull down of RC I chose to use single side PCM evaporator instead of more efficient double side PCM evaporator. Single side evaporator without RC fan is simpler to

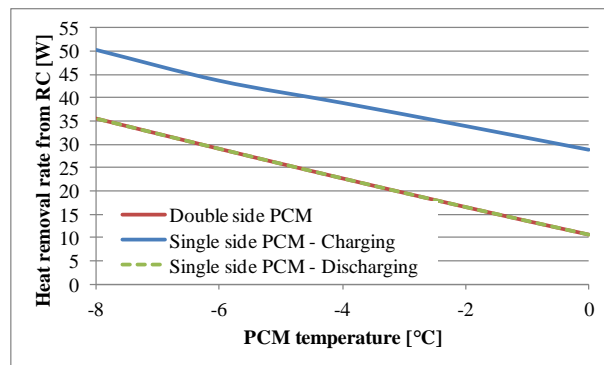


Figure 3.16 Heat removal rate from RC to PCM at various fusion temperatures of PCM

implement and should be sufficient to verify potential of the PCM technology in the contact with RC evaporator in SDE circuit.

3.3 Compartments heat load

The performance of the refrigerator-freezer cabinet is usually characterized by amount of heat that it absorbs from the ambient environment during the regular operation. The temperature gradient between ambient and compartment temperatures is the driver of the heat transfer and cabinet walls represents thermal resistances. Therefore the walls are made usually from low thermal conductivity materials such as polyurethane foams or vacuum insulation panels (VIP).

VIPs consists of a highly porous core material usually fiber glass, silica or aerogel with very low thermal conductivity sealed in an evacuated envelope made of air impermeable material such as aluminum foil. Properly manufactured VIPs generate thermal resistance some order of magnitude greater than that of standard polyurethane foams. The thermal conductivity value is ranging from 1.4 to 5 $\text{mWm}^{-1}\text{K}^{-1}$, which is only 1/15 to 1/5 that of polyurethane foam. Utilization of VIP can help to reduce the overall thermal load of RC by as much as 15% and of FC by approximately 3% and even gain some extra space inside the compartments.

On the other hand the main problems or disadvantages of VIPs are:

- Aging and loosing premium thermal resistance by air infiltration
- Thermal conduction across the edges through aluminum foil
- Still relatively high manufacturing cost

Heat loads of the compartments are measured by reverse heat leak test. Basic idea of the test is to reverse operating temperatures in the refrigerator by cold surrounding of the environmental room and warm compartment heated by electric heater to keep delta temperature equal to standard refrigerator operation. Measured electric power to the heater is assumed to be identical with heat load of the compartment during refrigerator operation.

Typical case of heat flows in the bottom-mount refrigerator-freezers is shown in the Figure 3.17. In my PCM – SDE prototype I want to match heat load of the RC with the heat removal rate by PCM (Q_{PCM}). If water is used as a PCM the heat removal rate is very small only approximately 11W as it was determined in the chapter 3.2.4 this value is slightly underestimated thus in reality it might be a bit higher. Typical RC heat load without VIP is about 26W at ambient temperature

25°C. By application of VIP the heat load can be reduced to around 22W. The compartment heat load can be further reduced by lowering ambient temperature to 20°C and reducing heat load by about 1/4.

Based on this theoretical assumptions the experimental prototype of PCM - SDE appliance was equipped by VIPs in the walls and doors

and ambient temperature in the environmental room was kept 20°C during all energy consumption tests. During the tests I observed complete melting of the PCM therefore these changes on the heat load side of the appliance were sufficient to allow successful utilization of water as a PCM in RC.

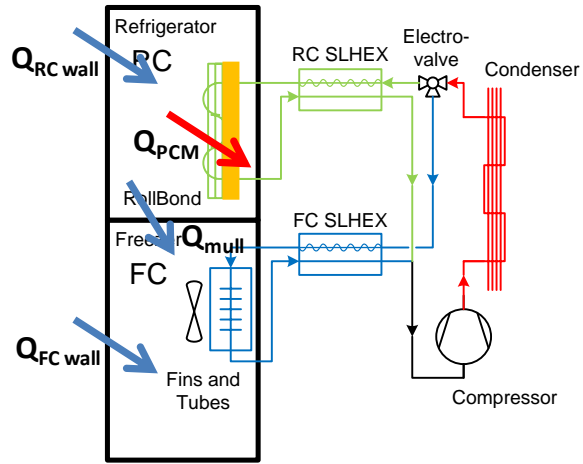


Figure 3.17 Heat loads of bottom mount refrigerator-freezer with indicated heat removal rate by PCM

3.3.1 Impact of heat loads on energy efficiency

3.3.1.1 Single compartment

Energy efficiency of single compartment refrigerator can be express in terms of system COP.

$$COP_{RC} = \frac{E_{removed}}{E_{electric}} = \frac{Q_{RC\ con}t + Q_{aux}t_{aux}}{P_{RC\ comp}t_{ON} + P_{aux}t_{aux}} \quad \text{eq 35}$$

The nominator consists of compartment heat load by conduction $Q_{RC\ con}$ through the walls, door and door's gaskets and auxiliary heat loads Q_{aux} of the fan, light, hot gas condensing in the evaporator during OFF period and other. Heat load by conduction typically represents the largest part of the total heat loads to the compartment. Numerator involves compressor power $P_{RC\ comp}$ during the ON periods and auxiliary power P_{aux} of all the other components of the system such as, fans, electro-valves, control board and more. Further on we can write total heat load of the compartment as:

$$Q_{RC} = \frac{Q_{RC\ con}t + Q_{aux}t_{aux}}{t} \quad \text{eq 36}$$

If we neglect all the auxiliary power consumptions we come to the conclusion that COP_{RC} is equal to compressor COP_{RCcomp} .

$$COP_{RC} = \frac{Q_{RC\ cont}t + Q_{aux}t_{aux}}{P_{RC\ comp}t_{ON}} = \frac{Q_{evap}t_{ON}}{P_{RC\ comp}t_{ON}} = COP_{RCcomp} \quad \text{eq 37}$$

At this point it's necessary to mention that higher heat load doesn't necessary results in less efficient refrigerator from COP point of view. But higher heat load will most probably mean higher overall energy consumption and thus also lower efficiency from energy efficiency index point of view (EEI – function of storage volume and overall appliance energy consumption not a COP). This is visible from the following equation for electric energy consumption:

$$E_{electric} = \frac{Q_{RC\ cont}t + Q_{aux}t_{aux}}{COP_{RC}} = \frac{Q_{RC}t}{COP_{RC}} = P_{RC}t_{ONRC} \quad \text{eq 38}$$

Each relative percent decrease in compartment heat load bring equal relative percent of energy consumption saving, Figure 3.18. Thus compartment heat load plays even stronger role than COP in decreasing energy consumption and improving EEI. Impact of relative improvement of COP on the relative improvement of energy consumption is shown in Figure 3.18. The advantage is that in SDE-PCM circuit the RC COP is completely independent from heat load of RC which is not true for standard SDE circuit.

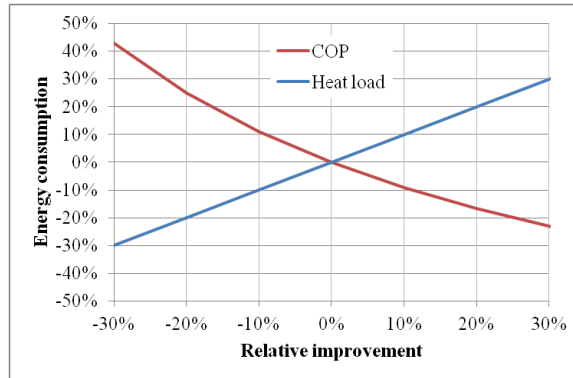


Figure 3.18 Impact of relative COP and heat load improvement on the energy consumption

3.3.1.2 Bottom-mount SDE refrigerator-freezer

Let's think about SDE system as two separate refrigeration circuits. The combined COP of two circuits can be considered as thermal heat removed from the compartments to the electric energy consumed by both circuits.

$$COP_{SDE} = \frac{Q_{RC}t + Q_{FC}t}{P_{RC}t_{ONRC} + P_{FC}t_{ONFC}} \quad \text{eq 39}$$

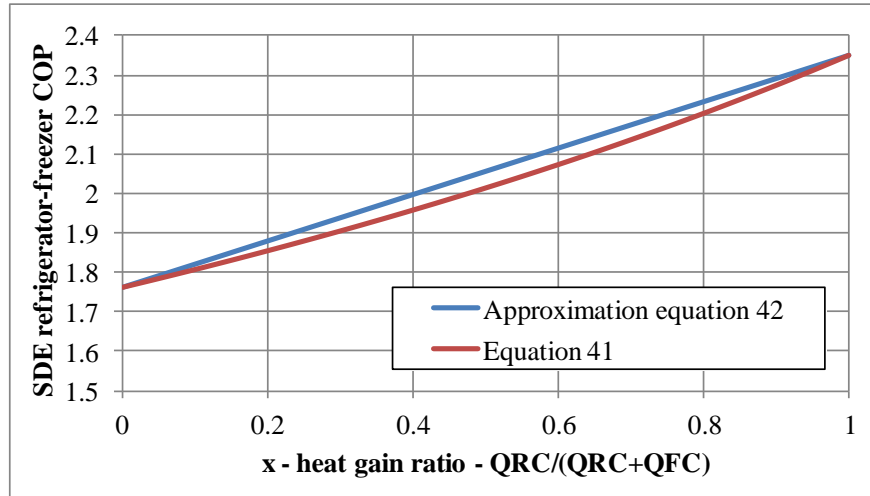


Figure 3.19 Overall SDE refrigerator-freezer appliance COP as a function of compartments heat load ration

In the next we substitute eq 38 into eq 39 for RC power and then we repeat it for the FC power. After several algebraic operations and implementation of RC heat load ratio:

$$x = \frac{Q_{RC}}{Q_{RC} + Q_{FC}} \quad \text{eq 40}$$

We obtain a SDE COP as a function of the two compartments COPs and heat load ratio as shown in the following equation.

$$COP_{SDE} = \frac{COP_{RC} COP_{FC}}{xCOP_{FC} + (1-x)COP_{RC}} \quad \text{eq 41}$$

Therefore in the refrigerator-freezer with SDE circuit overall system COP is dependent not only on the individual COPs of the compartments but also on the RC heat load ratio. Figure 3.19 shows the overall SDE appliance system COP as a function of x. Assuming that COP_{RC} is much higher than COP_{FC} , then the higher the ratio the higher is the system COP. The eq 41 can be very well approximated by simpler expression:

$$COP_{SDE} = xCOP_{RC} + (1-x)COP_{FC} \quad \text{eq 42}$$

The comparison of the two equations is visible in the Figure 3.19. The approximated equation overestimates the system COP at 0.5 RC heat load ratio by roughly 2% but anyway it can be used for quick estimations and behavior understanding.

3.3.2 Thermal load shifting with sub-cooling loop

In the previous chapter I have shown impact of the heat load ratio on the overall COP. The results lead me to the conclusion that it's more economic efficient to invest in the insulation of the freezer compartment which coincide with conclusions of Whirlpool, Figure 3.20. However it's necessary to understand that investing to the insulation of the RC has two positive effects, decreases heat load of RC and allows us to use PCM material with higher phase changing temperature. Thus higher evaporation temperature can be achieved during the compressor operation and resulting in increased COP_{RC} . In addition it could be interesting to compare possible heat load decrease by one m^2 of VIPs for RC and for FC, but economic analysis was not the target of this PhD activity.

The thermal load shifting is usually done on the cabinet insulation side by increasing thickness of the polyurethane foam or by implementing VIPs to the walls of the FC. The advantage of the SDE circuit is that thermal load shifting can be done also on the level of refrigeration circuit based on the subcooling of the high pressure liquid refrigerant during FC operation. The idea was considered innovative and patent application was successfully submitted to the European Patent Office EPO for registration (registration number 12182353.8).

I proposed a complex SDE circuit to shift part of the heat load from FC to RC and enhance overall COP according to the eq 42. The heat load is shifted from low temperature FC to high temperature RC by sub-cooling liquid refrigerant in RC PCM before being expanded to the freezer evaporator. The principle is clear from the p-h diagram Figure 3.21. I have introduced additional loop with second bi-stable electro-valve to the concept of SDE PCM refrigerator-freezer. Sub-cooling loop is marked by orange color in Figure 3.22. The loop starts after the second

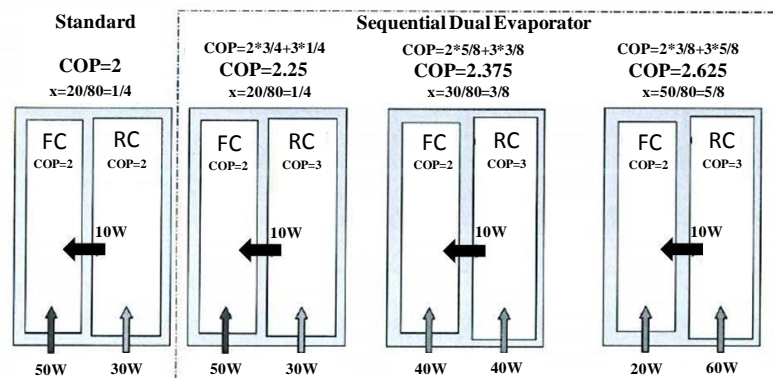


Figure 3.20 Thermal load shifting principle and impact on the appliance COP

diverting valve and enters the RC where it exchanges heat with PCM and then the cold liquid expands to the FC evaporator. Higher sub-cooling during FC operation results in higher cooling capacity delivered to FC evaporator for unchanged compressor power consumption.

Second bi-stable electro-valve placed on the FC loop allows the sub-cooling loop to be switched ON and OFF. Operation of the loop should be decided according to the amount of cooling capacity accumulated in PCM.

Simple steady-state numerical simulation showed energy consumption saving potential dependent on compartments' COPs and amount of heat exchanged between PCM and liquid refrigerant. Heat transfer rate between liquid and PCM is limited to refrigerant mass flow multiplied with the enthalpy difference between exit from the condenser and enthalpy of the refrigerant at PCM temperature. I've performed a case study where I evaluated potential of subcooling loop. The boundary conditions are following. $COP_{RC}=2.2$, $COP_{FC}=1.73$, $Q_{RC}=22.03W$, $Q_{FC}=25.86W$. The results are reported in the Figure 3.23. With increasing heat transfer during subcooling process the energy consumed by RC is increasing and FC decreasing. Larger cooling capacity provided to FC is shortening the cooling time and thus decreasing also the FC fan run time.

Simple steady-state numerical simulation showed energy consumption saving potential dependent on compartments' COPs and amount of heat exchanged between PCM and liquid refrigerant. Heat transfer rate between liquid and PCM is limited to refrigerant mass flow multiplied with the enthalpy difference between exit from the condenser and enthalpy of the refrigerant at PCM temperature. I've performed a case study where I evaluated potential of subcooling loop. The boundary conditions are following. $COP_{RC}=2.2$, $COP_{FC}=1.73$, $Q_{RC}=22.03W$, $Q_{FC}=25.86W$. The results are reported in the Figure 3.23. With increasing heat transfer during subcooling process the energy consumed by RC is increasing and FC decreasing. Larger cooling capacity provided to FC is shortening the cooling time and thus decreasing also the FC fan run time.

With increasing heat transfer during subcooling process the energy consumed by RC is increasing and FC decreasing. Larger cooling capacity provided to FC is shortening the cooling time and thus decreasing also the FC fan run time.

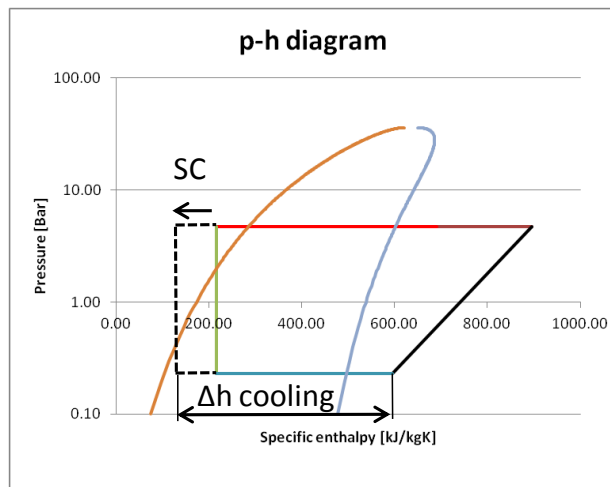


Figure 3.21 FC cycle operation with subcooling of the liquid refrigerant line in the RC PCM and increase in cooling capacity delivered to FC

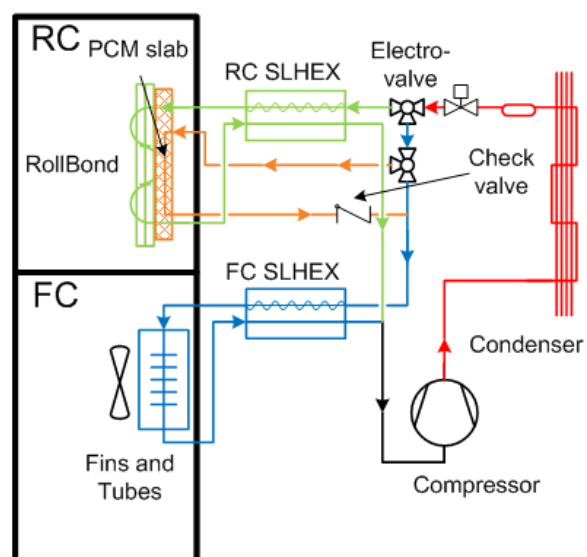


Figure 3.22 Concept of load shifting SDE circuit including sub-cooling loop in the RC PCM

Application of subcooling loop to the SDE refrigerator-freezer with PCM in contact with RC evaporator has a potential to save additional energy because of heat load shifting from FC to RC. The potential depends on the freezer and refrigerator COPs and amount of heat

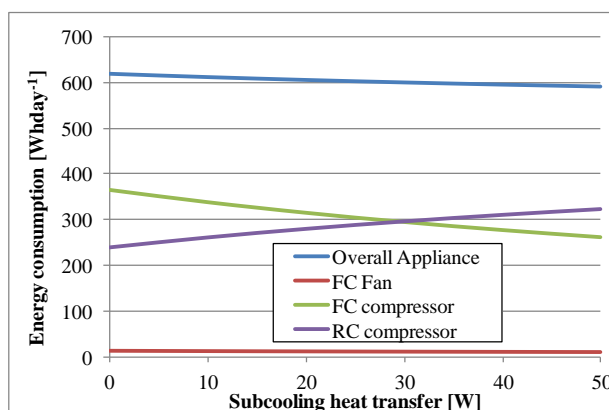


Figure 3.23 Case study of subcooling loop application to SDE refrigerator-freezer with PCM in RC

being exchanged in the subcooling loop. The subcooling loop might also be utilized to quickly defrost the PCM in RC.

3.4 Refrigerant charge migration

During the compressor OFF time there is a spontaneous movement of refrigerant mass (charge migration) to the evaporator in any refrigerator. One of the reasons for migration is a capillary tube used as an expansion device in the domestic refrigerators. At the end of the ON cycle there is a pressure difference build up between the condenser and evaporator. Capillary tube thus works in the first minutes after switching OFF the compressor as pressure equalization device between high and low side. There is large amount of refrigerant moving from the condenser to the evaporator during this initial period. After certain time mass distributes between evaporator, part is dissolved in the oil and relatively large part is present also in the compressor in vapor phase (Bjork, et al., 2006). In SDE circuit there is additional driver for refrigerant mass migration during the OFF period and that is temperature difference between RC and FC evaporators. In general the refrigerant in the refrigeration circuit tends to migrate to the place with minimum temperature. In SDE circuit minimum temperature is in FC. Thus during the prolonged OFF period the refrigerant will accumulate in the FC evaporator. If RC evaporator will depart after OFF period the refrigerant have to be first evacuated from FC evaporator. This is a reason for part of the transient losses in the SDE circuit.

Refrigerant mass migration happens also during the RC compressor ON period. RC evaporator operates at evaporation temperatures much higher than the

temperature of FC evaporator. Thus during RC ON period the vapor refrigerant at the exit from RC evaporator will further condense in the FC evaporator. This will reduce gradually refrigerant mass charge used in RC evaporator.

Based on the refrigerant charge migration behavior in SDE circuit I decided to implement electronic block

valve at the entrance to the capillary tubes. The block valve allows refrigerant mass pump out from the evaporator before RC operation. In addition I placed one way check valve at the suction tube of the FC evaporator to avoid refrigerant back flow to the FC evaporator, Figure 3.24. The check valve was applied to the prototype also in the study of (Won Jae, et al., 2011) but later on it was removed and the group claimed no usefulness of the valve. I have to comment that their evaporation temperature during RC operation was most probably very close to the freezer temperature and thus the function of check valve was unimportant. In any case in my refrigerator prototype design I placed manual closing valve in parallel to the check valve to eliminate its function if necessary.

3.5 Conclusions

Chapter 3, presents innovative conceptual solutions how to increase evaporation temperature in the SDE circuit during refrigeration compartment (RC) operation without passing to forced convection evaporator in RC.

In the first part I identified and analyzed heat transfer resistances of the RC roll-bond evaporator. The evaporator surface to RC air thermal resistance R_{air} is the bottleneck of the heat transfer to the evaporating fluid. From the previous experimental studies I estimated R_{air} to be approximately ten times higher than corresponding evaporator wall and refrigerant heat transfer resistance. I selected empirical correlation for convective heat transfer which most closely predicts air

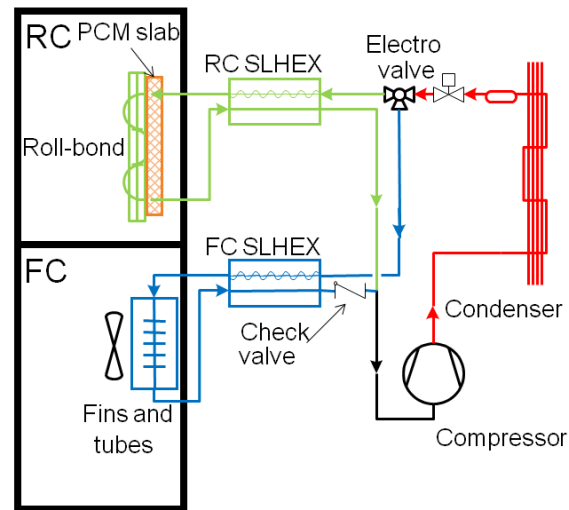


Figure 3.24 Conceptual design of SDE circuit with single side PCM in contact with RC evaporator, block valve between the filter and bi-stable and check valve at the exit from the FC evaporator

convective coefficient of the roll-bond evaporator and presented calculation of radiation heat transfer coefficient.

In the next I introduced concept of thermal accumulation based on the phase change material (PCM) attached to the RC evaporator. Convection and radiation heat transfer resistance on the evaporator surface was substituted by much higher thermal conduction in the PCM. I performed theoretical heat transfer analysis on the Whirlpool's RC roll-bond evaporator with thermal accumulation for two cases with PCM on one side and on both sides of the evaporator. Depending on the PCM temperature the compressor's COP_{RC} was estimated to be significantly (20% to 45%) higher than the COP_{RC} with evaporator without PCM. The design with PCM on both sides has 7% to 10% higher compressor COP_{RC} than single side PCM evaporator, but without RC fan in the compartment it has limited possibility to pull down temperature in RC during the start up. Thus design with single side PCM evaporator was selected for experimental testing.

To select proper PCM I performed a freezing and melting test with water and with water mixtures at different concentrations of ethylene glycol and NaCl. Most of the mixtures had significant supercooling and superheating effect except for the 6.3% mixture of water with NaCl with freezing temperature $-4^{\circ}C$. Thus pure water and water NaCl mixtures with concentration lower than 6.3% are suitable PCM materials for application in domestic refrigerator. Pure water was selected as a PCM for prototype testing.

I studied impact of PCM temperature on the COP_{RC} , evaporation temperature and heat transfer rate between RC and PCM (Q_{PCM}). Higher PCM temperature results in higher evaporation temperature and higher COP_{RC} but lower Q_{PCM} . To keep RC temperature during the PCM melting process at desired level ($4^{\circ}C$) Q_{PCM} has to be closely balanced with heat loads of the RC (Q_{RC}). Thus application of VIPs and lowering ambient temperature to $20^{\circ}C$ during the energy consumption tests is necessary.

Afterwards I showed impact of heat load ratio between RC and FC on the overall refrigerator-freezer appliance COP. Thermal load shifting from FC to RC can increase the overall efficiency of SDE refrigerator. I proposed an idea to shift load from FC to RC by subcooling liquid refrigerant in the RC PCM during FC operation. The idea was considered innovative and consequently patent application was filled up under registration number 12182353.8. Energy saving potential of the subcooling loop depends on the two COPs and heat transferred from liquid to the PCM.

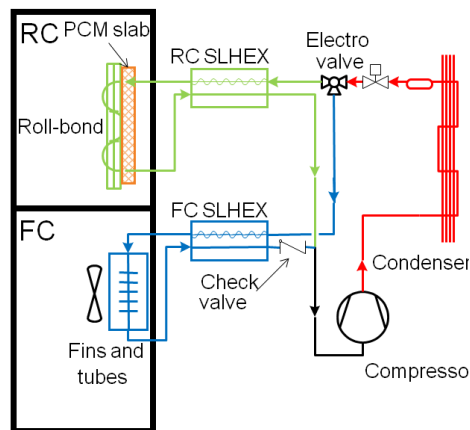


Figure 3.25 Prototype 1

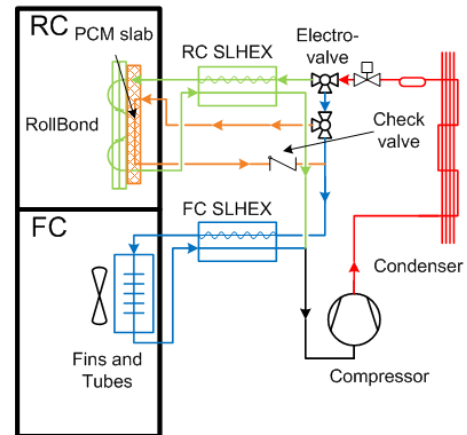


Figure 3.26 Prototype 2

Theoretically by adding block valve after the condenser and check valve after the FC evaporator I can reach additional energy saving in the SDE circuit by avoiding refrigerant mass migration.

Starting from these ideas I built with help of Whirlpool's model shop two conceptual prototype refrigerator-freezers. The two concepts of SDE circuit designs are:

1. SDE with single side visible PCM RC evaporator including block valve and check valve (Prototype 1, Figure 3.25)
2. SDE with single side visible PCM RC evaporator including subcooling loop for thermal load shifting from FC to RC (Prototype 2, Figure 3.26)

Experimental testing and results of prototypes are presented in the chapter 6.

4 Testing SDE circuit with variable speed compressor

Whirlpool Corporation developed and built prototype of bottom-mount refrigerator-freezer built-in appliance with variable speed compressor and visible roll-bond evaporator in RC as a part of the SDE technology assessment project. All the details of the prototype design were already described earlier in chapter 2.1. For further utilization of this existing prototype I equipped it with thermocouples and pressure transducers for measuring thermodynamic properties of the circuit and components. Compressor was connected with electronic inverter and frequency generator to allow compressor speed manipulation and manual switch was attached to the bi-stable electro valve.

4.1 Objective of the testing

I was interested in testing this prototype mainly from point of view to assess impact of compressor speed on the RC evaporation temperature and COP_{RC} . Decreasing compressor speed and hence also cooling capacity is one of the viable options to rise evaporation temperature and COP of SDE circuits as I explained in chapter 2.2.3. Thus I want to confirm the forecast.

Experimental results also helped in tuning simple steady-state simulation of refrigeration system introduced in chapter 5. It was used to predicting more closely the impact of evaporation temperature on the COP in the refrigeration circuit taking into account also condensing temperature.

Last but not least the purpose of this preliminary testing was also to get in touch and understand testing equipment and instrumentation typically used in Whirlpool laboratories for measurements and acquisition.

4.2 Prototype instrumentation, control and acquisition

The refrigeration compartment was equipped with air temperature probes according to the ISO 15502 standard (ISO, 2005). There were 3 temperature probes made of T type thermocouple inserted in the centre of solid cylinder made of brass with a mass of 25g and equal diameter and height about 15mm. The probes were distributed in the compartment over each other to capture temperature gradient in the compartment. Also ambient temperature was measured by the thermocouple with brass cylinder. Four thermocouples were

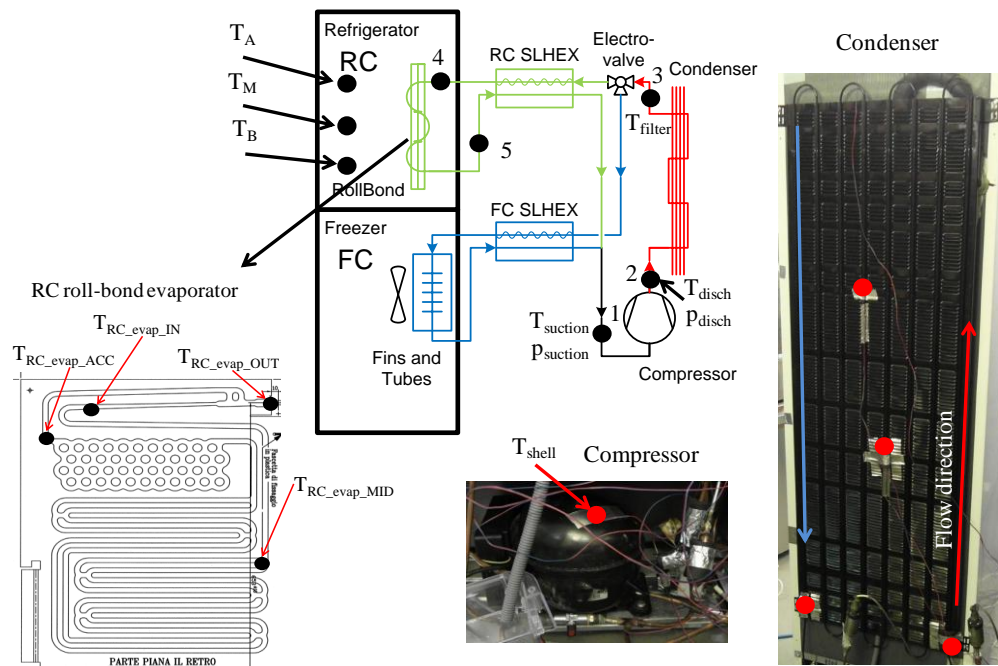


Figure 4.1 Prototype instrumentation with thermocouples and pressure transducers

taped directly to the surface of RC roll-bond evaporator with aluminum tape and the exact positions are shown in the Figure 4.1. 8 thermocouples were attached to the external part of the refrigeration circuit according to the Figure 4.1. 4 out of them were used to measure surface temperature of the condenser (inlet, 2x mid and outlet) other 3 were measuring temperatures to determine cycle operating conditions (suction temperature at the entrance to the compressor, discharge temperature and filter temperature to estimate subcooling) and the last thermocouple measured shell temperature of the compressor.

Two pressure transducers were welded to the circuit just before and right after the compressor. Pressure transducers were manually calibrated on the separate stand before welding to the circuit. Wattmeter was used to record electric power and

Instrument	Pressure transducer	Mass flow meter	Wattmeter energy meter	Thermocouple
Working principal	CVD	Coriolis		T-type thermocouple
Manufacturer	Gems-sensors	Micro Motion	Ohio Semitronics	Tewire
Type	6200F-F0-C0-B	CMFS010	GH-002DT52/250K	P-26-TT
Operating range	0.5-10Bar	max. 108kg/h	0-1000W	-40 to 350°C
Accuracy	0.15 % FS	0.3% at 0.2g/s	±0.05% FS	±0.5°C

Table 4.1 Summary of instruments utilized during the experimental testing

energy consumption. Technical description and accuracy of the used instrumentation can be found in the Table 4.1. Acquisition of temperatures, pressures and electric power was automated by existing Whirlpool hardware and software installed in the laboratories. The data were recorded approximately every 20 seconds.

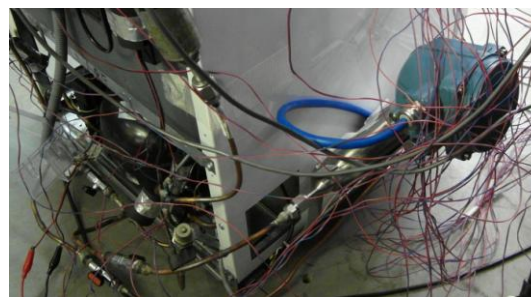


Figure 4.2 Coriolis mass flow meter attached to the suction line of the refrigeration circuit

Coriolis mass flow meter was attached in parallel to the suction line before the compressor and manual valves were welded to the suction line to allow directing the refrigerant flow to pass through it, Figure 4.2. Initial idea of using mass flow meter was to check the compressor data sheets of the manufacturer at various conditions. However at the end mass flow meter helped to estimate evaporation temperature when the low pressure acquisition system broke down and it was not possible to substitute it in a reasonable time. The details about mass flow meter are in the Table 4.1. Acquisition of data from the mass flow meter was done by Labview software using VISA interface and Modbus communication. The data were recorded to the separate computer in 15 seconds steps. Thus during the data analysis it was necessary to perform synchronization between two sources of data. At the moment of testing this prototype there was not available required hardware to perform automated control of the SDE refrigerator-freezer at the cycling running condition and switching between RC and FC. No standard control board could be used as SDE technology is not yet available on the market. Therefore manually operated control of the compressor speed and bi-stable electro-valve was necessary. Speed of the compressor was controlled by frequency modulator. Modulator was sending a square signal with amplitude 5V and required frequency to the compressor electronic inverter which controlled and protected compressor. Linear dependence between modulating

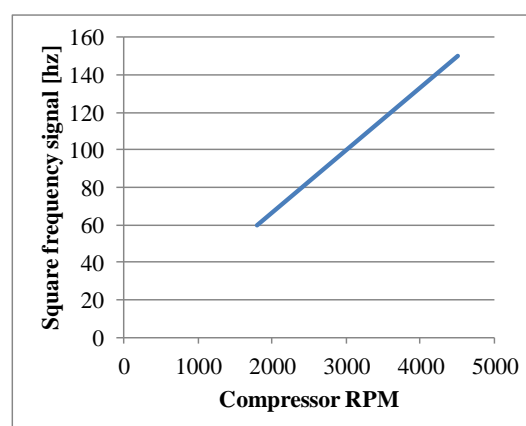


Figure 4.3 Relation between modulation frequency and compressor RPM

frequency and compressor RPM is shown in the Figure 4.3. Manual switch was constructed to control position of the bi-stable electro-valve and to decide between RC or FC operation. Electro-valve needs 4 half waves to switch from one position to another. Therefore small electronic circuit was built according to the sketch in the Figure 4.4.

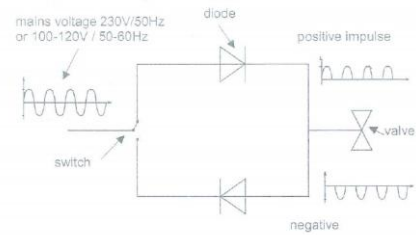


Figure 4.4 Electronic circuit for switching the bi-stable electro-valve

4.3 Test procedure

Ability to control compressor speed and electro-valve only in the manual mode limited possibilities for testing. Thus temperature cycling behavior and switching between RC and FC operation was not investigated during this experimental campaign. The only test I could perform was temperature pull down test of one compartment environment from ambient temperature with constant compressor RPM. I let the compressor running sufficiently long until steady-state constant temperature was reached in the compartment. I repeated the procedure at three different RPM of the compressor (1800RPM, 3000RPM and 4500RPM) and two ambient temperatures (22°C and 26°C) set by environmental room. Each pull down test lasted approximately one day including the heating up period necessary between the tests. Each test was divided into transient and steady-state part. I performed these tests only for refrigeration compartment because performance of RC operation is the more important in my study. Overview of performed tests is presented in Table 4.2.

T _{AMB}	1800 RPM	3000 RPM	4500 RPM
22°C	S, T	S, T	S
26°C	S, T	S, T	S, T

Table 4.2 Tests results obtained from the testing of existing Whirlpool's prototype, S – steady state, T - transient

4.4 Experimental results

4.4.1 Data processing

Data were acquired on two separate computers thus the first step was to perform time synchronization. In the next data were analyzed in MS Excel for production

of graphs and tables. Excel was connected with Refprop Version 8 add-in to calculate refrigerant thermodynamic properties where needed.

As I mentioned before, during the testing I realized that suction pressure transducer acquisition system was not working properly and was giving “strange” results. It seemed that the mistake was in the software part of the Whirlpool’s acquisition system for the particular stand where I was testing. It wasn’t possible to get it repaired in short term thus I had to find other way to estimate evaporation temperature indirectly.

The thermocouples attached to the evaporator surface gave the indication about behavior of the evaporation temperature but real evaporation temperature is normally several degrees Celsius lower. I decided to use compressor data sheets to evaluate evaporation temperature. There are two ways how to do it, either starting from measured compressor power or from measured mass flow determined by mass flow meter. The running conditions of the circuit were outside of the data tables provided by manufacturer hence I extrapolated existing power and mass flow data by using physical compressor model and then fitted the data with 10 coefficients model recommended by (EN 12900, 2002), full procedure of extrapolation is described in the Appendix I. Thus I obtained power and mass flow equations. The compressor data are evaluated at 32°C suction temperature and I further corrected them by ratio of densities of the suction gas ($\rho_{suction}$) at corresponding measured suction temperature:

$$P_{RPM} = f(T_{evap}, T_{cond}, 10xcoeff_p) \frac{\rho_{suction}}{\rho_{32^\circ C}} \quad \text{eq 43}$$

$$\dot{m}_{RPM} = f(T_{evap}, T_{cond}, 10xcoeff_m) \frac{\rho_{suction}}{\rho_{32^\circ C}} \quad \text{eq 44}$$

Inverting these equations for each measurement point I got the evaporation temperature (T_{evap}) profile as a function of refrigerant properties, 10 coefficients, measured condensing and suction temperatures and power or mass flow. Solving of the implicit equations was done by numerical iterations. The resulting two evaporation temperatures (determined from power $T_{evap_{Power}}$ and $T_{evap_{Mass\ flow}}$) have uncertainty higher than $\pm 5\%$ because already uncertainty of data in compressor data sheet is $\pm 5\%$. Time averaged two evaporation temperatures calculated from the tests are reported in the Table 4.3. I decided to use evaporation temperature determined by power because I am surer about precision of power measurement, in addition mass flow measurement includes oil mass fraction circulating in the system and it’s not known how much it is. Relatively

	$T_{amb} = 26^{\circ}\text{C}$			$T_{amb} = 22^{\circ}\text{C}$	
RPM	1800	3000	4500	1800	3000
$T_{evap_{Power}} [^{\circ}\text{C}]$	-28.9	-33.2	-36.4	-29.2	-33.4
$T_{evap_{Mass\ flow}} [^{\circ}\text{C}]$	-27.0	-34.0	-38.2	-27.0	-34.1
Calculated vs measured values					
Power from $T_{evap_{Mass\ flow}}$	6.6%	-2.9%	-6.8%	7.5%	-2.6%
Mass flow from $T_{evap_{Power}}$	-10.1%	4.9%	13.6%	-11.4%	4.2%

Table 4.3 Evaporation temperatures determined by numerical calculation from tests

high discrepancy between calculated errors for power and mass flow especially at minimum and maximum compressor RPM, suggests that data sheet values at these conditions are probably not very precise.

This estimation of evaporation temperature has also an impact on the absolute value of COP but the relative measure between various compressor RPMs is indicated correctly.

RC air temperature was obtained as an average of three thermocouples placed in the compartment between T_A , T_M and T_B thermocouples with brass cylinder. Measured profiles of the RC air temperature are reported in the Figure 4.5.

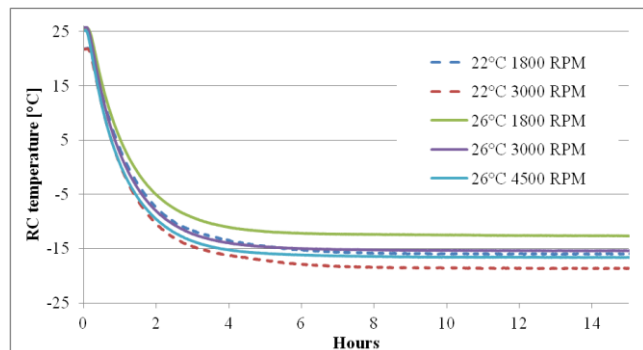


Figure 4.5 Measured average RC air temperatures during pull down tests performed at various RPM and ambient temperatures

4.4.2 Steady-state with continuously running compressor

After 15 hours of continuous running compressor the temperatures in the RC and of all the refrigeration circuit components stabilized. Steady-state with continuously running compressor was achieved. The results of these tests are thermal heat loads of the compartment at reached steady-state temperature which is directly equal to cooling capacity provided to the compartment. The cooling capacity is calculated from measured values according to the equation bellow:

$$Q_{evap} = \dot{m}(h_5 - h_3 + (h_1 - h_5)\epsilon_{SLHEX}) \quad \text{eq 45}$$

Where:

- \dot{m} is mass flow measured by coriolis device [gs^{-1}]
- h_1 , h_3 and h_5 are enthalpies determined from refrigerant's thermodynamic properties by pressures and temperatures in the points of the circuit shown in the Figure 4.1 [kJkg^{-1}]
- ε_{SLHEX} is capillary tube suction line heat exchanger efficiency taken from the Whirlpool's internal report and equals to 74%

I calculated Q_{evap} for all the tested conditions. Assuming that Q_{evap} is directly equal to heat load of the compartment I evaluated average thermal resistance of the complete RC compartment and results are presented in Table 4.4.

The compartment's thermal resistance is assembled from the convective and radiative heat transfer on the internal and external surfaces and conduction heat transfer within the walls. Convection and radiation heat transfers are dependent on the internal and external compartment temperatures. Compartment's walls are

	$T_{\text{amb}} = 26^{\circ}\text{C}$			$T_{\text{amb}} = 22^{\circ}\text{C}$		
RPM	1800	3000	4500	1800	3000	4500
Measured						
$T_{\text{amb}} [^{\circ}\text{C}]$	26.6	26.5	26.5	22.4	22.4	22.5
$T_{\text{evapPower}} [^{\circ}\text{C}]$	-33.6	-40.2	-43.3	-35.3	-40.1	-43.6
Mass flow [gs^{-1}]	0.197	0.211	0.227	0.187	0.199	0.203
$T_{\text{RC}} [^{\circ}\text{C}]$	-12.6	-15.4	-16.6	-16.0	-18.6	-19.1
Condensing pressure [Mpa]	0.517	0.523	0.529	0.470	0.471	0.476
$T_{\text{filter}} [^{\circ}\text{C}]$	32.4	33.0	33.5	28.2	28.4	28.7
$T_{\text{suction}} [^{\circ}\text{C}]$	24.7	25.0	25.5	20.7	20.7	21.2
$T_{\text{RC_evap_OUT}} [^{\circ}\text{C}]$	-24.6	-29.6	-31.0	-25.6	-31.5	-31.9
Calculated						
$T_{\text{cond}} [^{\circ}\text{C}]$	38.9	39.4	39.9	35.4	35.5	35.9
Evaporation pressure [Mpa]	0.039	0.028	0.024	0.036	0.029	0.024
$h_1 [\text{kJkg}^{-1}]$	599	600	601	593	593	594
$h_3 [\text{kJkg}^{-1}]$	277	278	279	266	267	268
$h_5 [\text{kJkg}^{-1}]$	522	516	514	521	513	513
ε_{SLHEX}	74%	74%	74%	74%	74%	74%
$Q_{\text{evap}} [\text{W}]$	59.5	63.2	67.9	57.5	60.8	61.9
$R_{\text{RC}} [^{\circ}\text{C}\text{W}^{-1}]$	0.66	0.66	0.64	0.67	0.68	0.67
Average $R_{\text{RC}} [^{\circ}\text{C}\text{W}^{-1}]$	0.652					

Table 4.4 Measured and calculated results from steady state analysis of pull down tests

made in majority from polyurethane (PU) foam and the PU's conduction coefficient is influenced by its temperature. Even though in the next the thermal resistance was supposed to be constant $0.652^{\circ}\text{C}\text{W}^{-1}$ so that I can evaluate thermal heat loads of the compartment at standard operating conditions and estimate energy consumption of the cycling RC at typical operating conditions.

4.4.3 Transient cooling of RC

Data between RC temperatures 8°C and 2°C were extracted from the results of pull down tests to imitate refrigerator cycling behavior between two set temperatures as it's visible in the Figure 4.6. These data gives practical idea about RC behavior during compressor ON cycle. Strong transient behavior at the beginning of real ON cycle is obviously not captured. It has an overestimating effect on the COP and also underestimates energy consumption. The heat load of the RC in this testing is higher because

freezer compartment is at the ambient temperature and there is additional load entering RC through mullion wall instead of heat leaving from RC to FC during standard operation. Higher RC thermal load however doesn't have a significant impact on the COP of the refrigeration circuit. On the other hand it influences the cycling frequency eq 30 and the

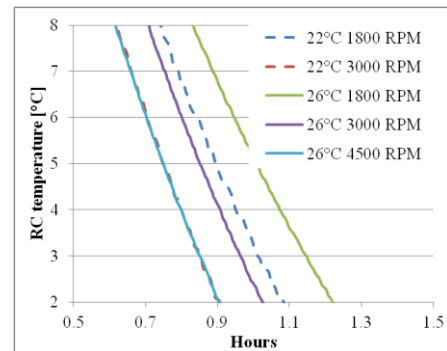


Figure 4.6 Extracted RC air temperature between 2°C and 8°C

higher the load the higher the frequency which causes higher energy consumption. Additional effect on the energy consumption might have thermal capacity of the refrigeration compartment walls which were not cold at the beginning of ON cycle as it is usual during typical appliance ON/OFF cycling. All these effects have impact on the energy consumption of the RC but only absent transient behavior at the beginning of the ON cycle effects the COP.

Extracted data were time averaged and are reported in the Table 4.5 for three tests at 26°C and two tests at 22°C . Evaporator surface temperature ($T_{\text{surf_evap}}$) was evaluated as an average between three thermocouples ($T_{\text{RC_evap_IN}}$, $T_{\text{RC_evap_MID}}$, $T_{\text{RC_evap_ACC}}$), which can be identified in the Figure 4.1. Refrigeration circuit subcooling (SC) was determined from difference between condensing temperature (T_{cond}) and filter/dryer temperature (T_{filter}). Compressor cylinder discharge

	T _{amb} = 26°C			T _{amb} = 22 °C	
RPM	1800	3000	4500	1800	3000
Tevap_{Power} [°C]	-28.9	-33.2	-36.4	-29.2	-33.4
T _{RC} [°C]	4.83	4.84	4.79	4.81	4.83
T _{RC_evap_IN} [°C]	-17.8	-19.3	-19.9	-18.0	-17.8
T _{RC_evap_MID} [°C]	-20.8	-22.7	-23.3	-20.3	-20.8
T _{RC_evap_ACC} [°C]	-15.5	-17.3	-19.0	-14.3	-15.5
T _{RC_evap_OUT} [°C]	-5.3	-5.9	-6.4	-5.1	-5.3
T _{surf_evap} [°C]	-18.0	-19.8	-20.7	-17.5	-18.0
T _{cond} [°C]	41.7	43.3	43.9	38.9	39.9
T _{filter} [°C]	35.3	37.1	37.8	31.7	32.8
SC [K]	6.3	6.2	6.2	7.2	7.1
T _{shell} [°C]	43.3	50.3	57.0	38.0	44.0
T _{cyl disch} [°C]	126	134	149	121	129
Q _{cond} [W]	83.9	111.7	132.5	84.2	113.8
Q _{comp} [W]	38.8	52.6	67.3	38.5	53.3
Q _{evap} [W]	74.8	97.6	110.8	76.6	101.0
Power [W]	44.0	62.8	83.6	43.2	62.0
Mass flow [gs ⁻¹]	0.273	0.306	0.324	0.279	0.314
COP	1.70	1.55	1.32	1.78	1.63

Table 4.5 Measured and calculated results from transient part of pull down tests

temperature (T_{cyl disch}) was calculated from thermodynamic properties of the refrigerant based on the following equations:

$$T_{real\ discharge} = f(p_{cond}, h'_2, R600a) \quad \text{eq 46}$$

$$h'_2 = h_1 + \frac{P}{\dot{m}} \quad \text{eq 47}$$

Where:

- h'₂ is enthalpy of the refrigerant at the cylinder discharge condition assuming no pressure drop [kJkg⁻¹]
- h₁ is enthalpy at suction condition to the compressor [kJkg⁻¹]
- P is measured power of the compressor [W]

- \dot{m} is measured mass flow [gs^{-1}]
- p_{cond} is condensing pressure [Mpa]

Heat rate dissipated at the condenser side Q_{cond} and from the compressor shell Q_{comp} were determined from cycle enthalpies and measured mass flow:

$$Q_{\text{cond}} = \dot{m}(h_2 - h_3) \quad \text{eq 48}$$

$$Q_{\text{comp}} = \dot{m}(h'_2 - h_2) \quad \text{eq 49}$$

Where:

- h_2 is enthalpy at compressor discharge condition [kJkg^{-1}]
- h_3 is enthalpy at subcooled refrigerant liquid at the filter/dryer [kJkg^{-1}]

Cooling capacity given to the compartment Q_{evap} is calculated according to the eq 45. And operation RC COP was evaluated by eq 37.

4.4.3.1 Results for COP and evaporation temperature

Results for evaporation temperature and COP are plotted also in the Figure 4.7 as a function of compressor RPM. It's possible to see that with decreasing compressor RPM the evaporation temperature is rising which perfectly corresponds with the theory described in the chapter 2.2.3. Moving from nominal 3000RPM to 1800 RPM led to increase in evaporation temperature from -33.2°C to -28.9°C which is 4.3K higher. However interesting part of the results is also that the evaporation temperature remains almost unchanged for different ambient

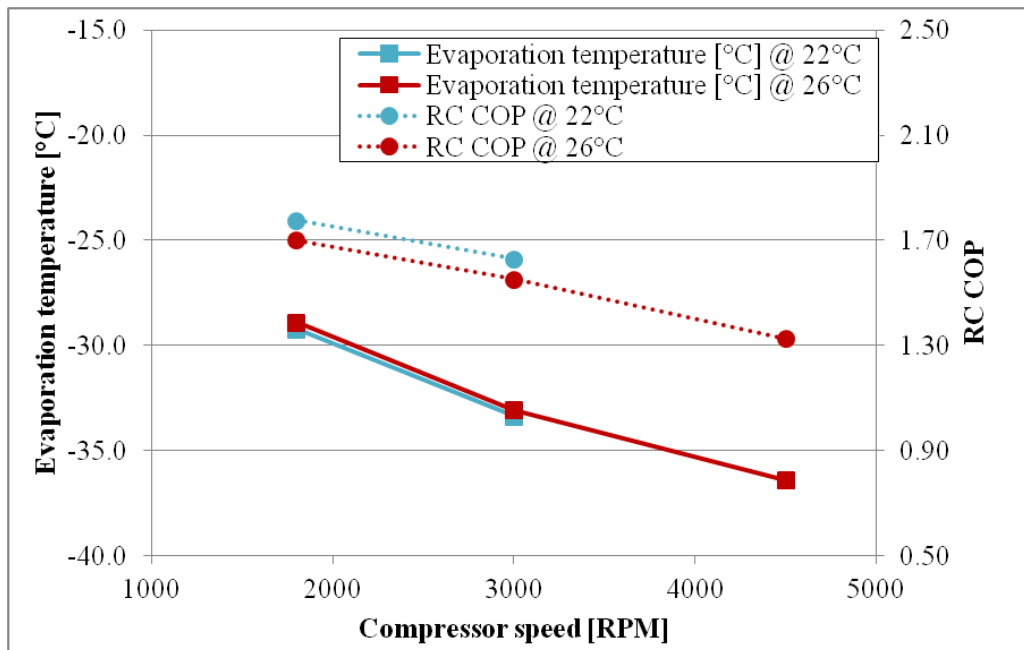


Figure 4.7 Evaporation temperature and COP as a function of compressor RPM

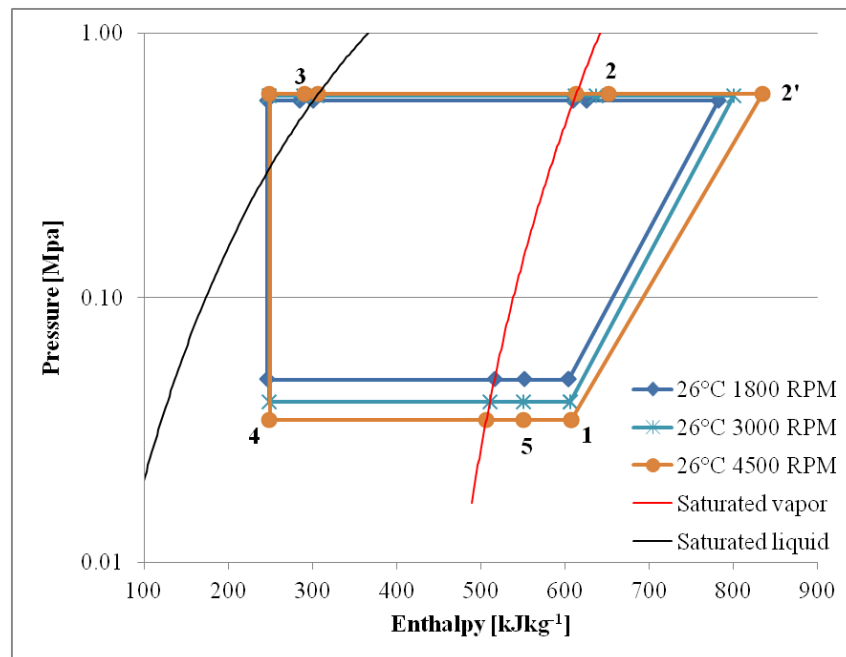


Figure 4.8 Refrigeration cycles with varying RPM in p-h diagram

temperatures. Thus the compartment heat load doesn't have a significant effect on the evaporation temperature.

Direct consequence of increased evaporation temperature in RC at lower RPM is also higher compartment COP. Reducing compressor RPM from 3000 to 1800 led to the measured improvement in COP from 1.55 to 1.70 and represented almost 10% COP increase. In the case of COP lower ambient temperature has also a small positive effect on the COP. It is mainly caused by slightly lower condensing temperature and slightly higher SC and thus also Q_{evap} .

The measured points of the refrigeration circuit were plotted for various tests to the pressure enthalpy diagram (p-h), Figure 4.8 and Figure 4.9. In the Figure 4.8 are compared three refrigeration cycles at the same ambient temperature with different compressor RPM. It's nicely possible to see the impact of RPM on the shape of the refrigeration cycles. The delta enthalpy on the evaporator side between points 4 and 5 is almost preserved for all RPMs even though evaporation temperature strongly increases. Significant change is though observed in the slope of the 1-2' line between 4500RPM and 3000RPM which represents compressor isentropic efficiency improvement from 59% to 64% respectively. Enthalpy difference between points h'_2 and h_2 describes amount of heat dissipated by the compressor shell. At higher RPM higher amount of heat has to be dissipated from high pressure refrigerant to the environment, large part of this increase is covered

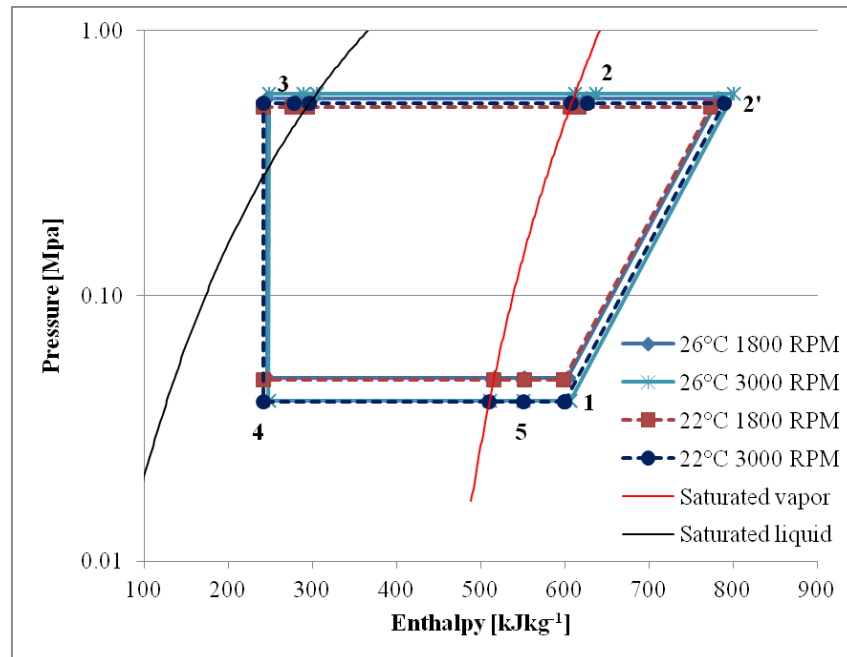


Figure 4.9 Refrigeration cycles with varying RPM in p-h diagram

by dissipation from the compressor shell. P-h diagram also shows minimal impact of RPM on the refrigerant subcooling. The Figure 4.9 compares four refrigeration cycles with two ambient temperatures and two RPM. Here is possible to observe almost negligible impact of the ambient temperature on the shape of the cycles, except lowering the condensing temperature.

4.4.3.2 Thermal resistances

Components exchanging heat in the RC cycle are mainly condenser, evaporator and compressor shell. From the measured results characteristic thermal resistances of all these components (R_{cond} , R_{shell} and R_{evap}) were evaluated and are reported in the Table 4.6. Resistances of condenser and compressor were further used in the steady-state simulation introduced in the chapter 5.

Evaporator thermal resistance was in addition split to air thermal resistance R_{air} and refrigerant-evaporator wall resistance R_{ref} based on the measured evaporator surface temperature. Comparing the results of measured air thermal resistance with simulation performed in chapter 3.2.4 and rerunning the simulation for 1800, 3000 and 4500RPM we can observe a match for the resistances at various speeds within 20% error band showed in the Table 4.6. In addition measured air heat transfer resistance varies stronger with RPM than the calculated one. In any case

the air thermal resistance remains the bottleneck of the heat transfer to the evaporating refrigerant. If we look at the refrigerant side thermal resistance we can see large discrepancy between simulation and measurement, where measured refrigerant resistance is much

higher than the estimated one. Besides measured refrigerant resistance in the evaporator varies slightly with RPM and reaches minimum at 3000 RPM, this may be related to refrigerant filling of the evaporator. Further investigations would be necessary to examine refrigerant two-phase and single-phase regions which strongly influence thermal resistance but this was not part of this PhD activity.

Compressor shell thermal resistance was calculated based on the heat dissipated from the shell Q_{comp} and the temperature lift between ambient temperature T_{amb} and cylinder discharge temperature $T_{cyl\ disch}$ (eq 46). Experimentally evaluated global heat transfer coefficients of the compressor UA_{comp} were in the next plotted as a function of $T_{cyl\ disch}$ and linear correlation was developed, Figure 4.10:

	Tamb = 26°C			Tamb = 22 °C	
RPM	1800	3000	4500	1800	3000
Measured					
$R_{cond} [^{\circ}CW^{-1}]$	0.180	0.150	0.131	0.196	0.154
$R_{comp} [^{\circ}CW^{-1}]$	2.558	2.049	1.824	2.561	1.989
$R_{evap} [^{\circ}CW^{-1}]$	0.451	0.390	0.372	0.415	0.385
Evaporator					
$R_{air} [^{\circ}CW^{-1}]$	0.611	0.504	0.461	0.584	0.453
$R_{ref} [^{\circ}CW^{-1}]$	0.291	0.276	0.283	0.246	0.318

Simulation results from chapter 3.2.4

$R_{air} [^{\circ}CW^{-1}]$	0.572	0.558	0.551
Error of R_{air}	-6%	11%	20%
$R_{ref} [^{\circ}CW^{-1}]$	0.08	0.08	0.08

Table 4.6 Measured thermal resistances of condenser, evaporator and compressor. Evaporator resistances compared to simulation.

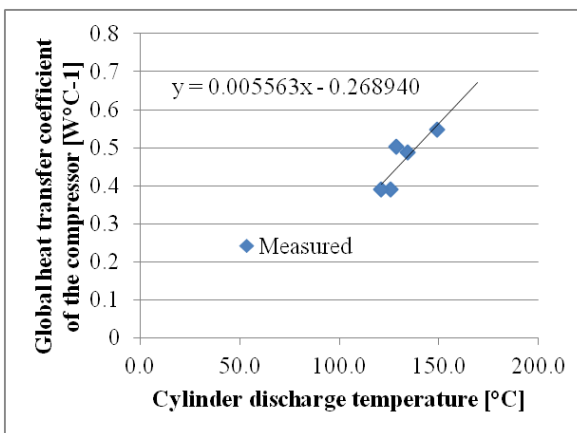


Figure 4.10 Global heat transfer coefficient of the compressor as a function of $T_{cyl\ disch}$

$$UA_{comp} = \frac{1}{R_{comp}} = 0.00556T_{cyl\ disch} - 0.269 \quad \text{eq 50}$$

According to the results in the previous chapter heat transfer rate from the compressor shell plays significant role in energy efficiency of the refrigeration circuit, therefore I used this correlation in the steady-state simulation in the chapter 5 to calculate this heat rate.

4.4.3.3 RC energy consumption

From the extracted data between 2°C and 8°C I could determine the energy consumption and time duration of compressor ON period. From steady-state results I estimated thermal resistance of the compartment and thus I was able to calculate heat load of the RC at different ambient temperatures. Heat load of RC at ambient temperature 26°C was calculated to be approximately 33.3W and at 22°C 27W which is 19% lower. All these results are summarized in the Table 4.7. In addition by using eq 23 and eq 30 the RC cycling frequency was determined and also the RC daily energy consumption could be estimated.

Predicted RC energy consumption based on the results from pull down tests is influenced by several factors such as missing transient behavior at the compressor start up, higher heat load of RC because FC was not operating and not considering the thermal capacity of the compartment in the cycling frequency calculation. However, the basic behavior of energy consumption related to the RPM and ambient temperature was preserved. Results of daily RC energy consumption and measured compressor ON time as a function of RPM and ambient temperature are plotted in Figure 4.11. It's possible to see that the compressor ON time decreases

RPM	T _{amb} = 26°C			T _{amb} = 22 °C	
	1800	3000	4500	1800	3000
Time of ON cycle [min]	23.3	18.9	17.2	20.5	17.0
Energy consumption [Wh/cycle]	17.1	19.8	24.0	14.7	17.6
RC heat load [W]	33.4	33.3	33.3	27.0	27.0
Energy removed in [Wh/day]	801	799	800	647	648
Frequency [1/day]	27.6	26.0	25.2	24.7	22.7
Energy consumption [Wh/day]	471	514	604	364	398
Energy consumption improvement	-8%	0%	17%	-29%	-23%

Table 4.7 RC energy consumption and cycling frequency results

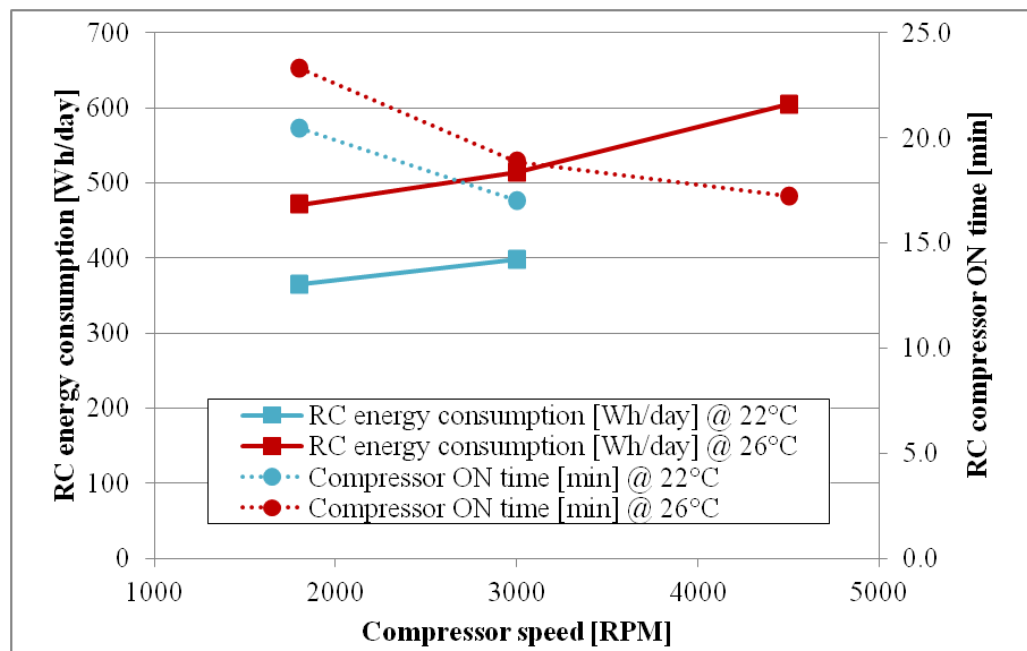


Figure 4.11 RC energy consumption and compressor ON time as a function of compressor RPM and ambient temperature

with higher RPM, because higher cooling capacity is delivered to the RC at higher RPM.

If 3000 RPM is considered to be nominal speed then, by running compressor at 1800 RPM we can save up to 8% of electrical energy during RC operation. On the other hand if we run the compressor at maximum 4500 RPM we will consume 17% more electrical energy. In addition if we decreased ambient temperature by 4°C from 26°C to 22°C we can save 23% of energy at nominal compressor speed or even 29% if RPM is lower to 1800 RPM.

4.5 Thermodynamic second law analysis

Second law analysis is not very often used in the refrigeration field. However to give a proper explanation of the efficiency improvement at low compressor RPM it is worth looking at the evolution of losses of each single process and component analyzed by second law of thermodynamics as a function of compressor speed. By quantifying losses I can judge which component has the highest potential to further improve efficiency. Important processes and components are easily recognizable in the temperature entropy (T-s) diagram. I have plot results of three tests at 26°C with three different compressor RPMs to the T-s diagram, Figure 4.12. From the first look it's possible to see that area of the diagram is

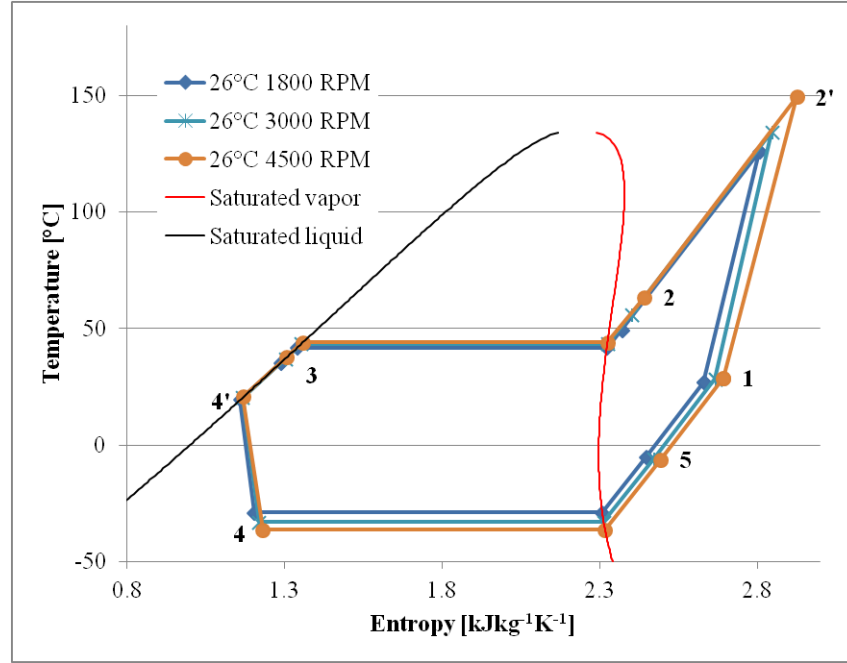


Figure 4.12 Refrigeration cycles with varying RPM in T-s diagram

significantly increased for higher RPM even though the changes of useful refrigeration effect (area under 4-5 line) are minor.

Following equations were applied to identify irreversible losses related to each component or process (Galliani, et al., 2006), (He, et al., 2008).

Compressor – compression process (1-2'):

$$Q_{irr\ comp} = \dot{m}((h_1 - h_{2'}) - (s_1 - s_{2'})T_{amb}) + P \quad \text{eq 51}$$

Compressor – shell heat dissipation (2'-2):

$$Q_{irr\ shell} = \dot{m}((h_{2'} - h_2) - (s_{2'} - s_2)T_{amb}) \quad \text{eq 52}$$

Condenser (2-3):

$$Q_{irr\ cond} = \dot{m}((h_2 - h_3) - (s_2 - s_3)T_{amb}) \quad \text{eq 53}$$

Capillary (4'-4):

$$Q_{irr\ cap} = T_{amb}\dot{m}(s_4 - s_{4'}) \quad \text{eq 54}$$

Evaporator (4-5):

$$Q_{irr\ evap} = \dot{m}((h_4 - h_5) - (s_4 - s_5)T_{amb}) - P_{carnot} \quad \text{eq 55}$$

Suction line heat exchanger (SLHEX) (3-4' and 5-1):

$$Q_{irr\ SLHEX} = \dot{m}((h_3 - h_{4'}) - (s_3 - s_{4'})T_{amb}) + \dot{m}((h_5 - h_1) - (s_5 - s_1)T_{amb}) \quad \text{eq 56}$$

In addition Carnot power was computed to assess system second law efficiency:

$$P_{carnot} = \dot{m}(h_4 - h_5) \left(\frac{T_{amb}}{T_{RC}} - 1 \right) \quad \text{eq 57}$$

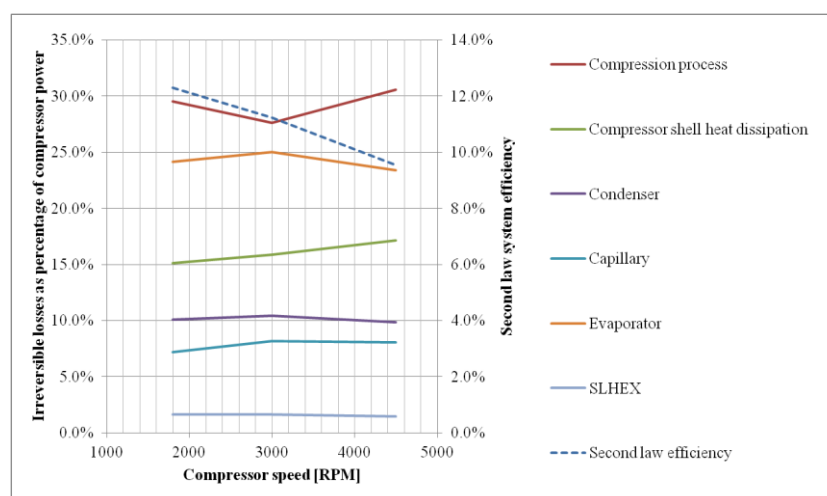


Figure 4.13 Irreversible losses of RC loop components and refrigeration cycle second law efficiency as a function of compressor RPM

All losses are integrated over the compressor ON time and in the following are expressed as percentage of electric power consumed by the compressor. Evolution of losses in the components at various speeds during 26°C ambient tests is shown in Figure 4.13.

From the second law analysis it can be concluded that the energy improvement at 3000RPM versus 4500RPM is caused exclusively by compressor, compression process and heat dissipation of the compressor shell. Losses of all other components are constant or increasing and causing degradation of system efficiency. On the other hand the efficiency improvement from 3000RPM to 1800RPM is mainly driven by compressor shell heat dissipation, evaporator and capillary tube. In this part the compression losses are rising because isentropic efficiency of the compressor is decreasing. I can conclude that this compressor was built to run at 3000RPM nominal speed.

Analysis also points out the components with highest irreversible losses. Compressor (compression process and shell heat dissipation) is on the first place with more than 40% of losses directly followed by evaporator with close to 25% of losses. Second law energy efficiency increases with lowering RPM from around 10% at 4500 RPM to almost 13% at 1800 RPM and causes increase in RC COP from 1.32 to 1.7 respectively.

4.6 Conclusions

I tested Whirlpool's existing prototype in the environmental chamber at two ambient temperatures. The manual control equipment allowed me to perform

temperature pull down tests of single compartment at various compressor RPM until steady-state temperatures were reached all around the running refrigeration circuit.

Even though pressure transducers were calibrated at the testing stand before starting the testing, acquisition of low pressure transducer was not working properly. Instead I used measured power to identify evaporation temperature by backward calculation through compressor data sheets. I understood that separate acquisition system for pressure transducers signal is required for further testing of appliance.

Test results were divided into steady-state with continuously running compressor and transient part between RC air temperature levels 2°C and 8°C. Steady-state results were used to calculate heat load and thermal resistance of the refrigeration compartment. I considered the refrigeration compartment thermal resistance to be average between all the measured results equal to 0.652°CW⁻¹.

Extracted data between 2°C and 8°C T_{RC} imitated real cooling period of RC at various compressor RPM. Confirming theoretical investigation evaporation temperature was rising with decreasing RPM. It raised by 7.5K from -36.4°C to -28.9°C by reducing compressor RPM from 4500RPM to 1800RPM. Evaporation temperature was also found to be independent from ambient temperature or compartment heat load. I determined also the compartment COP which reacts on the behavior of the evaporation temperature and it was rising from 1.32 to 1.7 with decreasing compressor RPM from 4500 to 1800RPM at 26°C. In addition lower ambient temperature had a slight positive effect on the operation COP.

By using thermal resistance of the compartment measured during steady-state I could determine also RC energy consumption per day. By reducing compressor RPM from 3000 to 1800RPM the daily energy consumption of the RC decreased by 8% from 514Wh/day to 471Wh/day. Reducing ambient temperature by 4°C we can save approximately 23% of electric energy and even 29% if also RPM of the compressor is reduced to 1800RPM.

Based on the heat transfer rates I calculated also thermal resistances of significant heat exchanging components such as condenser, evaporator and compressor shell. Evaporator resistance was further split to air side resistance and refrigerant side. Air resistance matched within 20% with predicted values from theoretical analysis. Refrigerant resistance was largely underestimated during the theoretical study. The air resistance remained to be the bottleneck of heat transfer to the evaporating liquid.

In the last part I performed second law analysis of the measured data at 26°C ambient temperature. From losses decomposition chart the compressor was identified as component with maximum share of the losses accounting for more than 40% of compressor power consumption. Evaporator was determined to be component with the second highest losses equal to almost 25% of compressor power. Energy efficiency improvement at 1800 compressor RPM arrives mainly from improvements in compressor shell and evaporator heat transfer and capillary tube. 3000RPM was identified as nominal speed of the compressor with minimum compression process losses.

5 Steady-state refrigeration circuit simulation

The purpose of my steady-state modeling was to estimate response of RC loop components of the SDE circuit to the increased evaporation temperature. The target was to predict mainly the impact on the RC COP. Placing phase change material in direct contact with the evaporator surface changes heat transfer mode from air natural convection and radiation to conduction in the PCM and the effect is increased evaporation temperature. However it's not so clear what effect has higher evaporation temperature on the compressor shell heat dissipation and condensing temperature which also influence the resulting COP.

There is large number of refrigeration circuit models introduced in the scientific literature. They range from first principle (Hermes, et al., 2008) to more empirical models (Gonçalves, et al., 2009) and from steady-state (Goncalves, et al., 2004) through quasi-steady (Borges, et al., 2011) to fully transient models (Carsten, et al., 2006). Most of the approaches are mathematically and numerically very complex and require also extensive model calibration before utilization. Most promising direction in modeling refrigeration circuit seems to be modular object oriented approach described by (Richardson, 2006). The model of any type of the refrigeration system (energy system) can be built from components which exchange information between them through structured framework based on the global balance equations of mass, momentum and energy. The component models are usually treated as “black box” objects and only inputs and outputs are important. Modular approach is used also in the commercial software for energy simulations such as Aspen and Dymola.

Without access to the refrigeration component libraries utilization of modular approach is still relatively difficult. Thus I decided to use the simplest steady-state modeling approach for refrigeration circuit very similar to the one presented in (Borges, et al., 2011). Main simplification is in prescribing condenser subcooling (SC) and evaporator superheat (SH). In my simulation both SC and SH were calculated based on the assumption of 10K approach point of condenser and evaporator. During the prototype testing at different compressor RPMs I could see that the SC and SH was almost invariant.

5.1 Model description

For further analysis of the RC loop efficiency in SDE circuit I developed a very simple numerical model. Model is a steady-state, based on compressor data sheets and experimentally measured overall heat transfer coefficients of compressor shell, condenser and evaporator. I considered several standard assumptions for models of refrigeration circuit; no pressure drop in heat exchangers, isenthalpic expansion in capillary and negligible kinetic and potential energy. Other assumptions which I took into account were introduced mainly to keep simplicity and speed of the model with reasonable results prediction:

- Uniform temperature 4.5°C in the RC
- Approach points of condenser and evaporator are constant 10K
- Compressor suction temperature is equal to the ambient temperature
- Constant efficiency of suction line capillary tube heat exchanger

Refrigeration circuit simulation model is built on four main components, compressor, capillary tube suction line heat exchanger, condenser and evaporator as it's possible to see in the Figure 5.1. Each component has to satisfy three balance equations (mass, momentum and energy). Mass balance equations are implicitly fulfilled by assuming single mass flow rate in the full system. Steady-state approach directly avoids any refrigerant mass accumulation in single components. Momentum balance equations are neglected by assumptions of no pressure drop, no kinetic and potential energies. Therefore only the energy balance equations remained to be solved. The system is composed of 19 equations comprising nonlinear equations of fluid state properties.

Each refrigeration circuit component has its energy balance equation from eq 58 to eq 62 and supplementary equations. Compressor model including heat dissipation model from the compressor shell is described by five equations from eq 63 to eq 67. Compressor power and mass-flow are corrected by suction gas density

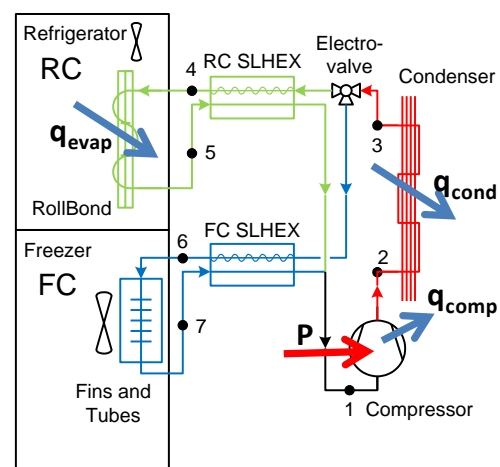


Figure 5.1 RC loop steady state-model

at suction temperature and are calculated by polynomials with 10 coefficients at various RPM. The coefficients were fitted to the compressor data sheet and extrapolated outside of the compressor operation envelope through isentropic and volumetric efficiency fits. The procedure is described in Appendix I. Compressor shell global heat transfer coefficient (UA_{shell}) is a linear function of cylinder discharge temperature fitted to the experimental results according to the eq 50. Heat transfer processes are described by eq 68 to eq 70 for evaporator, condenser and suction line heat exchanger. Suction line and capillary tube heat exchanger is modeled in the way that liquid subcooling happens before expansion and expansion in the capillary tube itself is isenthalpic. Suction line heat exchanger has constant heat transfer efficiency, equal to 74%. Condenser thermal resistances determined in chapter 4.4.3.2 are used in this simulation and eq 71 says that UA_{cond} is only a function of compressor RPM. Refrigerant states properties at different points of the refrigeration cycle are represented by eq 72 to eq 76. Effect of PCM on the refrigeration circuit operation condition is modeled simply as an increase in UA_{evap} value, even though theoretically this change is closer to increased air flow or area of the evaporator.

All the calculations are performed in MS Excel using macros and solver function. Fluid properties are imported to MS Excel calculation sheet with direct link to refprop database. Model can be easily implemented also to the engineering equation solver software (EES) which has an advantage of included refrigerant property database and much more efficient solver.

5.1.1 Mathematical model

Components energy balances:

$$P - q_{comp} = \dot{m}(h_1 - h_2) \quad \text{eq 58}$$

$$q_{cond} = \dot{m}(h_2 - h_3) \quad \text{eq 59}$$

$$q_{sthex hot} = \dot{m}(h_3 - h_4) \quad \text{eq 60}$$

$$q_{evap} = \dot{m}(h_5 - h_4) \quad \text{eq 61}$$

$$q_{sthex cold} = \dot{m}(h_1 - h_5) \quad \text{eq 62}$$

Compressor supplementary equations:

$$P = f(T_{evap}, T_{cond}, RPM) \frac{\rho_{25}}{\rho_{32}} \quad \text{eq 63}$$

$$\dot{m} = f(T_{evap}, T_{cond}, RPM) \frac{\rho_{25}}{\rho_{32}} \quad \text{eq 64}$$

$$q_{comp} = UA_{shell}(T_{cyl\ disch} - T_{amb}) \quad \text{eq 65}$$

$$UA_{shell} = 0.00556T_{cyl\ disch} - 0.269 \quad \text{eq 66}$$

$$T_{cyl\ disch} = f(T_{amb}, T_{evap}, T_{cond}, P) \quad \text{eq 67}$$

Heat transfer equations for evaporator, condenser and suction line heat exchanger with capillary tube:

$$q_{cond} = UA_{cond}(T_{cond} - T_{amb}) \quad \text{eq 68}$$

$$q_{evap} = UA_{evap}(T_{RC} - T_{evap}) \quad \text{eq 69}$$

$$q_{slhex\ hot} = \varphi_{slhex}q_{slhex\ cold} \quad \text{eq 70}$$

$$UA_{cond} = f(RPM) \quad \text{eq 71}$$

Refrigerant state properties:

$$h_1 = f(p_{evap}, T_{amb}) \quad \text{eq 72}$$

$$h_3 = f(p_{cond}, T_{amb} + \Delta T_{app\ cond}) \quad \text{eq 73}$$

$$h_5 = f(p_{evap}, T_{RC} - \Delta T_{app\ evap}) \quad \text{eq 74}$$

$$T_{cond} = f(p_{cond}, x_0) \quad \text{eq 75}$$

$$T_{evap} = f(p_{evap}, x_0) \quad \text{eq 76}$$

Variables and constants applied in the simulation model are summarized in the Table 5.1.

Variables:				
P	$q_{slhex\ hot}$	UA_{cond}	$T_{cyl\ disch}$	h_2
\dot{m}	q_{evap}	UA_{shell}	p_{cond}	h_3
q_{cond}	$q_{slhex\ cold}$	T_{cond}	p_{evap}	h_4
q_{comp}		T_{evap}	h_1	h_5

Constants:	
$T_{amb} = 25^\circ\text{C}$	$T_{RC} = 4.5^\circ\text{C}$
$\Delta T_{app\ cond} = 10\text{K}$	$\varphi_{slhex} = 0.74$
$\Delta T_{app\ evap} = 10\text{K}$	RPM
$x_0 = 0$	UA_{evap}

Table 5.1 Variables and constants of the refrigeration circuit model

5.2 Results of the simulation

After the compressor the RC evaporator is the second most inefficient component in the system and this is mainly because of high temperature lift between evaporation temperature and RC air temperature, therefore the numerical model was used to forecast RC COP at increased evaporation temperatures at various

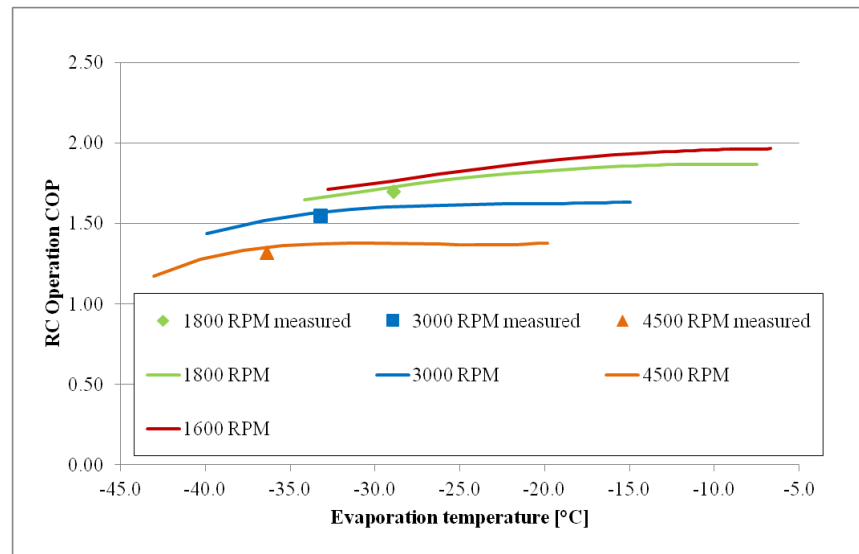


Figure 5.2 Impact of evaporation temperature on RC COP at various compressor RPM including comparison with measured COP

compressor RPM and the results are reported in the Figure 5.2. I displayed in the Figure 5.2 also measured RC COP from previous experimental chapter. Running compressor at minimum allowed speed 1600RPM and reserving evaporator heat transfer coefficient can bring further 4% increase in COP to 1.76 versus 1.7 at 1800RPM. In the Figure 5.2 it's also evident certain asymptotical behavior of the COP at increased evaporation temperatures. For minimum RPM this is reached at evaporation temperatures higher than -10°C where COP approaches maximum 1.97 equal to 16% improvement versus currently best measured COP at 1800RPM. The reason for limited and relatively small (only 16%) COP gain at high evaporation temperatures is caused by increasing condensing temperature. Higher mass flow pumped by the compressor at elevated evaporation temperature extracts more heat from the compartment and hence also more heat needs to be dissipated at the condenser side. Constant UA_{cond} then forces condensing temperature to rise.

In the following analysis I played also with the UA_{cond} . I simulated two different modifications, constant condensing temperature 45°C (dashed lines) and doubled UA value of the condenser (dotted line), Figure 5.3. Baseline was selected to be the best measured result at 1800RPM (0% COP improvement) 1.7 COP. The numerical model results showed rapid possibility for improvement in the RC COP up to 50% at evaporation temperatures higher than -10°C with modifications of UA_{cond} values.

Interesting is that the combined change on both the condenser and evaporator sides offers much more effect than just the simple sum of changes made separately. If only the UA_{cond} value is doubled the COP could increase by 14% at 1600 RPM. If only the evaporation temperature is raised to -10°C the COP could raise by 15%. But if we perform both changes in the same time the COP could approach 44% improvement which is 15% more than the simple sum of the changes described before.

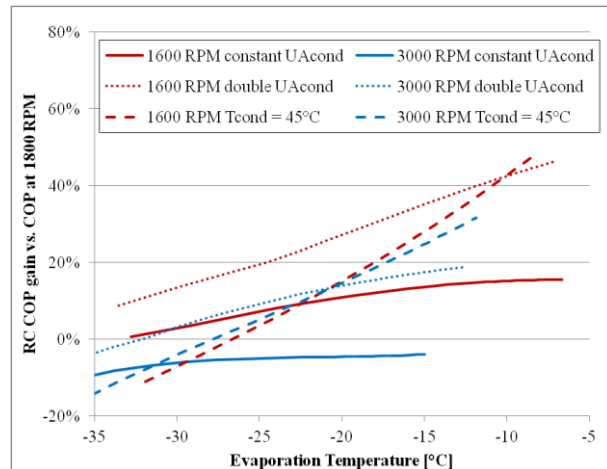


Figure 5.3 RC COP improvement with doubled UA_{cond} and at constant $T_{\text{cond}}=45^{\circ}\text{C}$ as a function of compressor RPM and evaporation temperature

5.3 Second law analysis

On the results of numerical simulation I performed the same second law analysis as in the chapter 4.5. I analyzed the same components and processes as before for three cases of changes in the condenser side with compressor running at constant 1600 RPM and increasing evaporation temperature.

1. No change on the condenser side
2. Doubled UA_{cond}
3. Constant condensing temperature

Irreversible losses of the components are plotted as a function of increasing evaporation temperature in the following figures for each case.

The first case is presented in the Figure 5.4. With increasing evaporation temperature (T_{evap}) the irreversible losses of evaporator, capillary tube and compressor shell are dropping down. Evaporator loss is decreasing the most

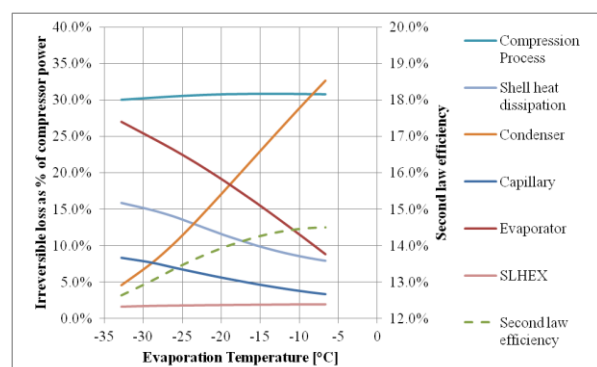


Figure 5.4 Decomposition of the losses for case 1

and at -10°C evaporation temperature reaches loss equal approximately to 12% of power consumption. Efficiency of compression process and SLHEX stayed almost constant with changing evaporation temperature. Condenser loss in % of the power is on the other hand rising significantly and at -10°C T_{evap} it's reaching almost 30% of power consumption. The second law efficiency gets to 14.5% at -10°C T_{evap} .

In the second case represented in the Figure 5.5 with doubled UA_{cond} value the trends are similar to the first case. However the condenser loss arrives to 22% of power consumption and the loss during the compression process is not anymore constant but it slightly rises. The second law efficiency approaches 18% at -10°C T_{evap} .

The third case in the Figure 5.6 with constant $T_{\text{cond}} = 45^{\circ}\text{C}$ shows slightly different behavior of the evaporator and also of the compressor process versus second case but the results at -10°C corresponds to each other. This is because condensing temperature in case two is changing with evaporation temperature and at -10°C T_{evap} it is very close to 45°C . Also the second law efficiency in the case three at -10°C T_{evap} is near to 18%.

In the Figure 5.7, I summarized results from all three cases at -10°C evaporation temperature and also the starting condition without any increase in evaporation temperature. On the left y-axis is the power consumption and on the right is reported cooling capacity. In the chart it's possible to see how much each component irreversible loss represents in watts. Carnot work represents minimum power required to run the cycle if it would be fully reversible one. Sum of all the losses

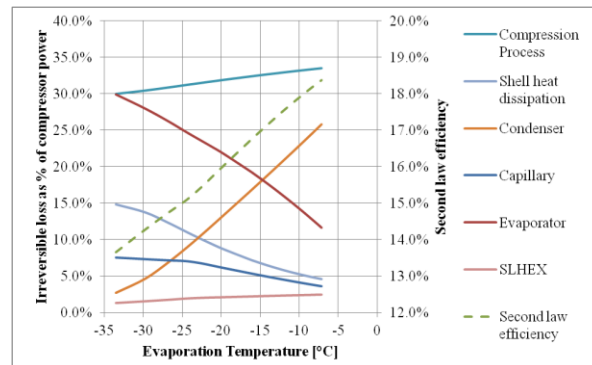


Figure 5.5 Decomposition of the losses for case 2 double UA_{cond}

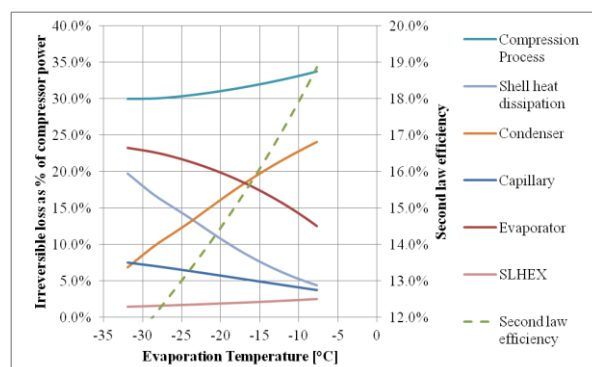


Figure 5.6 Decomposition of the losses for case 3 constant $T_{\text{cond}}=45^{\circ}\text{C}$

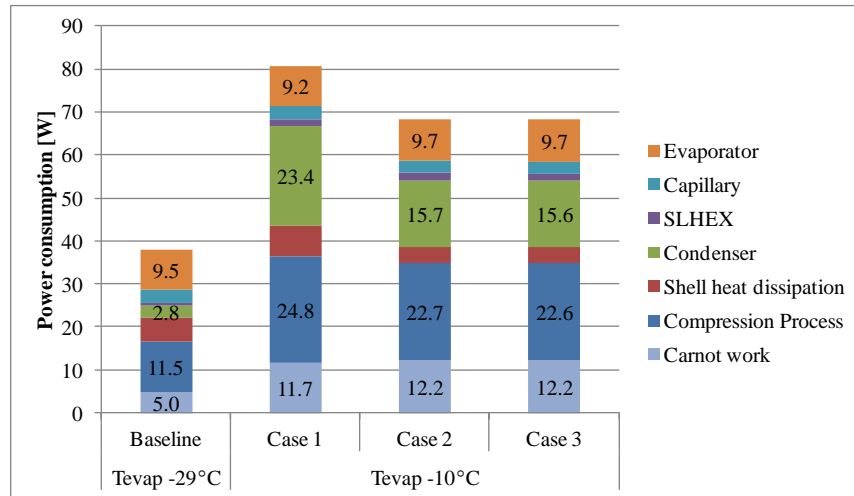


Figure 5.7 Comparison of irreversible losses for three cases and baseline in terms of power consumption, all at compressor speed 1600RPM

and of the Carnot work gives power consumption of the real compressor. In the first column the total power consumed is much smaller than for other cases even if baseline is the least efficient. The reason for that is a lower mass flow pumped at -29°C compared to -10°C evaporation temperature.

If we divide the columns by respective mass flow we obtain specific exergy losses related to each component. In other words specific exergy is in some sense representing area in the T-s diagram and it represents the second law losses of the components. The specific exergy is showed in the Figure 5.8 from where it's possible to see overall relative losses of the system and of each component. The baseline evaporating at -29°C is the least efficient and cases 2 and 3 are equally

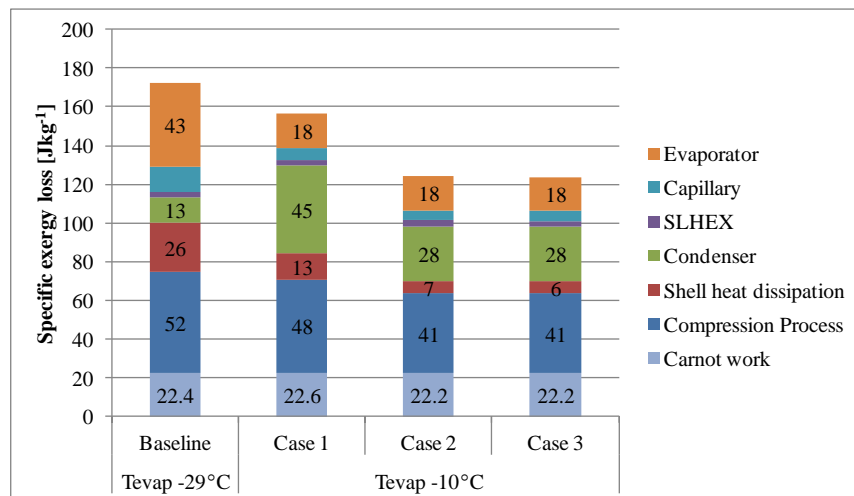


Figure 5.8 Comparison of irreversible losses for three cases and baseline in terms of specific exergy, all at compressor speed 1600RPM

most efficient. Moving from baseline to case 1 we can see that specific exergy losses of the condenser raised significantly and losses of evaporator and compressor decreased. In the further step to the case 2 and 3 the losses of the condenser were reduced by higher UA_{cond} value and the action reduced also the losses on the condenser side.

5.4 Conclusions

I developed a simple steady-state refrigeration cycle simulation based on the empirical data measured in the chapter 4. The purpose was to analyze the behavior of the refrigeration circuit components at increased evaporation temperature.

Running compressor at minimum RPM brings improvement in the COP. I showed that by increasing global heat transfer coefficient of the evaporator the evaporation temperature raises. Operating the refrigeration cycle at -10°C T_{evap} and at minimum speed 1600 RPM the COP can improve by 15% versus the measured value 1.7 at 1800 RPM in chapter 4. In addition if the change in evaporation temperature is complemented with the change on the condenser side the COP can increase up to 44% at the -10°C evaporation temperature.

From the second law analysis I determined that the components responsible for the improvement in the COP at elevated evaporation temperature are mainly evaporator, capillary tube and shell dissipation of the compressor. The components that degrade the improvement are mainly the condenser and slightly also compression process in the compressor.

Therefore I can recommend that the prototypes with PCM pocket attached to the evaporator should be equipped also by more efficient condenser or forced convection condenser.

The results of the chapter 4 and 5 were presented in summer 2012 at the 10th IIR Gustav Lorentzen Conference on Natural Refrigerants in Delft and also published in the conference proceedings (Visek, et al., 2012).

6 Experimental testing of conceptual prototypes

In the chapter 3 I performed theoretical analysis of sequential dual evaporation refrigeration system and made proposals of two conceptual SDE circuit designs including phase change material in contact with RC roll-bond evaporator Figure 6.1 and subcooling loop passing through PCM during freezer operation Figure 6.2. In this chapter I describe prototypes built according to the concepts and gathered experiences. After that I experimentally tested prototypes to confirm efficiency improvement potential. In the last part I discuss and analyze the experimental results for different various prototypes setups.

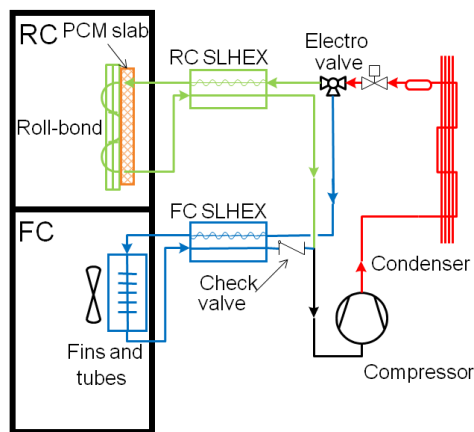


Figure 6.1 Prototype 1 (SDE-PCM)

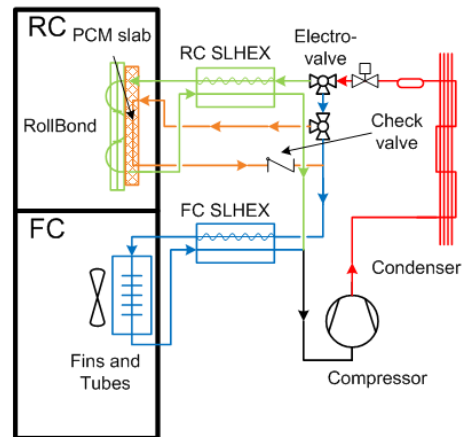


Figure 6.2 Prototype 2 (SDE-PCM-SC)

6.1 Objective of the experimental testing

Main objective of this experimental testing was to prove that placing PCM in direct contact with the RC roll-bond evaporator increases evaporation temperature and make the SDE refrigeration circuit run more efficiently.

Second objective was to verify that subcooling loop can shift load from freezer to refrigeration compartment and in this way increase overall appliance COP.

In addition I wanted to verify the importance of the FC check valve (FC-CV) and pump out (P/O) operation on the efficiency of the SDE circuit while dealing with refrigerant charge migration issues.

6.2 Prototype built

Both appliance prototypes were built based on the cabinet of bottom-mount built-in appliance. External dimensions of the refrigerator-freezer are 1735x540x514mm, height x width x depth. Storage volumes are 209 and 83 L for refrigerator and freezer compartments respectively. To further decrease cabinet heat loads low thermal conduction vacuum insulation panels (VIP) were placed in cabinet walls and doors before blowing the insulation foam Figure 6.3. The sizes and positions of VIPs are summarized in the

VIPs		
Position	Size [cm]	Pieces
Side walls	45x125	2x
RC door	30x40	2x
FC door	30x40	1x

Table 6.1 Vacuum insulation panels in the conceptual prototypes

Table 6.1. Global UA value for each compartment was estimated from the previously measured reverse heat leak tests performed by Whirlpool for various positions of the VIPs in the cabinet walls. Considered UA value for RC is $1.073\text{W}^\circ\text{C}^{-1}$ and for FC it is equal to $0.518\text{W}^\circ\text{C}^{-1}$. At 20°C ambient air temperature the RC and FC heat loads are 16.64W and 19.7W with 4.5°C and -18°C compartment air temperatures respectively. The cabinets were the same for both prototypes.

Both RC and FC suction line capillary tube counter flow heat exchangers (SLHEX) were foamed inside the back wall for appropriate insulation from ambient air. FC SLHEX was not changed versus standard bottom-mount electro-valve appliance. Capillary tube is soldered to the FC suction line surface with contact length 1.5m. Capillary tube has 0.6mm inner diameter and overall length 2.28m. It allows 4.9L/min volume flow of N_2 from the pressure 10Bar to the ambient pressure. RC SLHEX is new and it is counter flow capillary in suction tube heat exchanger. Heat exchange length is 1.4m. Original RC capillary tube had prescribed volumetric flow 4L/min of N_2 . New capillary tube has 0.8mm inner diameter and



Figure 6.3 VIP inserted in the side walls of the prototypes

allows 8L/min of N₂ from 10Bar pressure (which actually matched with SDE prototype built by Whirlpool in the past). Capillary with two times higher volume flow of N₂ was selected because volume flow of the refrigerant is expected to be 80% higher and pressure difference 10% lower.

FC evaporator was not modified versus serial production appliance. It was “no frost” fins and tube type with forced convection fan, mounted on the back wall in freezer compartment. Length of aluminum evaporator tube was 5.5m arranged in 2 rows and 9 tubes per row with approximately 50 aluminum fins.

Standard foamed-in RC evaporator was changed for natural convection visible roll-bond type with the size described in the Table 3.1. A metal construction was attached to back side of roll-bond to create a pocket for the phase change material. Welding of any structure to the aluminum evaporator plate was eliminated for complexity and potential cracking of the welds because of thermal contraction at low temperatures. Hence the solution was to screw the pocket to the evaporator plate and insert plastic bag to hold PCM and avoid leaks Figure 6.4. Pocket could store up to 2.2L of PCM, water was used as PCM. Evaporator with pocket was clamped to the compartment's back preserving 1 cm distance from the wall to allow air flow from both sides of the PCM evaporator.

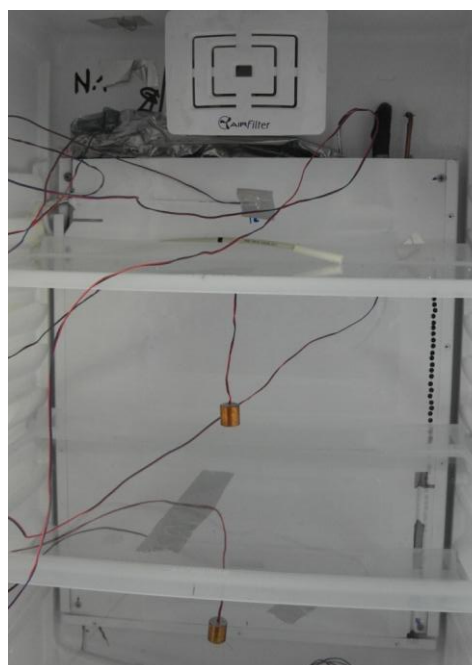


Figure 6.4 PCM pocket with plastic bag attached to the roll-bond evaporator

Condenser was steel natural draft with fins formed out of the steel sheet. It covered all the rear cabinet wall area. In case of necessity to simulate higher efficiency condenser the external fan with 5.5W power was utilized to blow air over existing condenser.

Compressor Embraco VEMZ9C variable speed type was used. The speed was adjustable by 5V square frequency signal in the range from 1600RPM to 4500RPM recommended by manufacturer and electronically limited by inverter.

Refrigeration circuit was charged by 42g of hydrocarbon R600a (isobutane). I determined the amount of refrigerant experimentally according to the FC

evaporator temperatures and suction temperature. Refrigerant was being added during FC operation until the three thermocouples attached to the inlet, middle and outlet of the FC evaporator started to show almost the same temperature. It means that there is no superheating in the FC evaporator. I continued adding refrigerant until suction temperature reached values close to the ambient temperature. By this condition I achieved that in the SLHEX exchanger was transferred most of the heat from the capillary to the suction gas and the suction line doesn't uselessly absorb heat from the ambient.

There were two bi-stable electro-valves placed on the liquid line after the filter/dryer. The first one took a function of block valve with one outlet completely sealed. Advantage of using bi-stable valve was that it consumed energy only during the short moment of switching which was almost negligible. The second valve operated as a diverter valve. It directed refrigerant flow either to RC or FC capillary tube. In the future, block and diverter functionality can be included in one stepper electro-valve and decrease appliance complexity.

6.2.1 Specific for Prototype 1 (SDE-PCM)

Ball check valve (one way valve) was inserted at the end of FC suction line before the junction with RC suction line to avoid back flow of refrigerant to FC evaporator. The valve was placed vertically to make sure that gravitational forces help the ball closing even at small pressure difference, Figure 6.5. The implemented check valve (BCV-603DY) is initially designed for fluorinated refrigerants according to manufacturer data sheet (Saginomiya, 2012). Thus the impact of mineral oil and isobutane on the gas sealing and long term reliability is not very clear. In parallel to the check valve was welded also manual bypass valve which allowed the refrigerant back flow if opened.

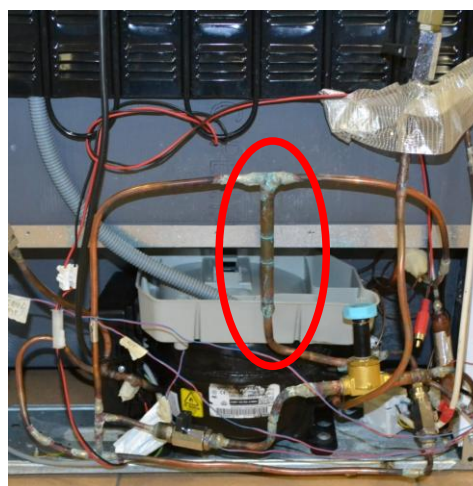


Figure 6.5 Vertical position of the check valve in the FC suction tube

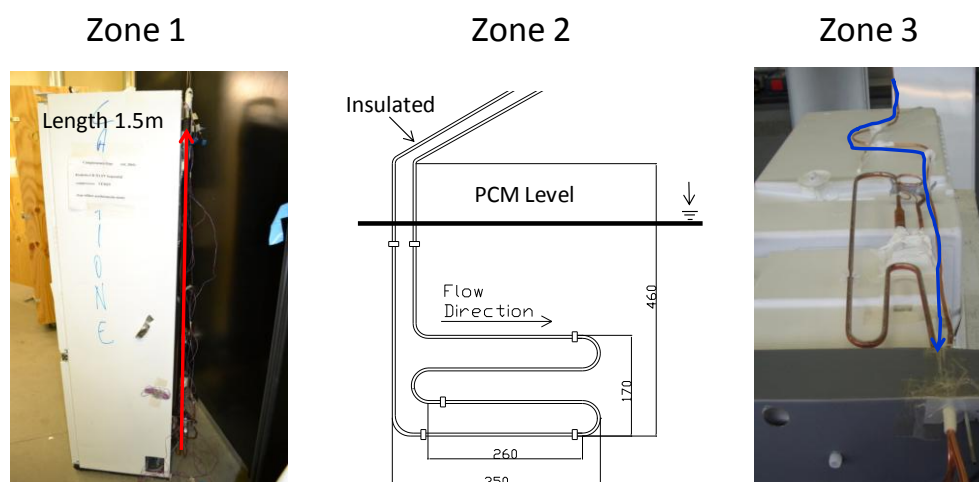


Figure 6.6 Three zones of the subcooling loop

6.2.2 Specific for Prototype 2 (SDE-PCM-SC)

Right after the second bi-stable on the freezer loop is added third electro valve which directs the flow either directly to FC capillary tube or to the subcooling loop. The subcooling loop is made of the copper tube with inner diameter 4.2mm and total length 4.5m which can be divided into 3 zones of approximately equal length 1.5m, Figure 6.6. First zone is a strait tube going on the external part of the back wall where additional few degrees of subcooling are gain by ambient cooling. At the end of the first zone the tube enters refrigeration compartment and starts the second zone in the PCM where it forms a coil of 1.5 m length. In the second zone significant subcooling down to frozen PCM temperature can occur. Afterwards subcooling loop exits the PCM and passes through the foam of the back cabinet wall down to meet the original freezer loop and freezer capillary tube. Just before joining the original freezer loop there is a check valve on the subcooling loop to avoid refrigerant back flow if subcooling loop is switched off.

6.3 Testing equipment

All the testing was performed at Whirlpool laboratories in Cassinetta di Biandronno in Italy in the environmental room with possibility to set ambient temperature and preserve it within range of $\pm 0.5^{\circ}\text{C}$.

6.3.1 Acquisition and control

For the control of the prototype appliances Whirlpool uses a dedicated control box built on the CompactDAQ boards of National Instruments. The ports of the box

allow acquiring signals from NTC sensors and door sensors in the compartments. Digital output board of the box controls compressor speed and actuators such as light, fans, heater and one electro-valve. Signals from 16 T-type thermocouples can be acquired by the box as well. Control box is connected to the computer and Labview is used to program the software part of the control and acquisition.



Figure 6.7 Field point acquisition and control setup

connected to the computer and Labview is used to program the software part of the control and acquisition.

After the experience with malfunctioned acquisition of the suction pressure by the environmental room stand described in chapter 4 I decided to build alternative acquisition system for pressure transducers from older National Instruments components available in the laboratory. In addition the control functionality for two more bi-stable electro-valves was required to operate my prototypes. Some extra ports for thermocouples were also useful. I assembled the acquisition and control hardware from Field point modules described below and showed in the Figure 6.7:

- communication module FP-100
- relay module RLY-420
- analog signal acquisition module AI-100
- thermocouple acquisition module TC-120

Except the communication module each module had 8 ports. To control switching of the two electro-valves I used 4 ports of RLY-420 and small electric circuit made of relay and diodes as drawn in the Figure 4.4. One more port was used to control condenser fan. Two ports of AI-100 were recording voltage signal from the pressure transducers and 8 ports of TC-120 were used for thermocouple readings. I connected the Field point system with computer through serial port cable and I configured it in the Measurements and Automation Explorer (MAE) software for further use in Labview.

The acquisition system of the testing stand in the environmental room was still utilized for reading the electric power and energy consumption.

6.3.2 Control strategy

The serial production appliance control board could not be used for sequential circuit prototypes. I modified the state machine program in Labview used by Whirlpool to control appliances without board. I had to implement specific control strategy of compartment operation sequence of SDE circuit. The control algorithm worked online and in each cycle acquired signal from the NTC and made decisions about switching of the actuators.

Order of operation sequence of FC and RC was based on the NTC readings from each compartment hence the control algorithm is very flexible and can adjust itself to different loads of the RC and FC. The temperature band was decided for each compartment 3°C to 6°C in RC and -18°C to -21°C in FC. As circuit operates in alternative mode prioritization between compartments was really necessary. Basic idea was that FC had a priority to be cooled. Therefore if RC was running and FC asked to be cooled in the same time circuit switched to FC mode and after returned to finish cooling of RC.

This control strategy is very simple and sufficient for determination of appliance's energy consumption but it doesn't handle unusual running conditions. Labview program was managing both control systems (DAQ and Field point) in parallel.

Speed of compressor during RC and FC mode was preset in the control and fixed to 54Hz (1620 RPM) and 100Hz (3000 RPM) respectively. The speed choice was done according to our previous experience with this circuit, in order to minimize energy consumption of RC and to preserve temperature pull down capability in FC (Visek, et al., 2012). Slightly higher RC speed than 1600RPM was used in order to avoid unwanted irregular compressor tripping which was sometimes observed at minimum RPM.

Further on, phase of pump out (P/O) was introduced to the control strategy to deal with refrigerant migration issues. The purpose of P/O phase was to extract as much refrigerant from cold FC evaporator as possible and made it available for the use in the warmer RC evaporator. I considered three different control sequences, one without P/O and two with P/O performed in different order:

1. No P/O performed
2. P/O before RC start
3. P/O after FC, bi-stable electro-valve in RC position during OFF period, FC-CV obligatory

Main difference between sequence 2 and 3 is in number of P/Os actually performed during the tests. In case 2, it's equal to RC starts and in case 3 to FC stops, the two numbers can be very different as possible to see in the Figure 6.8.

Part of the control software in Labview was also recording data. The data from positions of the switches, thermocouples and pressure transducers were directly stored in MS Excel format in 20s intervals. This was at the end of each test synchronized with power measurements recorded by the stand.

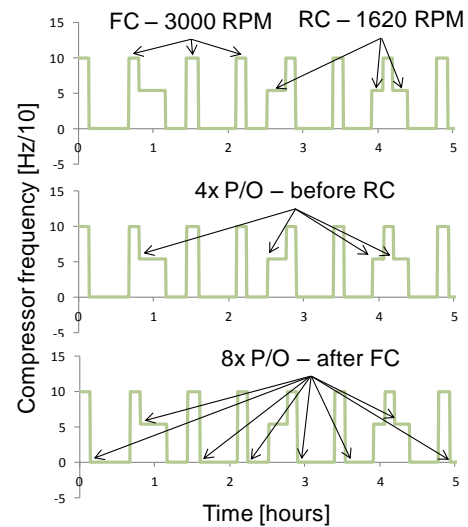


Figure 6.8 Flexible SDE control strategy with visualization of two different positions of the P/O phase

6.4 Instrumentation

Appliance prototype was instrumented with 6 standard T-type thermocouples attached to the external part of the refrigeration circuit according to the Figure 6.9a. Further 4 and 3 thermocouples were placed on the RC and FC evaporators described in the Figure 6.9b and Figure 6.9c respectively. Additional 4 thermocouples were placed inside of the pocket with the phase change material, two in the height of 10cm and other two in 28cm from the bottom of the RC evaporator. Besides, 7 weighted thermocouples were measuring air temperature; 1 ambient temperature and 3 thermocouples spaced in each compartment. The ISO 15502 norm (ISO, 2005) was followed in the RC but not in the FC. Weighted thermocouples were hanged in each of the 3 drawers in the freezer and there were no packages in the freeze. Moreover RC and FC had installed separate NTCs thermistors, guiding control mechanism. Pressure transducers were located at the compressor inlet and outlet. They were manually calibrated before physically added to the circuit calibration tables are showed in Appendix II. Electric power and energy consumption was recorder by wattmeter. Accuracy of the instruments was already reported in the Table 4.1.

Prototype 2 SDE-PCM-SC was instrumented with two additional thermocouples attached to the tube at the entrance and at the exit of the subcooling loop.

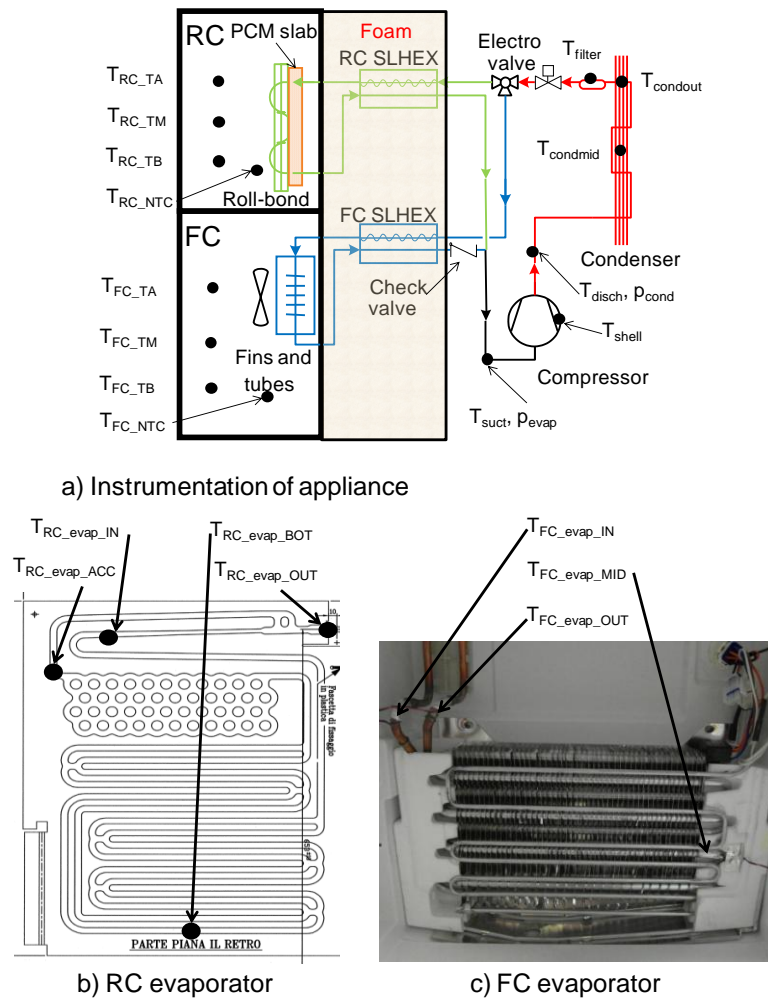


Figure 6.9 Positions of thermocouples and pressure transducers in the Prototype 1 SDE-PCM

6.5 Experimental refrigerant pump out optimization

Refrigerant pump out phase is a special procedure implemented to the sequential dual evaporator refrigeration circuit in order to extract refrigerant from cold FC evaporator and make it available for warmer RC evaporator. Various sequences for P/O phase were tested in the work of (Won Jae, et al., 2011) and 2.6% to 5.9% improvement was reported. They examined also the impact of P/O duration time on the energy consumption and depending on the position of P/O in the control sequence their optimum P/O duration was between 60s and 120s.

I was mainly interested to understand impacts of FC fan, P/O duration time and compressor speed during P/O on the RC evaporation temperature and energy consumption of P/O phase. I performed tests at following parameters:

- Duration of P/O (0s, 120s, 180s, 240s)

- FC evaporator fan (ON, OFF)
- Compressor RPM (1620, 3000)

Based on the results I defined optimal parameters of the P/O phase and used it during the following appliance energy consumption tests.

6.5.1 Test procedure for pump out

Technically the P/O was performed by closing block valve placed after the filter/dryer and the compressor was left running for certain period of time. This way it pumped out refrigerant fluid from both evaporators to the condenser where it was accumulating. All the P/O tests were performed on the SDE-PCM prototype with 2.2L of water as a PCM and recording was done after appliance reached cyclic-steady condition. Ambient temperature was 20°C, controlled by environmental room.

To minimize differences between test results the forced operation sequence FC-P/O-RC was imposed instead of flexible control. Optimization criteria were P/O energy consumption and amount of refrigerant pumped out. Energy consumption was measured directly. Amount of refrigerant extracted during P/O phase was the more important and harder to measure criteria. Precise measurements of refrigerant mass distribution are possible as shown in (Bjork, 2005) but more complex experimental setup is necessary. Thus I applied following indirect measures to decrease complexity of testing and to judge about extracted refrigerant amount:

- Pressure at the compressor inlet
- Surface temperature of FC evaporator
- RC evaporation temperature after P/O

Pressure was measured by pressure transducer. It reflects actual dynamically changing evaporation temperature of the refrigerant and pressure change in time can be interpreted as boiling intensity. FC evaporator surface temperature was captured by thermocouple close to the bottom of the evaporator. It indicates presence of evaporating liquid refrigerant in the FC evaporator when compared with evaporation temperature.

RC evaporation temperature was calculated by refrigerant property library from measured compressor suction pressure after the P/O phase. Pressure drop in the RC suction channel was neglected and average was obtained by integration of temperature over first 10 minutes of RC operation after P/O was stopped. Higher

RC evaporation temperature indicates higher amount of refrigerant pumped during P/O. Energy consumed during P/O is an integral under power curve recorded during P/O. Typical P/O analysis is shown in Figure 6.10.

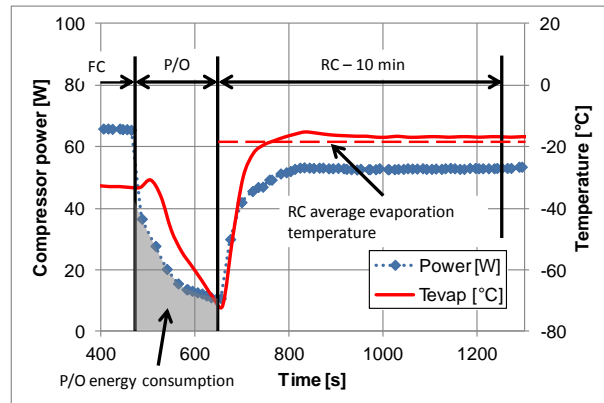


Figure 6.10 Typical P/O analysis performed on the temperature, power and pressure (evaporation temp)

6.5.2 Experimental results of pump out

Impact of FC fan operation, duration of P/O phase and compressor RPM on P/O operation performance are discussed separately.

6.5.2.1 FC fan ON/OFF

After the block valve closed the circuit, vapor pressure at the compressor inlet decreased rapidly and liquid trapped in the evaporators started to evaporate to restore lower thermodynamic equilibrium temperature. $T_{FC_evap_MID}$ surface thermocouple attached close to the bottom of the FC evaporator Figure 6.9c showed decrease of temperature after the P/O started which is visible in the Figure 6.11. For case with FC fan OFF the surface temperature dropped significantly right after the P/O started (red line) and after reaching minimum it moderately

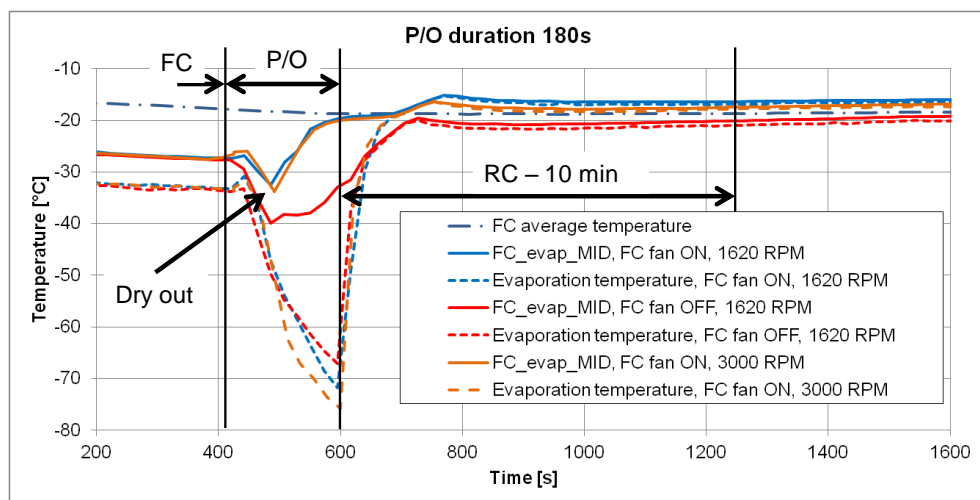


Figure 6.11 Temperature profiles for P/Os at 180s duration for FC fan ON and OFF and at two different compressor RPMs 1620 and 3000

grew.

On the other hand with FC fan ON the surface temperature and pressure right after the P/O start slightly increased because the heat transfer to the evaporator was enhanced by the fan and caused evaporation of the liquid thus more vapor increased pressure. After a short moment both pressure and temperature initiated to decline as the compressor was pumping the refrigerant mass away to the condenser until the temperature reached minimum at approximately 60s. Afterwards the pressure continued to drop down but the surface temperature was rising till it reached FC air temperature after 180s visible in the Figure 6.11. The temperature minimum meant a dry out of the liquid refrigerant at the thermocouple position. The thermocouple was not mounted exactly at the lowest point of the evaporator and thus even after indicated dry out there could be some remaining liquid refrigerant in the FC evaporator. But as the surface temperature approached FC air temperature it's less probable that there is still some liquid

Compressor	P/O duration	FC FAN	P/O energy consumption	Tevap RC
RPM	[s]	ON/OFF	[Wh/period]	[°C]
1620	0	OFF	0	-22.4
	120	OFF	0.86	-22.8
		ON	0.97	-18.5
	180	OFF	1.05	-21.2
		ON	1.21	-17.0
240	ON	1.51	-17.2	
3000	180	ON	2.04	-18.1

Table 6.2 Results of experimental tests for P/O energy consumption and RC evaporation temperature at various parameters of P/O

refrigerant left in the FC evaporator.

Clearly the FC fan increased heat transfer to the evaporator and helped to extract liquid refrigerant from the evaporator. The positive impact of FC fan on refrigerant removal was also visible on the increased average RC evaporation temperature during the RC operation following P/O phase presented in the Figure 6.11 and in the Table 6.2.

Power consumption of the FC fan is only 3.6W and it increased energy consumption during the P/O with FC fan ON Table 6.2, but the rise is almost negligible compared to overall appliance consumption.

6.5.2.2 P/O duration

P/O duration plays significant role as it directly influences energy consumed and it delays the start of RC cooling period. Energy consumption as a function of the time is reported in the Figure 6.12. After approximately 120s at 1620 RPM the energy

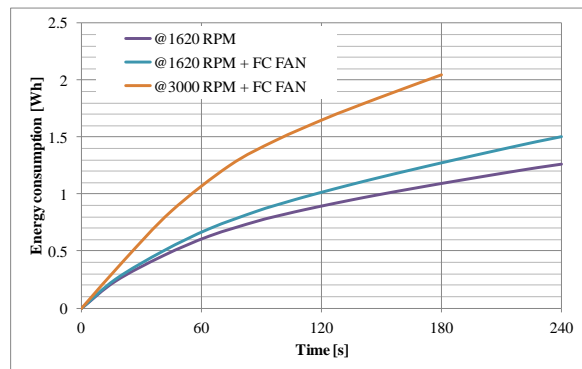


Figure 6.12 Experimentally determined P/O energy consumption as a function of duration, compressor RPM and FC fan operation

consumption line flattened to almost linear dependence on time thus the power became almost constant. Difference between 120s and 180s at 1620 RPM was only 0.2 Wh per one P/O. The measurements showed that the longer the P/O the lower the suction pressure could be reached at the end of P/O. It's important to mention that low suction pressure means very high pressure ratio across the compressor valves which caused extremely low volumetric efficiency and decreased mass flow. Extrapolation analysis of compressor data sheet revealed that at evaporation temperature of -60°C (pressure ratio around 40) volumetric efficiency is only approximately 30% and at -65°C (pressure ratio 60) approaches 0% as showed in the Figure 6.13. Thus no mass is being pumped anymore. Therefore prolonged operation at very low suction pressures is meaningless. Theoretically evaporation temperature should asymptotically reach -65°C . In reality even temperatures below -65°C were achieved Figure 6.11 but the measurement can be misleading because pressure transducer worked far outside of the recommended pressure range.

P/O duration has also an impact on the RC evaporation temperature after P/O phase. Measurements with P/O length 180s led to highest

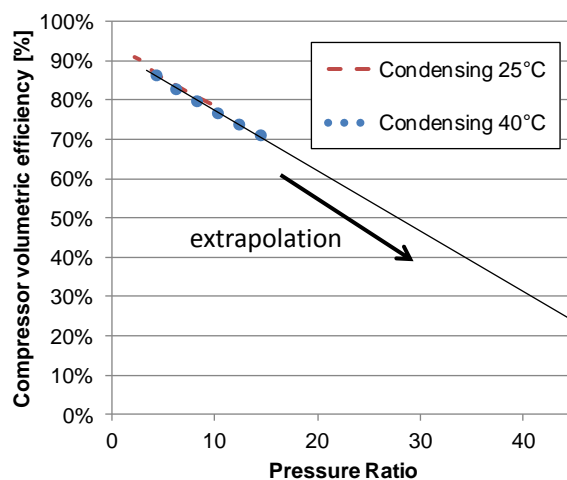


Figure 6.13 Extrapolation of compressor volumetric efficiency to very high pressure ratio

average RC evaporation temperatures around -17°C . Prolonging P/O phase to 240s didn't bring further temperature increase but shortening of the phase to 120s decreased evaporation temperature to -18.5°C as showed in the Table 6.2. Duration of 180s was taken as optimum. However, 20s values recording frequency and 60s time step in the evaluated parameter were quite long and further refinement would be helpful in the future assessments.

6.5.2.3 Compressor RPM

Most of the tests were performed at the 1620RPM, only during one P/O with duration 180s and FC fan ON the RPM was changed to 3000RPM. At higher compressor RPM, suction pressure dropped faster and also reached lower value at the end (Figure 6.11– evaporation temperature). Thus it was assumed that higher refrigerant amount was pumped out during the same running time. RC evaporation temperature after 3000RPM P/O although didn't confirm the assumption because it was approximately 1°C lower than during the P/O with 1620RPM visible from the Table 6.2. In addition P/O at 3000RPM consumed 2.04Wh/period which was almost double energy compared to 1620RPM. 3000RPM P/O would have to last only 80s to have the same energy consumption as 180s P/O at 1620RPM. Interesting is that RPM doesn't have almost any impact on the FC evaporator surface temperature and it reaches FC air temperature after 180s displayed in the Figure 6.11. Hence the decision was to take 1620RPM as optimum. However further tests at 3000RPM and shorter P/O duration time would be helpful in confirming the decision.

6.5.3 Conclusion for pump out optimization

Optimum parameters of P/O were experimentally defined. FC fan operation had major positive effect on the refrigerant amount pumped to the condenser. Compressor speed showed strong influence on the P/O energy consumption and minor effect on P/O efficiency, thus minimum 1620RPM was chosen as an optimum. Duration of 180s was selected in order to be on the safe side that most of the refrigerant fluid was extracted at any condition. In the future, the decrease in P/O length is possible.

6.6 Testing procedure for energy consumption tests

All the energy consumption tests were performed on the cyclic-steady condition of the prototype appliance in the environmental room with stable ambient temperature. The air temperature in RC was kept between 3°C and 6°C and in FC between -18°C and -21°C. Compressor speed was preset to 1620RPM and 3000RPM for RC and FC operation respectively. Optimum P/O parameters defined in the chapter 6.5 were used for all P/O sequences. Acquisition length for energy consumption tests differentiated for non PCM and PCM refrigerator setup. The length was 24 hours for non PCM and at least two full RC periods for PCM prototype. In PCM prototype single RC period was reaching in some cases extremely long duration of 15 to 18 hours, thus 2 periods were more than 30 hours. The energy consumption results were scaled to 24 hours of operation with measurement unit Wh/day. In evaluation of the PCM prototypes it's very important to calculate energy consumption only from complete RC periods. Otherwise significant energy consumption errors could occur.

6.6.1 Data processing

After the data were recorded by acquisition system I had to process them to achieve comparable results for various tests.

Average compartments' air temperatures were obtained as an average of three weighted thermocouples placed in each compartment. The averages differed between the tests. For valid comparison of the tests following temperature correction procedure was applied on the energy consumption results. Basic assumption is that COP remains constant and only the compressor's run time changes with small correction of compartment air temperature.

1. Based on measured ambient and internal temperatures the actual compartment heat gain Q_{XC} was calculated. Global heat transfer coefficients of RC and FC were determined beforehand from measured reverse heat leakage tests ($UA_{RC} = 1.073$ and $UA_{FC} = 0.518$ W/°C).

$$Q_{XC} = UA_{XC}(\bar{T}_{amb} - \bar{T}_{XC}) \quad \text{eq 77}$$

2. I determined relative difference (RD) between actual compartment heat load and heat load at constant internal air temperatures T_{XC} (4.5°C and -18°C for RC and FC respectively) and constant ambient temperature T_{amb} .

$$RD_{XC} = \frac{UA_{XC}(T_{amb} - T_{XC})}{Q_{XC}} = \frac{Q_{XC} T_{XC}}{Q_{XC}} \quad \text{eq 78}$$

3. According to the Figure 3.18 relative improvement of the heat load has the effect of the same relative improvement on the energy consumption. I applied the correction solely to the electrical energy $E_{XC \text{ comp}}$ consumed by compressor during XC operation without P/O, FC fan and condenser fan because these are not influenced by differences in the heat load.

$$E_{XC \text{ comp cor}} = RD_{XC} E_{XC \text{ comp}} \quad \text{eq 79}$$

4. In the next I reconstructed energy consumption for each compartment by adding P/O and fans consumptions. P/O energy consumption was fully added to RC operation even though it cools partially also FC.

$$E_{RC \text{ cor}} = E_{RC \text{ comp cor}} + E_{P/O} + 24 n_{RC} P_{cond \text{ fan}} \quad \text{eq 80}$$

$$E_{FC \text{ cor}} = E_{FC \text{ comp cor}} + 24 n_{FC} P_{FC \text{ fan}} \quad \text{eq 81}$$

5. RC and FC compressor run times were recalculated by following equations.

$$n_{RC \text{ cor}} = \frac{n_{RC} E_{RC \text{ cor}}}{E_{RC \text{ comp}} + E_{P/O} + 24 n_{RC} P_{cond \text{ fan}}} \quad \text{eq 82}$$

$$n_{FC \text{ cor}} = \frac{n_{FC} E_{FC \text{ cor}}}{E_{FC \text{ comp}} + 24 n_{FC} P_{FC \text{ fan}}} \quad \text{eq 83}$$

6. Utilizing eq 35 I could determine the RC and FC COPs and by employing eq 41 I calculated SDE circuit overall COP.

$$COP_{RC} = \frac{24 Q_{RC \text{ 4.5}^\circ\text{C}}}{E_{RC \text{ cor}}} \quad \text{eq 84}$$

$$COP_{FC} = \frac{24 Q_{FC \text{ -18}^\circ\text{C}} + 24 n_{FC \text{ cor}} P_{FC \text{ fan}}}{E_{FC \text{ cor}}} \quad \text{eq 85}$$

$$COP_{SDE} = \frac{COP_{FC} COP_{RC}}{\frac{Q_{RC \text{ 4.5}^\circ\text{C}}}{(Q_{RC \text{ 4.5}^\circ\text{C}} + Q_{FC \text{ -18}^\circ\text{C}})} COP_{FC} + \frac{Q_{FC \text{ -18}^\circ\text{C}}}{(Q_{RC \text{ 4.5}^\circ\text{C}} + Q_{FC \text{ -18}^\circ\text{C}})} COP_{RC}} \quad \text{eq 86}$$

6.7 Prototype 1 SDE-PCM experimental results

The tests performed with prototype 1 SDE-PCM are summarized in the Table 6.3. Changes to the appliance setup and to the position of P/O phase in the control strategy were performed. The tests are numbered and the test numbers are used also while presenting results. All the tests were carried out at the 20°C ambient temperature.

The measured results of energy consumption tests were corrected to the unique RC = 4.5°C and FC = -18°C temperatures according to the procedure described in the chapter 6.6.1. Corrected values are reported in the Table 6.4 and original measured values are in Appendix III. Regularly the measured FC average air temperatures at different tests were very close to each other with standard deviation of only 0.1°C. Measurements of RC temperature had larger standard

Test #	Control	Refrigerator components			
		SDE	PCM	FC - CV	Cond fan
1	NO P/O	X			
2		X	X		
3	P/O before RC	X		X	X
4		X	X		
5		X	X	X	
6		X	X	X	X
7	P/O after FC	X		X	
8		X	X	X	

Table 6.3 Various setups of the prototype 1 SDE-PCM experimentally tested for energy consumption

deviation 0.7°C between the tests and maximum temperature correction was 0.91°C. RC average temperature was typically higher when PCM was present in the compartment because during compressor OFF cycle temperature was rising very modestly once it exceeded 4°C which is showed in the Figure 6.14. The reason for that is close match between heat absorbed by PCM pocket and heat gained by RC from the ambient expressed by the equation:

$$UA_{PCM}(T_{RC} - T_{PCM}) = UA_{RC}(T_{AMB} - T_{RC}) \quad \text{eq 87}$$

Test	SDE appliance		RC			FC		
	Energy	COP	Energy	Run time	COP	Energy	Run time	COP
#	[Wh/day]	-	[Wh/day]	-	-	[Wh/day]	-	-
1	533	1.67	197	18.9%	2.02	336	20.2%	1.46
2	521	1.71	186	15.6%	2.14	335	19.4%	1.46
3	554	1.61	210	15.3%	1.90	344	19.9%	1.42
4	529	1.69	180	11.1%	2.21	349	19.2%	1.40
5	525	1.70	179	10.3%	2.23	346	19.0%	1.41
6	503	1.77	167	10.5%	2.39	336	19.5%	1.46
7	516	1.73	189	14.2%	2.11	327	19.1%	1.49
8	531	1.68	179	9.2%	2.24	353	20.0%	1.39

Table 6.4 Corrected values of energy consumption tests of prototype 1 SDE-PCM

The close match allowed proper freezing and melting of the PCM which can be observed in Figure 6.14. T_{PCM} was taken as an average between four thermocouples immersed in the PCM and measurements showed that at the beginning of charging sequence the temperature was above 0°C thus PCM was in the liquid state. Then phase changing freezing is visible at 0°C and at the end of the charging process some sub-cooling of the ice was reached. Importance of suitable design of UA_{PCM} and UA_{RC} for completing PCM melting process is evident from the eq 87. If T_{PCM} is considered constant it is also understood that ratio between UA values has to be adjustable to actual ambient temperature and RC thermostat setting. Thus appliance production design have to have a variable speed RC fan and/or dumpers for air flow distribution to deal with off design temperature conditions.

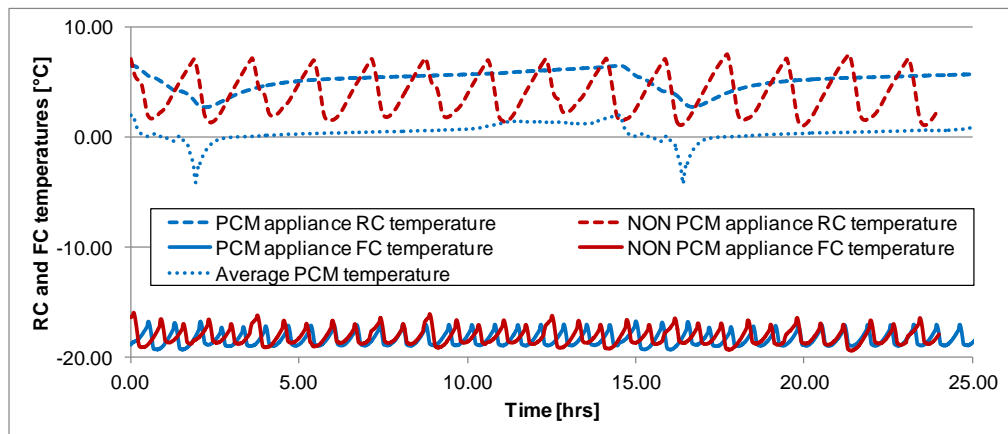


Figure 6.14 Principal differences between PCM and Non PCM experimental results

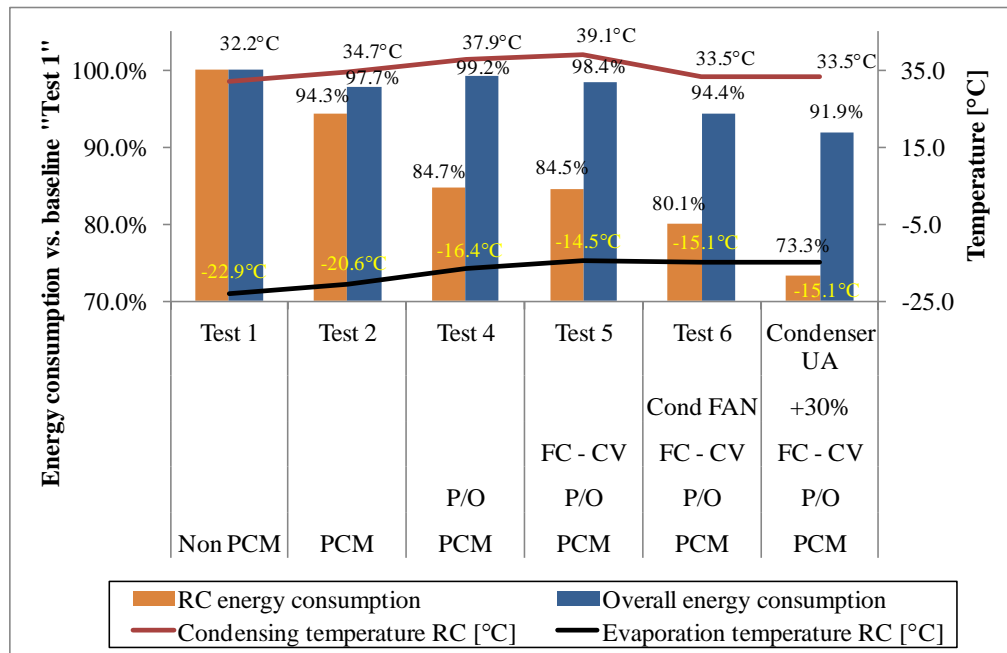


Figure 6.15 Impact of PCM, P/O, FC-CV and condenser fan on the energy consumption and RC average operating condensation and evaporation temperatures

I divided the experimental result into three groups:

1. Baseline SDE appliance analysis which includes test 1.
2. Impact of PCM, condenser fan and refrigerant migration components which include test numbers 1, 2, 4, 5 and 6. The improvements of energy consumption for overall appliance and separately for RC are summarized in the Figure 6.15. Operating temperatures are also reported. Summary of improvements in terms of RC COP, FC COP and SDE COP are presented in Figure 6.16 and reflects from other angle of view prototype energy consumption improvements.
3. Study of the impact of P/O phase position (control strategy) on the energy consumption of the prototype with and without PCM in contact with roll-bond evaporator. Test included in this study are 1, 2, 3, 6, 7 and 8. The overall results for these tests are showed in the Figure 6.20.

6.7.1 Baseline circuit

Baseline appliance was prototype 1 with completely removed PCM pocket. Simple flexible control strategy without any P/O phase was applied to the baseline prototype and tested for energy consumption as the “Test 1”. Appliance energy consumption was 533Wh/day out of which 197Wh/day belonged to RC and the rest to FC. RC evaporation temperature was -22.9°C which is already 6.1°C

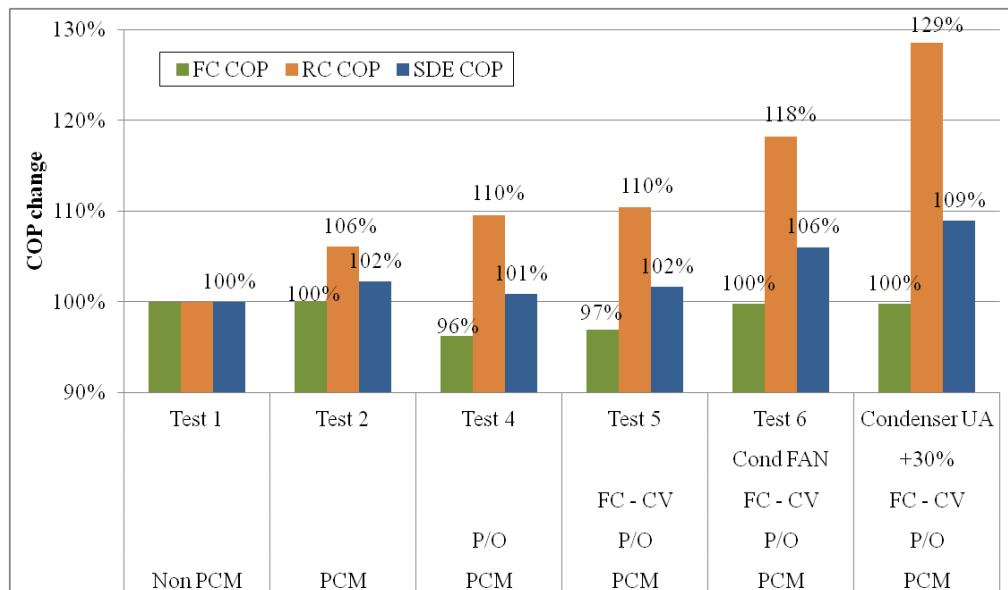


Figure 6.16 Impact of PCM, P/O, FC-CV and condenser fan on the COP of the compartments and SDE system

higher than FC evaporation temperature. It already showed positive potential of SDE circuit versus series evaporators cycles where the RC evaporation temperature is the same as the FC one. Still enormous temperature lift 26.9K was measured in the baseline between RC evaporation temperature and RC air temperature and this offered large potential for further energy efficiency improvements in the following tests. Compressor run time was 19% and 20% with average ON/OFF period duration 67 and 42 minutes for RC and FC respectively.

6.7.2 PCM in contact with RC evaporator

Basic idea of PCM in the contact with RC evaporator is to increase evaporation temperature by improving evaporator heat transfer coefficient and to store excess cooling capacity in the latent heat of PCM. In the “Test 2” only PCM (2.2L water) was placed in the pocket and no additional changes were made to the control and circuit versus baseline. Results of measurements with PCM in the pocket showed very modest increase in evaporation temperature during RC operation by only 2.3°C from -22.9°C to -20.6°C and were disappointing. It led to improvement of 5.7% in energy consumption during RC operation and 2.3% overall as presented in the Figure 6.15. It is relatively small improvement and doesn't match with enthusiastic theoretical estimations.

Such a small evaporation temperature raise was most probably related to insufficient refrigerant mass in the RC evaporator during RC operation.

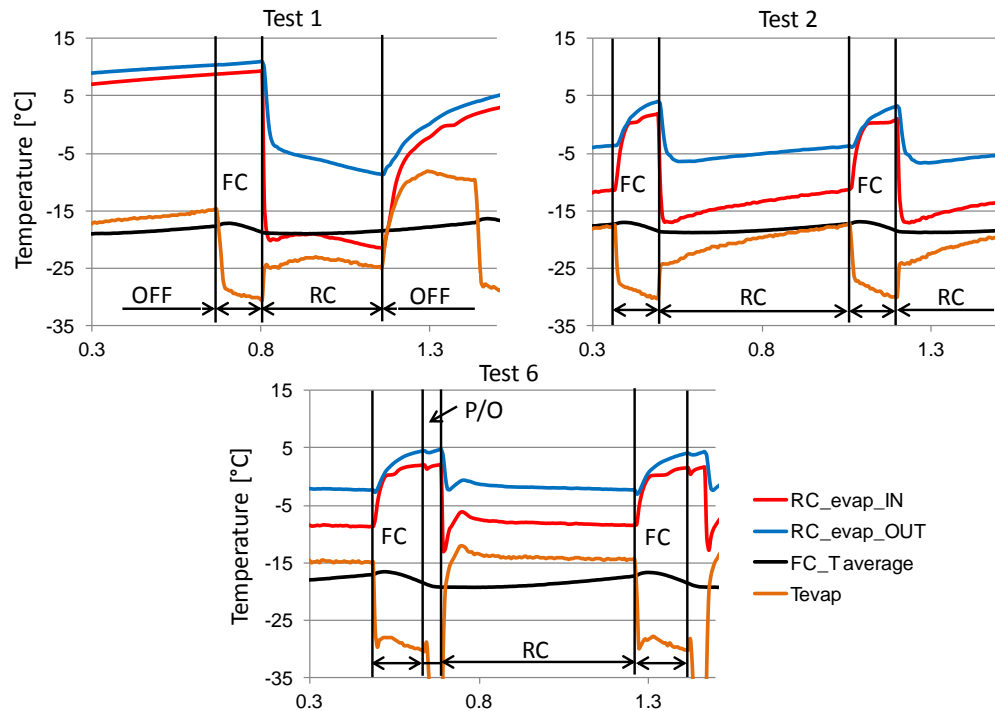


Figure 6.17 Temperature profiles of the RC evaporator and evaporation temperature during different tests (Test 1 – No PCM, Test 2 – PCM, Test 6 – PCM + P/O + FC-CV)

Refrigerant tends to naturally migrate to FC evaporator as it's colder than RC evaporator. When electro-valve switched to RC mode, refrigerant only slowly started to move from FC loop to the running RC loop by help of compressor. This was visible on the gradually increasing evaporation temperature Figure 6.17 ("Test 2"). Even at the end of the RC ON period the RC evaporation temperature didn't exceed FC air temperature. Hence there was still some liquid refrigerant remaining in the FC evaporator even at the end of RC operation.

PCM in the RC had though positive effect on the RC compressor run time which decreased from 18.9% to 15.6% thus compressor was surely delivering higher cooling capacity. One complete RC period had duration of more than 18 hours versus 67min during baseline test. PCM extremely increased resistance of the RC to the electric grid power failure.

6.7.2.1 P/O before RC

In the "Test 4", pump out (P/O) phase was introduced to the control mechanism and placed before RC operation to deal with insufficient charge during RC operation. Refrigerant was pumped from FC evaporator and stored in the condenser from which it was directly released to the RC capillary after P/O was concluded. Experimental results showed significant grow by 6.5°C in the RC

evaporation temperature from -22.9°C to -16.4°C . It brought also noteworthy improvement of 15.3% in energy consumption of RC without taking into account P/O phase consumption. But overall energy consumption increased versus “Test 2” and only negligible improvement of less than 1% was observed versus baseline as it’s reported in the Figure 6.15.

6.7.2.2 FC suction tube check valve (FC-CV)

In addition to P/O also the FC-CV was activated in the circuit during the “Test 5” to avoid back flow of refrigerant to the FC evaporator during RC operation and OFF cycle. RC evaporation temperature rose by 8.4°C from -22.9°C to -14.5°C . On the other hand together with evaporation temperature also the condensing temperature was rising significantly from 32.2°C to 39.1°C . This means that higher amount of heat was absorbed by evaporator and also higher heat load needed to be dissipated by the condenser. The condenser had to exchange approximately 200W with the air which is 50% more heat than during the baseline test. Interesting is that the same condenser dissipates around 200W also during the FC operation at 3000RPM and condensing temperature is reasonable 34.6°C . It could indicate that the condensing temperature is growing because of too high restriction on the capillary side or too less refrigerant and vapor is entering the capillary tube. Therefore I looked at the subcooling during RC operation and it is only 1°C higher than during baseline operation. To be sure about correct value of SC the thermocouple should be immersed in the liquid. Also sight glass and pressure transducer on the liquid line would be helpful in the future testing.

COP of compressor increased by 9% at this condition calculated from the compressor data sheet. RC energy consumption decreased by 9% from 197 to $167+12$ Wh/day considering P/O phase being fully part of RC operation. Energy consumption decomposition between RC, FC and P/O for the tests is reported in the Figure 6.19. But overall appliance energy consumption decreased only by negligible 1.7%. Thus FC-CV allowed increase of RC evaporation temperature by extra 2°C and overall saved only approximately 1% of energy consumption.

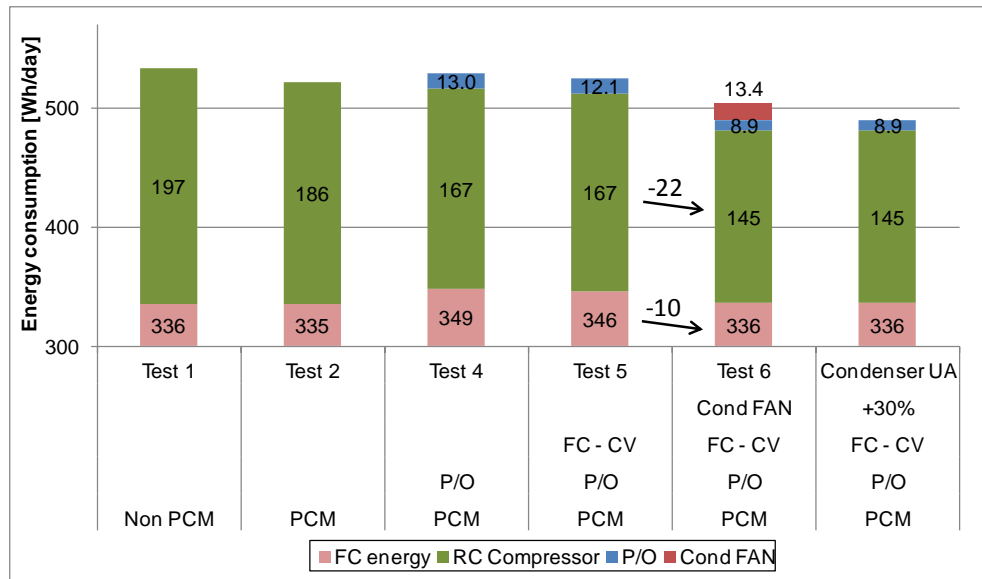


Figure 6.19 Actual energy consumption decomposition between FC, RC, P/O and condenser fan for the PCM and components tests

Single RC period duration was 14 hours 20 minutes with compressor run time 9.7% and 1.4% P/O run time. Long PCM charging period was interrupted by FC cooling period several times what is visible in Figure 6.18. FC during RC charging period and shortly after consumed approximately 11Wh/day (3.5%) more energy. Higher FC consumption penalized the overall energy consumption. The first reason for increased FC energy consumption during RC charging was already warm condenser and compressor which absorbed less heat from the refrigerant fluid. The second reason might be related to the necessity for

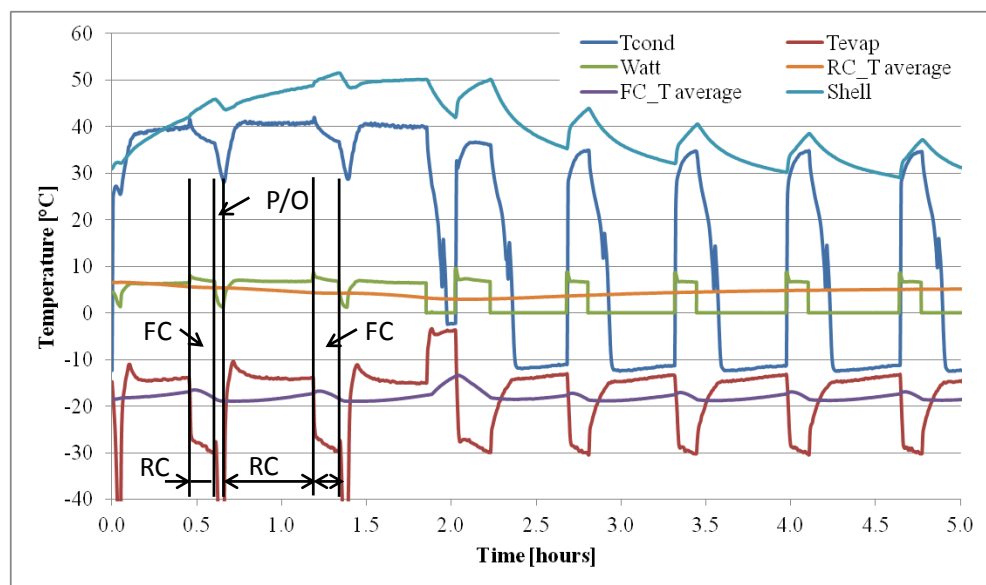


Figure 6.18 Long PCM charging period in RC interrupted by several FC cooling cycles

refrigerant fluid migration from RC to FC evaporator after switching to FC operation.

6.7.2.3 Condenser fan

Increased heat dissipation requirement on the condenser when PCM is present in RC brought penalty to the compressor efficiency in terms of higher condensing temperature. Simulation performed in chapter 5 predicted large RC COP improvement if evaporation temperature is increased and condenser temperature is kept constant. Thus external fan was mounted under the existing condenser to increase air heat transfer coefficient. Power consumption of the fan was 5.5W. During the “Test 6” the control software was modified to run this fan only during the RC operation. The RC condensing temperature was pushed down to 33.5°C and it brought important improvement of 19.9% in RC energy consumption including condenser fan electricity. Overall appliance energy consumption dropped by 5.6% versus the baseline. Performance of fan accounted for approximately 30% increase in the UA value of the condenser. In the next I assumed that 30% increase in UA value was done by modifications to the condenser, capillary tube and refrigerant charge hence I could remove fan’s energy consumption 13 Wh/day. The results can be seen in the last column of Figure 6.15, Figure 6.16 and Figure 6.19. RC energy usage decreased by 26.7% and it resulted in appliance overall energy saving of 8.1%. More efficient condenser could positively impact also FC power consumption but this was not part of the analysis.

6.7.3 Control strategies

Control mechanism in SDE circuit plays very important role in achieving high energy efficiency. Three control strategies were experimentally compared. Each control approach was tested with and without PCM to be able to evaluate combination impact on the energy efficiency. All three approaches are based on flexible RC and FC operation sequence which depends only on NTC readings in corresponding compartment and the priority is always given to the FC. In principal this is an alternative approach to the fixed sequences FC-P/O-RC or RC-P/O-FC presented in (Won Jae, et al., 2011). Advantage of flexible sequence is an ability to operate compartments completely independently in case RC and FC periods have very different durations. This was the case of the tests with PCM

when duration of one RC period was as long as 15 - 18 hours and one FC period lasted only 50min.

Other important advantage is possibility to simply switch OFF unused compartment just by setting the thermostat to temperature higher than ambient environment. This feature can be interesting during longer vacation leave when it's sufficient to operate only freezer with long lasting frozen food or for events when freezer is empty but refrigerator should still run. Worth mentioning is also a possibility of converting freezer into refrigerator just by thermostat setting.

As it was shown already before, P/O is a crucial phase to move refrigerant from FC evaporator to RC evaporator. Refrigerant P/O phase can be attached either to the end of the FC operation or just before running RC. Both cases were tested and compared to NO P/O case. Energy consumption results of NO P/O tests without and with PCM ("Tests 1 and 2") were already discussed in the paragraph 6.7.1 and 6.7.2. Appliance set up in "Test 1" was considered to be baseline also for energy consumption comparison of control strategies, presented in Figure 6.20.

6.7.3.1 P/O before RC

"Tests 3 and 6" were performed with P/O phase before RC with FC-CV and condenser fan running only during RC operation but electricity consumed by fan was not taken into overall energy consumption calculation.

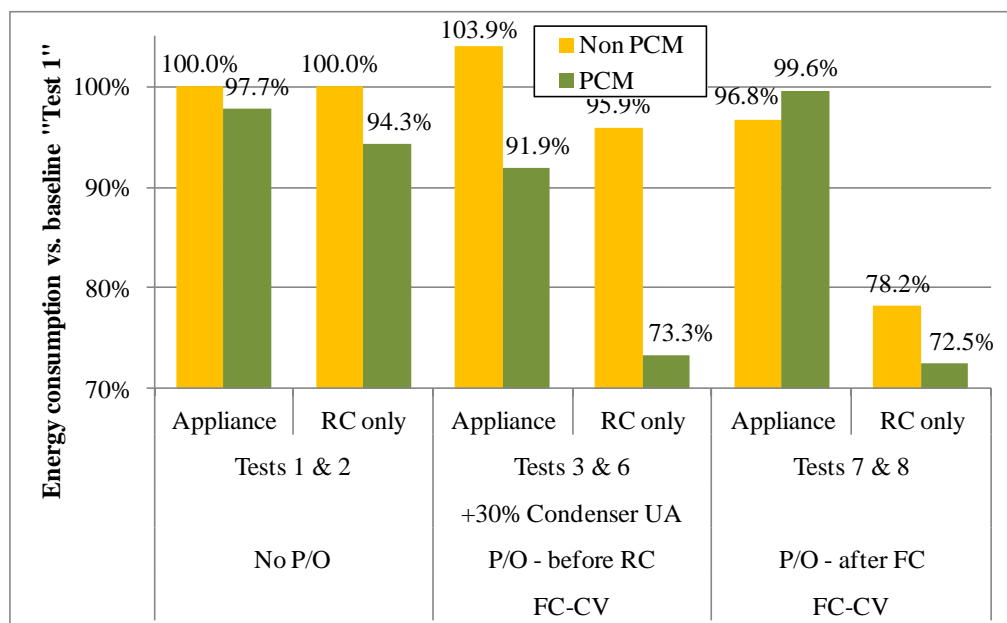


Figure 6.20 Impact of P/O phase position in the control strategy on the energy consumption of the prototype with and without PCM

“Test 3” was carried out without PCM in RC. Although RC consumption decreased almost by 20% the overall appliance consumption was 3.9% higher than during “Test 1”. RC was more efficient because more refrigerant was flowing to the roll-bond evaporator and filled it better. During one day of operation approximately 18 P/Os were performed and consumed 31Wh which became significant share of overall energy consumption Figure 6.21. 1.7Wh were used per P/O instead of 1.2Wh measured previously, which was caused by higher initial evaporation pressure. Moreover FC consumed 8Wh more because it needed to pull back large amount of refrigerant charge back to FC evaporator 18 times a day.

Only 5 P/Os per day were observed during the “Test 6” with the same control mechanism and implemented PCM. Significant 41Wh of energy was saved during RC for only a small cost of 9Wh spent during P/O versus “Test 2” without P/O and with PCM. Obviously the P/O before RC control strategy starts to be more efficient when less P/Os are necessary, thus makes it ideal for PCM extended duration RC periods. In principal FC-CV is not obligatory for this control mechanism and some costs can be saved for relatively small penalty in energy efficiency.

6.7.3.2 P/O after FC

The control strategy where P/O is run at the end of each FC period was tested

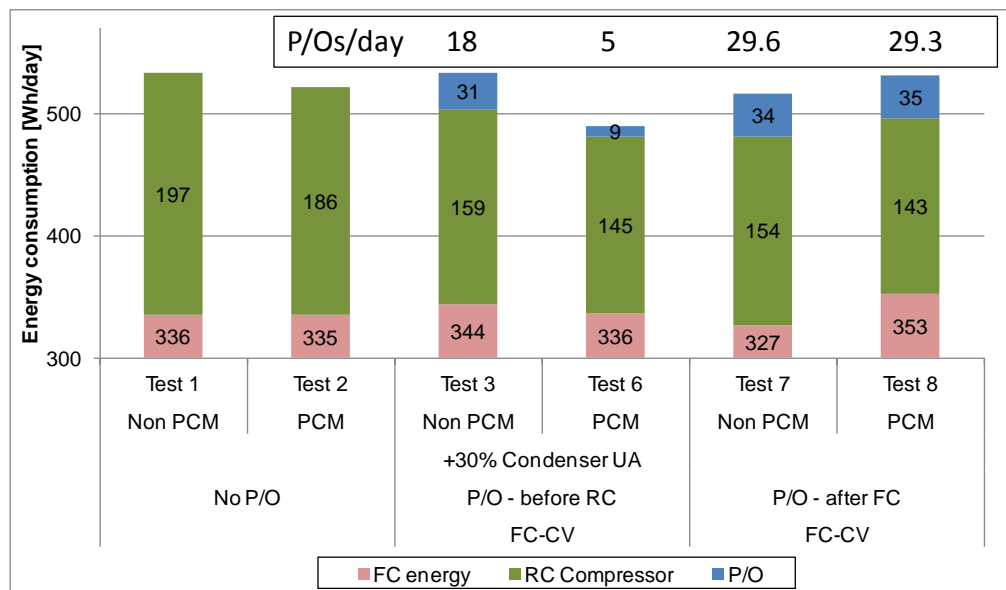


Figure 6.21 Actual energy consumption decomposition between FC, RC and P/O for the control strategy testing

during “Tests 7 and 8”. Labview program had to be modified versus previous tests and FC-CV became mandatory piece of the refrigeration circuit. Prototype during the “Test 7” was run without PCM and performed 3.2% better than during the “Test 1”. The number of P/O performed per day was equal to 29.6 which was higher than during the “Test 3”. But energy consumed per P/O was only 1.16Wh. RC started only 16 times per day thus 13.6 P/Os were actually “wasted” every day, thus there is still a potential for improvement in this control strategy. Energy consumption of RC dropped significantly by 43Wh/day versus “Test 1” and by 26Wh versus “Test 3” Figure 6.21.

There are several reasons for such a major improvement. The first one is efficient refrigerant P/O at the end of FC. While FC is running the refrigerant is distributed between condenser and evaporator. The amount of refrigerant in the FC evaporator is lower compared to the compressor OFF period when the entire refrigerant charge accumulates in this evaporator. Thus P/O at the end of FC needed less energy for pumping refrigerant and moreover P/O cooling effect was utilized in FC and made FC run time shorter and brought also 9Wh energy saving during FC. Another reason for energy saving relates to the expansion of accumulated refrigerant to RC evaporator from the condenser after P/O finished by switching bi-stable electro-valve to RC position during OFF period. The RC OFF period was extended and RC run time decreased. Condenser fan was not applied during RC but it could have additional positive effect on the energy consumption, estimated to roughly extra -1% of overall energy consumption.

The energy results of “Test 8” were surprising when refrigerator with PCM consumed overall 16Wh/day more energy than during the “Test 7” without PCM. Energy consumption decomposition between FC, RC and P/O showed in the Figure 6.21 that RC was actually more efficient and consumed 11Wh/day less than during the “Test 7”. But the penalty of almost 26Wh/day appeared in the FC operation. It was related to already warm condenser and compressor at some FC starts as previous mentioned and to refrigerant charge migration from RC to FC evaporator at the beginning of FC operation. Condenser fan applied during RC operation could possibly decrease both RC by 22Wh/day and FC by 10Wh/day estimated from previous tests Figure 6.19. In total 29.3 P/Os were performed per day and consumed 35Wh, however RC started only 4.2 times thus 25.1 P/Os were “wasted” and increased the need for charge migration. Hence it was concluded that control strategy with P/O after FC was not properly adapted to the case with PCM and further work is necessary.

6.7.4 Formulation of new control strategies

From all the testing performed with different control strategies I tried to formulate the optimal control sequence of SDE-PCM refrigerator-freezer.

Fixed sequence RC-FC-P/O-OFF where electro-valve is switched to RC position during OFF period seems to be the optimum. In this way RC has available maximum refrigerant charge directly from the beginning of the cycle. During RC operation charge is distributed between condenser and RC evaporator hence after switching to FC operation only the part of the charge from RC evaporator needs to migrate to FC loop. P/O performed at the end of FC provides additional cooling to FC, extracts most of the refrigerant from the evaporator and partially cools also RC at the end of P/O. Approach to run RC at the same frequency as FC have to be thought of to make use of every P/O phase.

Other optimal sequence could be performing P/O after each FC operation and store all the refrigerant in the condenser until either RC or FC ask to be cooled. By this way the refrigerant distribution time at the start up could decrease and there would be no need for fixed sequence. The disadvantage if this control strategy is large pressure difference on the compressor side during the start up. Most of the compressors are low starting torque engines thus they could not start up until the pressure difference is very small. The unloaded start electro-valve could solve the situation.

I sincerely recommend testing these two strategies in the future development of SDE-PCM concepts.

6.8 Heat transfer analysis

In general the driver of high RC efficiency is high evaporation temperature and ability to efficiently dissipate increased heat on the condenser side. Condenser heat dissipation was approached by experimental application of condenser fan and was already discussed. Nevertheless almost 15°C remaining temperature lift between PCM and refrigerant fluid temperatures, which is present throughout the experiments, still offers significant potential for improvement. To better understand the persistent restrictions simplified analogy with electrical circuit introduced in 3.2.4 was used to analyze heat transfer between evaporating refrigerant fluid and RC air. Three circuits were examined Figure 6.22:

1. plain roll-bond evaporator
2. roll-bond evaporator with PCM during charging process

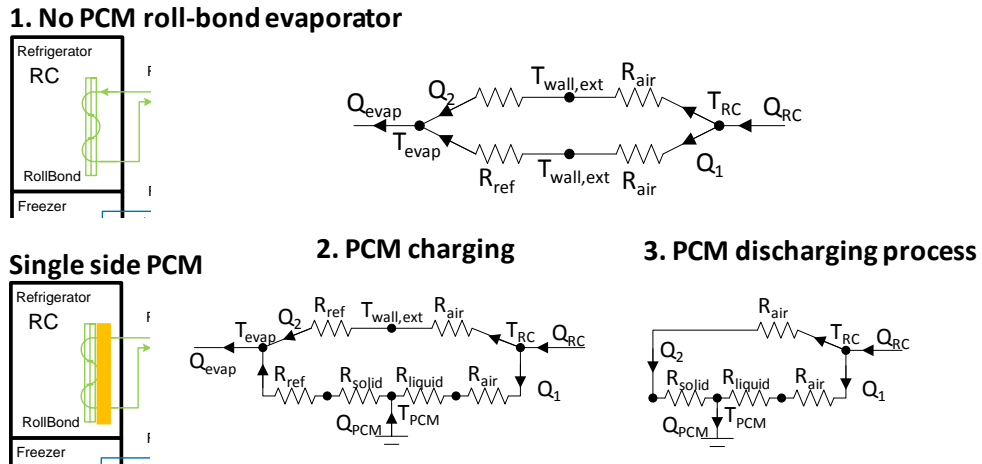


Figure 6.22 Heat transfer model used to evaluate options for further increase of evaporation temperature by placing PCM in contact with evaporator

3. roll-bond evaporator with PCM during discharging process

And impact of 5 different modifications on evaporation temperature and compressor COP were studied (cases) Table 6.5:

1. No PCM
2. Water as PCM on one side
3. Water and R_{air} decreases to 1/3
4. Water and R_{ref} decreases to 1/2
5. PCM on one side with $T_{PCM} = -5^{\circ}C$

Refrigerant (R_{ref}) and natural convection radiation (R_{air}) thermal resistance values were calculated from experimental results of the “Test 3” without PCM according to the Figure 6.22 and were reported in the Table 6.5. In the analysis roll-bond temperature $T_{wall,ext}$ was assumed to be uniform and value was taken equal to average between $T_{RC_evap_IN}$ and $T_{RC_evap_BOT}$ thermocouples. Compartment temperature T_{RC} was obtained as average between three weighted thermocouples

Case	Calc	Measured			Evap.	Air	PCM						
	T_{evap}	T_{evap}	$T_{wall,ext}$	T_{RC}			T_{PCM}	R_{ref}	R_{air}	t_{solid}	R_{solid}	t_{liquid}	R_{liquid}
	[$^{\circ}C$]	[$^{\circ}C$]	[$^{\circ}C$]	[$^{\circ}C$]			[$^{\circ}C$]	[$^{\circ}C/W$]	[$^{\circ}C/W$]	[mm]	[$^{\circ}C/W$]	[mm]	[$^{\circ}C/W$]
1. NO PCM		-23.1	-16.3	4.0		0.132	0.394						
2. Water	-15.3	-15.1		5.3	0	0.132	0.394	5	0.01	5	0.039		
3. Water + $R_{air}/3$	-13.1			5.3	0	0.132	0.131	5	0.01	5	0.039		
4. PCM + $R_{ref}/2$	-11.1			5.3	0	0.066	0.394	5	0.01	5	0.039		
5. $T_{PCM} -5^{\circ}C$	-17.6			5.3	-5	0.132	0.394	5	0.01	5	0.039		

Table 6.5 Simulated cases and values used to calculate evaporation temperature

and T_{evap} is equal to evaporation temperature during RC operation determined from suction pressure. Cooling capacity was determined from compressor data sheet at measured suction and discharge pressures. R_{ref} contained forced convection heat transfer from evaporating refrigerant to the evaporator wall and conduction within the aluminum wall. R_{air} thermal resistance on the air side was approximately 3 times higher than R_{ref} as it's possible to see in the Table 6.5.

Calculated resistances were further used in the analysis of PCM circuits according to Figure 6.22. Solid and liquid resistances of the PCM are estimated from water and ice properties and solid-liquid interface position. During the PCM charging process thickness of ice is growing and of water decreasing. For simplicity 5mm thickness of ice and 5mm thickness of water were fixed with thermal conduction coefficients $2.2\text{W}/^\circ\text{C}$ and $0.56\text{W}/^\circ\text{C}$ respectively. Contact and plastic bag resistances are neglected and all the resistances are considered constant throughout the calculation for simplicity. Heat transfer rates in each circuit branch were calculated. T_{evap} in PCM circuits was determined from balance between Q_{evap} and cooling capacity taken from the compressor data sheet. Measured value of T_{evap} during "Test 5" with PCM is reported for comparison and only 0.2°C difference was found, Table 6.5. Choice with 3mm thickness of ice could lead to perfect match between measured and calculated T_{evap} temperatures. However the purpose of the calculation is to point out critical places not to predict exact performance so the ice thickness was left to be 5mm.

In the investigation with PCM pocket, case 2, Q_{evap} grew by 43% versus the case 1 and led to the increase in evaporation temperature and efficiency, Table 6.6. On the other hand it's important to mention that heat rate Q_{RC} from RC air decreased significantly to less than half during the charging process thus RC temperature pull down performance suffered considerably.

In case 3 with PCM I simulated only one third of R_{air} thermal resistance which

Case	Compressor data sheet					Charging		Discharging	Q_{PCM} [W]
	T_{cond} [$^\circ\text{C}$]	T_{evap} [$^\circ\text{C}$]	Q_{evap} [W]	Power [W]	COP		Q_{RC} [W]	Q_{RC} [W]	
					W/W	%			
1	29.6	-23.1	103	41	2.53	-	103		
2	33.5	-15.3	147	51	2.86	0%	51	20	96
3	33.5	-13.1	162	54	3.02	5%	101	44	61
4	33.5	-11.1	177	56	3.17	11%	43	21	134
5	33.5	-17.6	133	49	2.71	-5%	67	39	65

Table 6.6 Compressor COP improvements and heat transfer rates for the simulated cases

could be achieved by forced convection fan. Similar pull down performance was observed as for case 1. Evaporation temperature grew by modest 2.2°C and could bring extra 5% compressor COP during RC operation versus case 2. However Q_{RC} discharging equals 44W which is much higher than RC heat gain at 4°C and would lead to compartment temperatures closer to 0°C and purposeless cabinet heat gain increase. Risk of fresh food freezing could occur as well. ON/OFF RC fan could be helpful in this situation as it could operate only during the pull down and stay off during most of the discharging process. Even better solution could be speed controlled RC fan which could react quickly to the increased heat load to RC and absorb it to the PCM. This topic is subject for further research and development in the SDE-PCM field.

The most significant thermal resistance which still restricts RC evaporation temperature is R_{ref} . In the simulation case 4, I reduced R_{ref} to half and significant 4.2°C increase in evaporation temperature was observed which would lead to extra 11% compressor COP during RC if condensing temperature was assumed to remain constant. In order to decrease R_{ref} two steps need to be performed:

1. Study of charge distribution in the system has to be carried out, followed by determination of optimal internal volume of the evaporators to assure sufficient refrigerant filling of both evaporators.
2. It is necessary to define fins design which could extrude into the PCM material and improve conduction heat transfer and heat exchange area of the evaporator.

Phase changing temperature has also a strong impact on the performance of the system. In the case 5 I simulated PCM temperature equal to -5°C. Evaporation temperature dropped by 2.3°C versus case 2 and brought 5% penalty in compressor COP. In addition Q_{RC} discharging is two times higher than RC heat gain and would lead to sub cooling RC even to temperatures below 0°C which is undesirable.

6.9 Prototype 2 (SDE-PCM-SC) experimental results

I experimentally tested for energy consumption prototype 2 with subcooling loop at two different setups, with subcooling loop turned ON and OFF. The measured results were analyzed in the same way as it was shown in 6.6. Results were disappointing because they didn't show theoretically expected energy efficiency improvement. Even degradation of performance was visible when compared to

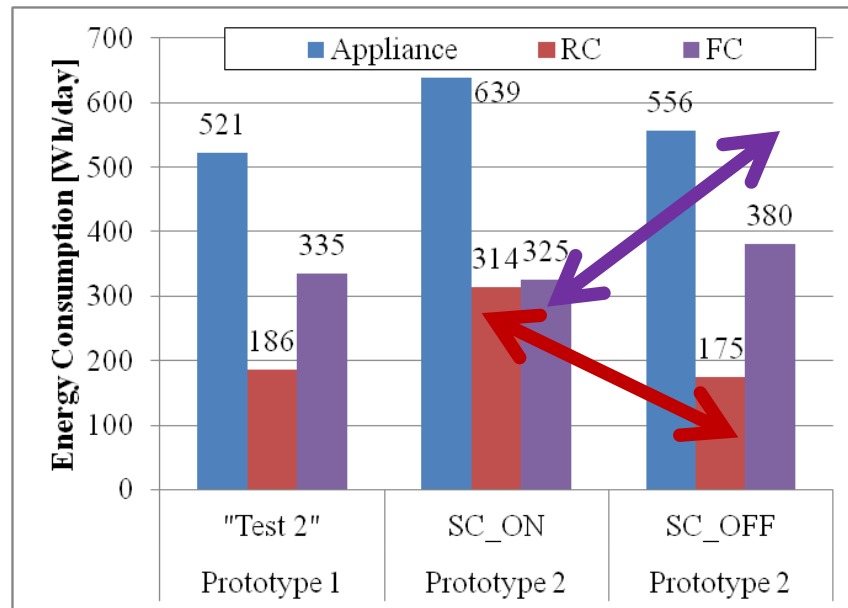


Figure 6.23 Comparison of energy consumption of prototype 2 with subcooling loop turned ON and OFF and prototype 1 as a baseline

the prototype 1 without subcooling loop, Figure 6.23. Energy consumption results illustrated that load shifting mechanism could work, because FC energy consumption decreased and RC energy consumption increased when sub-cooling loop was turned ON. However the relative energy consumption decay during FC operation was much smaller than the increment of energy consumption during RC operation.

From the temperature profiles measured at four different points inside of the PCM for the two setups of prototype 2 I could conclude that PCM in the RC was completely utilized when subcooling loop was turned ON. Complete melting of the PCM was achieved at the end of the RC OFF period. On the other hand when SC was turned OFF one of the PCM thermocouples was still showing remaining ice at 0°C.

6.9.1 Efficiency degradation issues of prototype 2

Based on the temperature and pressure readings before and during FC operation, see Figure 6.24, I identified several issues in the prototype 2 refrigeration system causing efficiency degradation.

Even though the prototype 2 was charged by 50g of R600a which is 8g more than prototype 1, the three thermocouples (FC_evap_IN, FC_evap_Mid and FC_evap_OUT) attached to the FC evaporator showed insufficient charge refrigerant charge. FC_evap_out was higher than the other two which means there

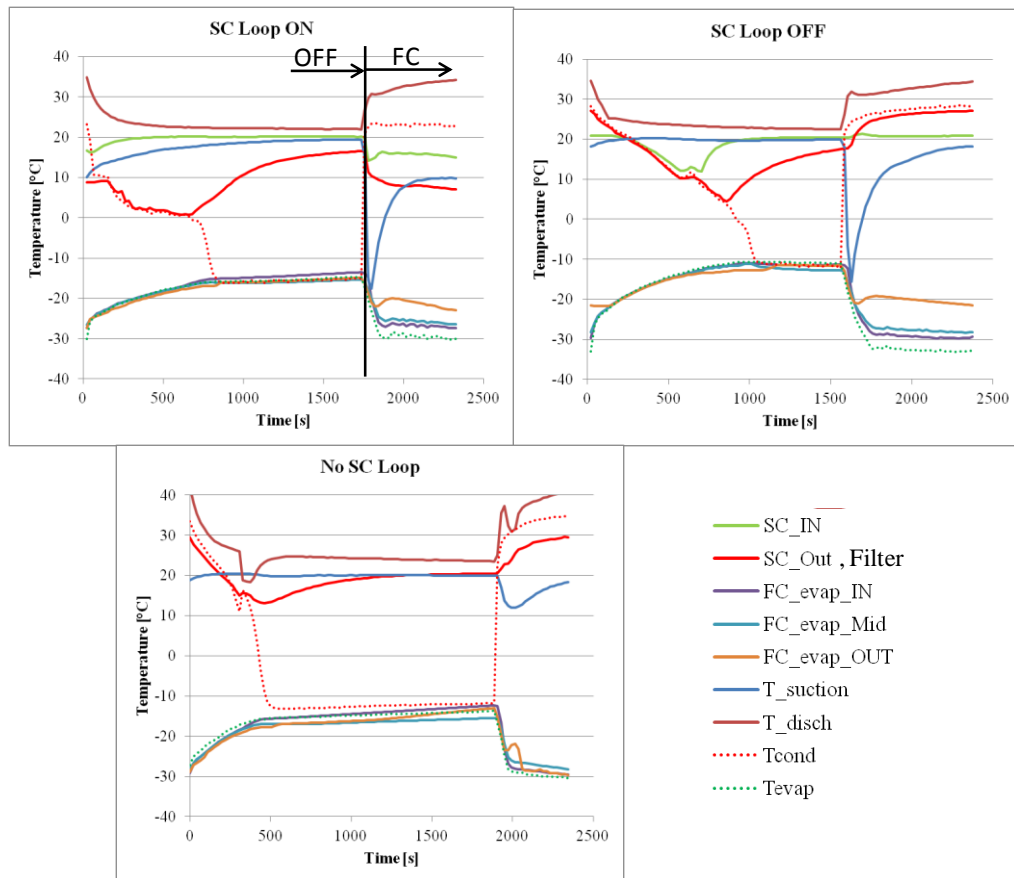


Figure 6.24 Comparison of OFF period before FC and FC operation for two setups of prototype 2 and baseline setup of prototype 1

is certain superheating length of the evaporator. On the other side already 50g of refrigerant was causing compressor flooding at the start up, which is visible on the suction temperature reading. In addition T_{cond} was significantly lower during SC_ON testing versus SC_OFF. This means that the subcooling region moved further to the PCM and more condenser area was available for condensing. However it's possible that some of the refrigerant condensation was occurring in the PCM. In this way less heat was transferred to the ambient and more to the PCM. All these problems indicate improper design of the subcooling loop in respect to the available amount of the refrigerant in the system. Internal volume of 4.5m long loop can accommodate additional 36g of liquid refrigerant R600a and this amount would cause severe problem to the compressor reliability. Thus the loop has to be designed again taking into consideration also refrigerant mass charge.

Another significant problem identified from the Figure 6.24 is low suction temperature during SC_ON operation. FC suction line capillary tube heat

exchanger was not modified and hence less heat was recuperated. The temperature of the liquid entering the FC capillary tube is indicated as SC_OUT (or Filter for prototype 1) which is considerably lower for the SC_ON operation than for other two cases. Efficient SLHEX is very important especially in the circuit

with R600a refrigerant which I demonstrate with the results of a simple calculation in the Figure 6.25. I compared impact of SLHEX on the system performance with different refrigerants. The 0% COP is valid for the system without SLHEX. The colors represented different evaporation temperatures with constant condensation pressure. The COP improvements are calculated for ideal suction line heat exchanger. From the selected usual refrigerants utilized in the small refrigeration systems isobutane is the most sensitive refrigerant on good design of the suction line heat exchanger. Prototype's FC suction line heat exchanger has to be redesigned together with the subcooling loop.

Next issue of the subcooling loop design is extremely long 1.5m tube between end of the subcooling in the PCM and entrance to the capillary tube. Even though the tube is insulated in the foam of the back wall, it absorbs heat from the foam which again increases liquid temperature after it was subcooled and degraded energy efficiency. Additional issue of such a long subcooling tube is extremely long time for reaching pressure equalization between condensing and evaporating pressure during OFF period. Once the capillary tube liquid seal is broken remaining liquid in the loop and in the condenser starts to evaporate and absorbs heat from the ambient. It's visible on the thermocouples SC_IN, SC_OUT and Filter. For prototype 2 the temperatures at these positions are much lower and last longer under ambient temperature than for prototype 1. This has negative effect on the system energy efficiency. The optimum design of the loop could expand the subcooled liquid immediately after exiting PCM and flowing to the FC evaporator by shortest possible way.

I described three major topics which cause energy efficiency degradation of the prototype 2. These issues require redesign of the subcooling loop and of the FC suction line heat exchanger and tuning of the system and it was not performed as a part of this PhD research.

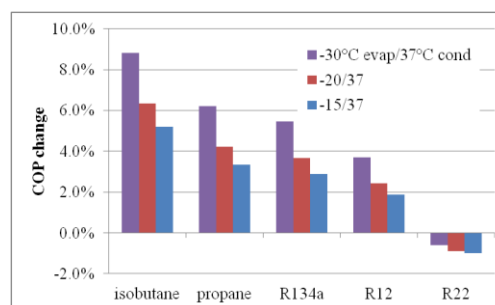


Figure 6.25 Impact of SLHEX on the system COP with various refrigerants

7 Conclusions and contribution

Based on the literature review I selected sequential dual evaporator (SDE) refrigeration system as one of the potentially most efficient cooling circuits to be applied in the domestic refrigerator-freezer appliance. However refrigerator with such a circuit was not yet commercialized and hence I was eager to identify principal drawbacks of the SDE system:

- excessive cooling capacity pumped by the volumetric compressor at elevated refrigerator compartment (RC) evaporation temperature
- reduced heat transfer rate to the evaporator at high evaporation temperature lead to forced convection heat transfer in RC
- refrigerant mass charge migration between FC and RC evaporator
- overall appliance COP is dependent on the RC heat load ratio

7.1 Preliminary testing

In the first step I wanted to understand how variable speed compressor could impact SDE circuit performance. On the existing Whirlpool SDE prototype I experimentally tested effect of compressor RPM on the RC evaporation temperature and COP. Results showed that only reducing compressor speed from 3000 to 1800RPM during RC operation brought 10% increase in RC COP and RC evaporation temperature grew by 4.3°C.

By applying approach of second law of thermodynamics to the measured results I could determine losses in the components of the refrigeration circuit. Compressor was identified with the highest losses accounting more than 40% of electric power consumed. RC evaporator was a second most inefficient component with losses accounting around 25% of power input. The reason was very high temperature lift (33.7°C) between evaporating refrigerant and RC air temperatures even at minimum compressor RPM.

7.2 Concepts of SDE circuit with PCM

Based on the theoretical and experimental analysis of the SDE refrigeration circuit I proposed two innovative concepts with advanced technologies to overcome main drawbacks of the SDE system in refrigerator-freezer appliance.

The first innovative concept included variable speed compressor to allow reduction of cooling capacity pumped by compressor at the elevated evaporation

temperature during RC operation. The pocket filled with PCM was attached to one side of the visible RC roll-bond evaporator in order to increase heat transfer coefficient and to store excess of cooling capacity in the frozen PCM. PCM thermal accumulation brought stability to RC air temperature and extended RC resistance to the electricity black outs. Heat from the RC air was continuously absorbed to the PCM and reduced heat transfer rate necessary to keep compartment within specified temperature range. Thus the heat transfer to the PCM can be driven by natural convection which has positive effect on the fresh food preservation and saves forced convection fan power.

To deal with refrigerant mass migration issues two components were added to the system. Electronic block valve was attached to the liquid line after the condenser to be able to perform refrigerant pump out from the evaporators. And check valve was placed on the FC suction line to avoid refrigerant back flow to the evaporator during RC operation and OFF periods.

The second conceptual idea in addition to the first one implemented supplementary loop attached to the freezer liquid line, which by passing through RC PCM can further subcool liquid refrigerant and shift load from the FC to RC. By this approach overall SDE COP could be improved by increasing RC heat load ratio. The idea was considered innovative and Whirlpool Corporation decided to fill up the patent application.

The two novel concepts were turned into two appliance prototypes built in cooperation with Whirlpool Corporation research center in Italy which also sponsored this research activity.

Pure water was chosen as PCM because it met many selection criteria such as compatibility with food environment, low supercooling/superheating effect, cyclic stability, availability, cost and good thermal conductivity in solid and liquid state. Phase changing temperature 0°C gave high potential for increasing RC evaporation temperature but limited heat absorption rate from RC air. Therefore low thermal conductivity vacuum insulation panels were implemented in the RC walls to decrease compartment heat load and match it with small heat absorption rate of the PCM.

I proposed modifications to the acquisition and control hardware to be able to experimentally test the prototypes in the environmental rooms of Whirlpool laboratories.

7.3 Experimental results

Optimum parameters of P/O were experimentally defined. FC fan operation had major positive effect on the refrigerant amount pumped to the condenser. Compressor speed showed strong influence on the P/O energy consumption and minor effect on P/O efficiency, thus minimum 1620RPM was chosen as optimum. Duration of 180s was selected to be on the safe side that most of the refrigerant was extracted at any condition.

SDE prototype was tested with and without phase change material. RC evaporation temperature in the prototype with PCM was increased by 7.8°C which brought 26.7% energy consumption decrease during RC operation and 8.1% overall appliance energy saving. Properly performed P/O and activated FC-CV were crucial to reach high evaporation temperatures during RC. Moreover condenser global heat transfer coefficient had to be improved by 30% to reach overall energy efficiency improvement.

Heat transfer analysis showed still available potential for further increase of evaporation temperature and RC energy efficiency. Thermal resistance between evaporating refrigerant and external evaporator wall temperature was detected as next critical place in the heat transfer to the evaporating refrigerant. Refrigerant charge distribution measurements and modification to the RC evaporator have to be done in order to decrease this thermal resistance.

In the prototype with PCM in RC, temperature pull down capabilities were identified as insufficient. Thus variable speed fan or other solution is necessary for production appliance. Variable speed fan could have an advantage of modulating amount of heat absorbed to the PCM and keeping RC temperature very stable.

Three different control strategies were tested and results showed that proper control of the P/O operation has a crucial impact on the overall efficiency of the SDE-PCM appliance. Two additional control strategies were proposed and could lead to even better results in energy efficiency.

Second concept with subcooling load shifting mechanism didn't prove to be more efficient but showed that the load shifting could work. However the design of the subcooling loop has to be modified to avoid extensive refrigerant charge, heat gains from the ambient and losses in the suction line heat exchanger.

7.4 Further work

Several fields were identified as interesting for future studies:

- Dedicated design of RC evaporator with thermal accumulation for SDE-PCM appliance
 - Internal volume for refrigerant charge match with FC evaporator
 - Thermal resistance between evaporating refrigerant and PCM
 - Adjustable heat transfer rate from RC environment to PCM
 - PCM selection with lower phase change temperatures
- Optimization of capillary tube and condenser design for SDE-PCM appliance
 - Forced convection versus natural convection condenser
 - RC capillary tube impact on the increase of condensing temperature during RC PCM charging sequence
 - Liquid line sight glass and pressure temperature measurements
- Optimization of control strategy considering PCM thermal accumulation
 - Sequence to minimize refrigerant mass charge migration in SDE circuits
 - Unloaded compressor start to allow further control sequences
- Redesign load shifting mechanism based on sub-cooling between freezer and refrigerator compartments
 - Design of the subcooling loop to minimize refrigerant mass charge and heat gain from ambient
 - Dedicated capillary tube for the subcooling loop

8 Bibliography

Abhat A. Low temperature latent heat thermal energy storage: Heat storage materials [Journal] // Solar Energy. - Stuttgart : Elsevier, 1983. - 4 : Vol. 30.

Azzouz K., Leducqa D. and Gobinb D. Enhancing the performance of household refrigerators with latent heat storage: An experimental investigation [Journal] // International Journal of Refrigeration. - Cedex : IIR, 2009. - 7 : Vol. 32.

Baskin E. Delafield F. Performance of a Two-Cycle Refrigerator/Freezer Using HFC Refrigerants [Journal] // ASHRAE Transaction. - USA : ASHRAE, 1999. - 2 : Vol. 105. - pp. 310-318.

Bertoldi P. and Atanasiu B. Electricity Consumption and Efficiency Trends in European Union - Status Report 2009 [Report]. - Ispra : JRC Scientific and Technical Reports, 2009.

Bjork Erik A simple technique for refrigerant mass measurement [Journal] // Applied Thermal Engineering. - Stockholm : Elsevier, 2005. - 8-9 : Vol. 25.

Bjork Erik and Palm Bjorn Refrigerant mass charge distribution in a domestic refrigerator, Part I: Transient conditions [Journal] // Applied Thermal Engineering. - Stockholm : Elsevier, 2006. - 8-9 : Vol. 26.

Borges Bruno N. [et al.] Transient simulation of household refrigerators: A semi-empirical quasi-steady approach [Journal] // Applied Energy. - Florianopolis : Elsevier, 2011. - 3 : Vol. 88.

Carsten Heinrich and Berthold Kai A Modelica Library for Simulation of Household Refrigeration Appliances Features and Experiences. - Dresden : Institute for Air Conditioning and Refrigeration, Department Refrigeration and Cryogenics, 2006.

Cur Nihat O [et al.] Dual evaporator refrigerator with non-simultaneous evaporator [Patent]. - US, 1995.

DOE Preliminary technical support document: Energy efficiency program for consumer products: Refrigerators and freezers [Report]. - 2009.

DOE TECHNICAL REPORT: Analysis of Amended Energy Conservation Standards for Residential Refrigerator-Freezers [Report]. - 2005.

EN 12900 Refrigerant compressors — Rating conditions, tolerances and presentation of manufacturer's performance data // Standard. - 2002.

Engineeringtoolbox [Online]. - 2013. - http://www.engineeringtoolbox.com/thermal-conductivity-d_429.html.

European Commission Directive 2010/30/EU of the European Parliament and of the Council with regard to energy labelling of household refrigerating appliances [Report]. - 2010.

Galliani A. and Pedrocchi E. Analisi exergetica [Book]. - Milano : Polipress, 2006.

Gan A. Klein S., Reidl D. Analysis of Refrigerator/Freezer Appliances Having Dual Refrigeration Cycles [Journal] // ASHRAE Transaction. - 2000. - pp. 185-191.

Ge H. and Bullard C. W. Experimental Investigation of a Refrigerator with a Dual Temperature Evaporator [Report]. - Urbana-Champaign : ACRC, 1999.

Gin Benjamin and Farid Mohammed M. The use of PCM panels to improve storage condition of frozen food [Journal] // Journal of Food Engineering. - Auckland : IJR, 2010. - 2 : Vol. 100.

Gonçalves Joaquim M., Melo Cláudio and Hermes Christian A semi-empirical model for steady-state simulation of household refrigerators [Journal] // Applied thermal engineering. - Sao Jose : Elsevier, 2009. - 8-9 : Vol. 29.

Goncalves Joaquim Manoel and Melo Claudio Experimental and Numerical Steady-State Analysis of a Top-Mount Refrigerator [Conference] // International Refrigeration and Air Conditioning Conference Purdue. - Purdue : Purdue e-Pubs, 2004.

Guoliang Ding, Chunlu Zhang and Zhili Lu Dynamic simulation of natural convection bypass two-circuit cycle refrigerator-freezer and its application Part I: Component models [Journal] // Applied Thermal Engineering. - Shanghai : Elsevier, 2004. - 10 : Vol. 24.

He M., Song X. and Zhang J. Available energy analysis of new tandem double-capillary tube refrigeration system for refrigerator-freezer [Journal] // Frontiers of Energy and Power Engineering in China. - Xinxiang : Springer-Verlag, 2008. - 1 : Vol. 2.

Hermes Christian J.L. and Melo Claudio A first-principles simulation model for the start-up and cycling transients of household refrigerators [Journal] // International Journal of Refrigeration. - Florianopolis : IIR, 2008. - 8 : Vol. 31.

Hermes Christian, Melo Claudio and Negro Cezar A numerical simulation model for plate-type roll-bond evaporators [Journal] // International Journal of Refrigeration. - Florianopolis : Elsevier, 2008. - 2 : Vol. 31.

Incropera F. [et al.] Fundamentals of heat and mass transfer [Book]. - 2007.

ISO ISO-15502 Household refrigerating appliances — characteristics and test methods // ISO International Standard. - 2005.

Janssen M.J.P and Jonge H. de Stationary simulation of domestic refrigeration cycles (Theory) [Report]. - Netherlands : Philips Research, 1991.

Jaster H. Refrigerator system with dual evaporators for household refrigerator [Patent]. - US Patent, 1990.

Jung D.S. Radermacher R. Performance simulation of single-evaporator domestic refrigerators charged with pure and mixed refrigerants [Journal] // International Journal of Refrigeration. - USA : IIR, July 1991. - 4 : Vol. 14. - pp. 223-232.

Kelman S. and Bullard C. W. Dual Temperature Evaporator Refrigerator Design and Optimization [Report]. - Urbana-Champaign : ACRC, 1999.

Kim K. Radermacher R. R22/R152b Mixtures and Cyclopropane RC270 as substitutes for R12 in single evaporator refrigerators [Journal]. - USA : ASHRAE, 1993. - Vol. 99.

Kim Man-Hoe, Lim Byung-Han and Chu Euy-Sung The Performance Analysis of a Hydrocarbon Refrigerant R-600a in a Household Refrigerator/Freezer [Journal]. - Suwon : KSME International Journal, 1998. - 4 : Vol. 12.

Lavanis M., Haider I. and Radermacher R. Experimental Investigation of an Alternating Evaporator Duty Refrigerator/Freezer [Journal] // ASHRAE Transaction. - USA : ASHRAE, 1998. - Vol. 104.2. - pp. 1103-1111.

Liu Zhijing [et al.] Test Results of Hydrocarbon Mixtures in Domestic Refrigerator/Freezers [Conference] // Int. CFC and Halon Alternatives Conf. - USA : Center for Environmental Energy Engineering, 1994.

Martinez Isidoro [Online]. - 2011. - <http://webserver.dmt.upm.es/~isidoro/bk3/c07sol/Solution%20properties.pdf>.

MEglobal Product guide Ethylen Glycol [Online]. - 2008. - 2011. - <http://www.meglobal.biz>.

Öko-Recherche Comparison of global projections of HFC emissions with regard to 100 year GWP and 20 year GWP metric [Report]. - Germany : Öko-Recherche, 2011.

Oro E. [et al.] Improving thermal performance of freezers using phase change materials [Journal] // International Journal of Refrigeration. - Lleida : IIR, 2012. - 4 : Vol. 35.

Park J K [et al.] Dual-controlled indirect refrigerator/freezer using two capillary tubes and an air flow switching system [Conference] // Purdue international refrigeration and air conditioning conference. - Purdue : Purdue e-Pubs, 1998.

Presutto Milena Preparatory Studies for Eco-design requirements for EuPs, Task7 [Report]. - Brussels : European Commission, 2008.

Richardson David An object oriented simulation framework for steady-state analysis of vapor compression refrigeration system and components // PhD Thesis. - 2006.

Saginomiya Check Valves [Online]. - 2012. - <http://www.saginomiya.co.jp/eng/auto/syousai.php?File=pdf/acv.pdf&Mode=777&Type2=acv&NameType=CHECK%20VALVES&Type3=china/controlsC1>.

Sand J. R., Rice C. K. and Vineyard E. A. Alternative Refrigerants and Refrigeration Cycles for Domestic Refrigerators [Report]. - Oak Ridge : OAK Ridge National Laboratory, 1992.

Simmons K. E., Haider I. and Radermacher R. Independent Compartment Temperature Control of Lorenz-Meutzner and Modified Lorenz-Meutzner Cycle Refrigerators [Journal] // ASHRAE Transaction. - 1996. - pp. 1085-1092.

Tulapurkar Chetan [et al.] Phase change materials for domestic refrigerators to improve food quality and prolong compressor off time [Conference] // Purdue International conference of refrigeration and air conditioning. - Purdue : Purdue e-Pubs, 2010.

Visek Matej [et al.] Performance improvement of sequential dual evaporator refrigeration cycle in domestic refrigerator-freezer charged with R600a: Prototype testing [Conference] // 10th IIR Gustav Lorentzen Conference on Natural Refrigerants. - Delft : Delft, 2012.

Won Jae Yoon, Hae Won Jung and Hyun Joon Chung Performance optimization of a two-circuit cycle with parallel evaporators for a domestic refrigerator freezer [Journal] // International Journal of Refrigeration. - Seoul : IIR, 2011. - 1 : Vol. 34.

Won S. Jung D. and Radermacher R. An experimental study of the performance of a dual-loop refrigerator/freezer system [Journal] // International Journal of Refrigeration. - USA : IIR, 1994. - 6 : Vol. 17. - pp. 411-416.

9 Appendix I

The Embraco compressor data sheets include data of the VEMZ9C compressor envelope determined for various RPM. (1600, 2000, 3000 and 4500). The envelope extends from -35°C to -10°C evaporation temperature and from 35°C to 55°C condensing temperature. All the data are reported at ASHRAE32 condition which means 32°C suction temperature of the compressor and 32°C of liquid temperature. To determine 10 coefficients for describing mass flow, power and cooling capacity according to EN12900 I entered the data from the data sheet at one compressor RPM to the software ASEVAL2. Software calculated isentropic and volumetric efficiency of the compressor based on the compressor displacement and choice of the refrigerant. Then I selected a fit of volumetric efficiency by equation:

$$\vartheta_{vol} = A_0 + A_1 T_{cond} + A_2 T_{cond}^2 - (B_0 + B_1 T_{cond}) p_i^C \quad \text{eq 88}$$

The coefficients A, B and C were calculated by least squares method. In the next step also isentropic efficiency was fitted by equation and coefficients calculated by least squares:

$$\vartheta_{is} = \left(A_0 + A_1 \frac{T_{cond}}{100} + A_2 \left(\frac{T_{cond}}{100} \right)^2 \right) \vartheta_{vol} \frac{p_i^B - C}{D_0 + D_1 p_i^{(e_0 + e_0 \frac{T_{cond}}{100})}} \quad \text{eq 89}$$

The maximum relative errors for both volumetric and isentropic fits are reported in the Table 9.1 for various compressor RPMs.

After the data were successfully fitted to the efficiency curves which are visible in the Figure 9.1 and Figure 9.2 I could generate 10 coefficients of the EN12900

	RPM	Efficiency	
		Volumetric	Isentropic
Max. relative error	1600	-0.62%	-1.62%
	2000	0.40%	-0.82%
	3000	-0.48%	-1.44%
	4500	0.23%	0.37%
Mean error	1600	0.28%	0.59%
	2000	0.18%	0.32%
	3000	0.15%	0.66%
	4500	0.07%	0.18%

Table 9.1 Maximum relative and mean error of the isentropic and volumetric equations fits

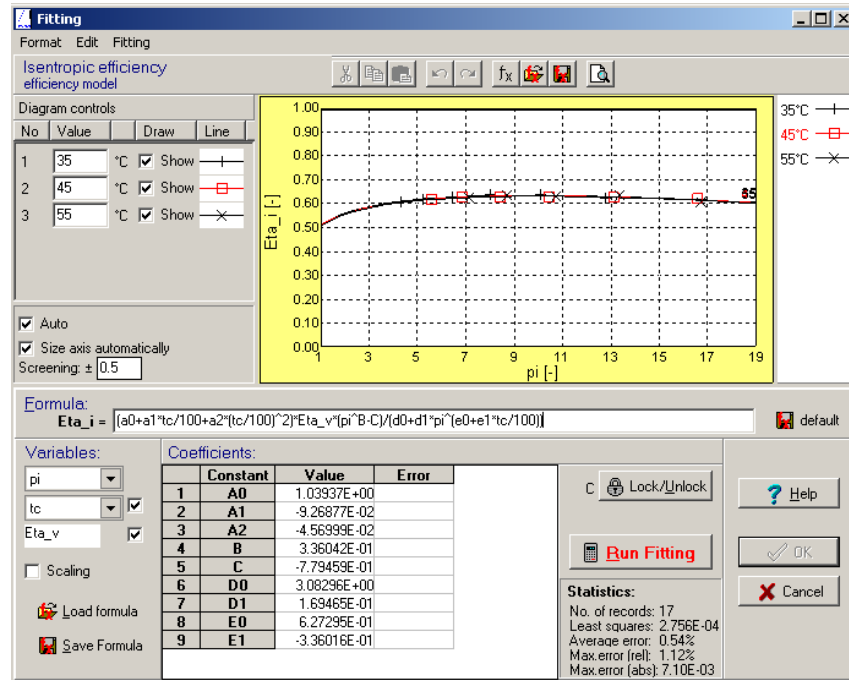


Figure 9.1 Fit of isentropic efficiency for 1600RPM

polynomial for the extended envelope for evaporation temperatures from -35°C to 0°C. The procedure was repeated for each RPM of the compressor and 10 coefficients were determined and reported in the Table 9.2. ASEVAL calculation should be based on the experimental outcomes to obtain more accurate results but these were not available thus I used data sheets.

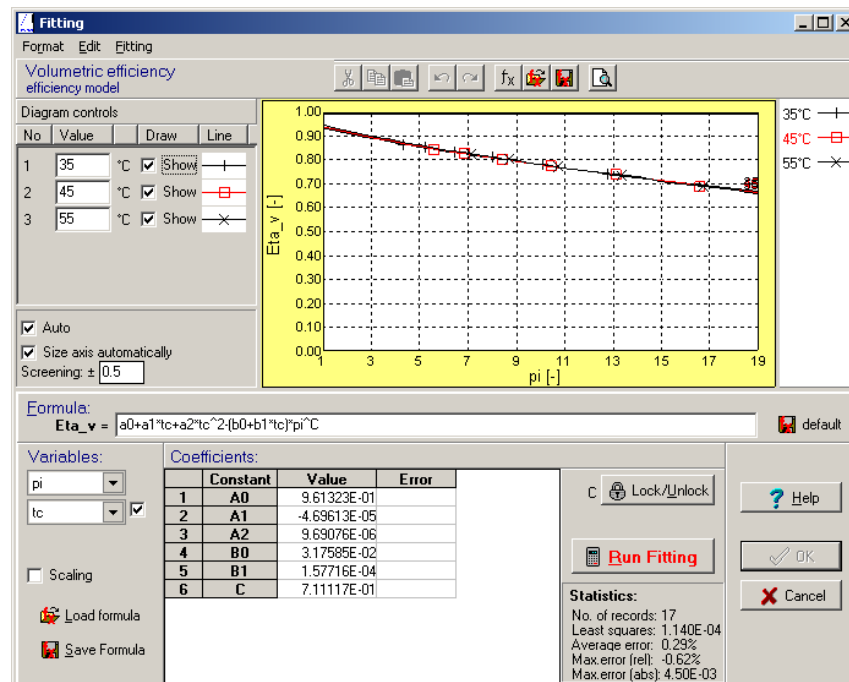


Figure 9.2 Fit of volumetric efficiency for 1600RPM

1600RPM			2000RPM		
Mass flow	Cooling capacity	Power	Mass flow	Cooling capacity	Power
9.20E-01	2.85E+02	1.10E+01	9.90E-01	3.50E+02	3.80E+01
3.36E-02	1.05E+01	-1.18E+00	4.01E-02	1.28E+01	5.40E-02
-3.90E-03	-2.45E-01	1.93E+00	3.39E-03	-2.49E-01	1.67E+00
4.81E-04	1.45E-01	-3.61E-02	5.68E-04	1.74E-01	-1.35E-02
-3.92E-05	8.35E-04	6.19E-02	-3.47E-05	-2.84E-03	4.56E-02
4.83E-05	-1.41E-03	-9.47E-03	-8.98E-05	-2.50E-03	-3.87E-03
2.85E-06	7.95E-04	-2.60E-04	3.19E-06	9.28E-04	-1.05E-04
-5.46E-08	5.93E-05	5.29E-04	-3.27E-07	-3.89E-05	3.32E-04
2.83E-07	-4.46E-06	-1.61E-04	1.73E-07	4.01E-06	-3.27E-05
-3.19E-07	-1.21E-05	1.42E-05	4.78E-07	-1.32E-05	-1.23E-05
3000RPM			4500RPM		
Mass flow	Cooling capacity	Power	Mass flow	Cooling capacity	Power
1.16E+00	5.32E+02	4.58E+01	1.41E+00	7.89E+02	2.81E-01
5.78E-02	1.93E+01	-1.42E+00	8.42E-02	2.89E+01	-6.88E+00
2.31E-02	-7.35E-01	3.55E+00	5.31E-02	-6.79E-01	8.64E+00
8.45E-04	2.61E-01	-6.15E-02	1.21E-03	3.94E-01	-1.94E-01
3.09E-05	-1.05E-02	1.22E-01	1.24E-04	-5.23E-03	3.14E-01
-4.58E-04	5.89E-04	-2.41E-02	-1.03E-03	-5.90E-03	-7.44E-02
4.89E-06	1.39E-03	-4.88E-04	6.68E-06	2.10E-03	-1.43E-03
-2.01E-07	-2.72E-05	1.09E-03	3.78E-08	-4.54E-05	2.91E-03
-3.46E-07	8.11E-05	-4.43E-04	-1.17E-06	9.13E-06	-1.39E-03
2.62E-06	-2.32E-05	7.21E-05	5.80E-06	-4.19E-05	2.33E-04

Table 9.2 Coefficients of the polynomial from EN12900 for VEMZ9C compressor at various RPM reported for the 32°C suction temperature and 32°C liquid temperature

10 Appendix II

Calibration tables of pressure transducers for prototypes 1 and 2

Prototype 1

Calibration done on FP AI 100

Channel 1 and 3

Atmospheric pressure

1.005 Bar

Low pressure	FP3	High pressure	FP1
Transducer range	0-10Bar	Transducer range	0-10Bar
Set pressure [bar]	Read value [V]	Set pressure [bar]	Read value [V]
1.005	0.824	1.005	0.810
7.005	5.807	7.005	5.793
4.005	3.318	4.005	3.310
1.005	0.824	1.005	0.810
Linear fit pressure=(ax+b)			
a	1.20400	a	1.20398
b	0.01238	b	0.02655

Prototype 2

Calibration done on FP AI 100

Channel 1 and 3

Atmospheric pressure

0.9797 Bar

Low pressure	FP1	High pressure	FP3
Transducer	0-10Bar	Transducer range	0-25Bar
Set pressure [bar]	Read value [V]	set pressure [bar]	Read value [V]
0.9797	0.855	0.9797	0.242
6.9797	5.782	10.9797	2.736
3.9797	3.334	5.9797	1.492
0.9797	0.848	0.9797	0.242
Linear fit pressure=(ax+b)			
a	1.21600	a	4.00875
b	-0.05931	b	0.00656

11 Appendix III

Test #	Appliance [Wh/day]	RC						FC				
		T _{RC} [°C]	Compressor [Wh/day]	Run time	P/O [Wh/day]	Run time	Cond fan [Wh/day]	TFC [°C]	Compressor [Wh/day]	FC fan [Wh/day]	Run time	
1	536	3.94	211	20.2%	0.0	-	-	-18.25	325	17.8	-	
2	498	5.19	178	14.9%	0.0	0.0%		-18.25	320	16.9	20.6%	
3	541	4.04	164	15.7%	30.6	3.8%	20.7	-18.13	328	17.2	20.0%	
4	505	5.31	160	10.7%	13.0	1.3%		-18.15	333	16.7	19.3%	
5	497	5.41	157	9.7%	12.1	1.4%		-18.11	329	16.4	18.9%	
6	481	5.29	138	10.1%	8.9	1.0%	13.4	-18.27	321	17.0	19.6%	
7	502	3.82	160	14.5%	34.4	6.2%		-18.43	313	16.6	19.3%	
8	502	5.36	136	8.8%	35.5	6.1%		-18.20	336	17.3	20.0%	

Measured values of energy consumption tests performed on the Prototype 1